

https://dspace.org/

Fabrication of nanomaterial-based printed electrode sensors for electrochemical determination of heavy metals

Ntuli, Letta Mahlohonolo

2021
https://hdl.handle.net/10539/32966

Downloaded from a DSpace repository. https://dspace.org/



Fabrication of nanomaterial-based printed electrode sensors for electrochemical determination of heavy metals

by

Letta Mahlohonolo Ntuli

Thesis in fulfilment of the requirement for the degree

MSc (Engineering)

Submitted to the

School of Chemical and Metallurgical Engineering, Faculty of Engineering and the Built Environment, University of Witwatersrand, Johannesburg, South Africa

Supervisors: Prof. Jean Mulopo, Dr. Palesa Diale

October 2021

Dedication

To my grandmother, *Mogoshadi!*

Acknowledgements

First, I would like to acknowledge my previous and current supervisors for the guidance in their respective fields especially for cementing my research interest. Special thanks to Professor Jean Mulopo for his supervision and patience, support, valuable wisdom throughout the project. I am indebted to my co-supervisor Dr Palesa Diale for giving me the opportunity to carry out this project in her laboratory, her priceless help and inspiring guidance throughout my studies. CSIR and CSIR merSETA Bursary Programme are acknowledged for financial support and allowing me to use their unlimited resources when needed.

Special thanks to Dr Abongile Jijane and Ms Ntsoaki Mphuthi for kindly allowing me to use Mintek NIC facilities and offering their time and expertise to assist me with the screen-printing process.

For discussions and recommendations mostly electrochemistry related, I would like to gratefully thank Dr Tshimangadzo Munonde and Clementine Louw.

To my friends, Rebone Chaba, Mlungisi Ngoma and Siphiwe, thank you for your immeasurable love and always lending me an ear when the research work became too much, thank you deeply for your unwavering support.

Finally, I would like to give gratitude to my family, my mother, my aunt, my son and all my entire family for your love and constant care," *KE A LEBOGA*".

Declaration

I Letta Mahlohonolo Ntuli declare that this dissertation is my own unaided work. It is being submitted to the degree of Master of Science in Engineering to the University of the Witwatersrand, Johannesburg. It has not been submitted before for any other degree or examination in any other University.

Signature: 

_13_th day of ____October_____ 2021

- **Table of Contents**

Dedication ..... **ii**

Acknowledgements ..... **iii**

Declaration ..... **iv**

ABSTRACT **1**

LIST OF ABBREVIATIONS AND SYMBOLS **2**

STRUCTURE OF THE DISSERTATION **4**

1. CHAPTER 1: INTRODUCTION **5**

1.1. Background 5

1.1.1. Evolution of paper-based diagnostic devices 9

1.2. Problem Statement 11

1.3. Study Objectives 12

1.4. Research questions 13

1.5. References ..... **Error! Bookmark not defined.**

CHAPTER 2: LITERATURE REVIEW **2**

2.1. Introduction to electrochemistry 2

2.2. Types of electrochemical signals 3

2.2.1. Cyclic Voltammetry 3

2.2.2. Square-Wave Voltammetry 4

2.3. Working Electrode carbon material 6

2.3.1. Graphene 6

2.3.2. Graphene oxide 6

2.4. Screen-printing 7

2.5. Heavy metals detection by nanomaterials application 11

2.6. Conductive Inks 18

2.6.1. Properties of the conductive inks used in printing 18

2.6.2. Rheological Properties of printing inks 20

(a) Viscosity 20

2.7. References 23

3. CHAPTER 3: EXPERIMENTAL PROCEDURE 29

3.2. Materials and Methods 30

3.2.1. Chemicals 30

3.1.2. Preparation of reagents for electrochemical analysis 30

3.1.3. Synthesis of graphene oxide, graphene oxide ink, and graphitic carbon nitride. 30

3.2. Material characterisation techniques 30

3.2.1. X-ray diffraction (XRD) 30

3.2.2. Raman Spectroscopy 30

3.2.3. Fourier transform infrared (FTIR) spectroscopy 31

3.2.4. Ultraviolet-visible spectroscopy (UV-Vis) 31

3.2.5. Scanning Electron Microscopy (SEM) 31

3.2.6. Transmission Electron Microscopy (TEM) 31

3.2.7. Rheology 31

3.2.8. Thermographic Analyser (TGA) 32

3.3. Modification of the paper SPES with g-C_3N_4 32

3.4. Electrochemical analysis with cyclic voltammetry (cv) and square wave anodic stripping (SWASV) 32

3.5. References 33

4. CHAPTER 4 : GRAPHENE OXIDE NANOPARTICLE CONDUCTIVE INKS: SYNTHESIS, CHARACTERIZATION, AND FABRICATION OF ELECTROCHEMICAL PRINTED PAPER-BASED ELECTRODES. 34

4.1. Introduction 34

4.2. Materials and method 35

4.3. Results and discussion 36

4.3.1. Structural studies on GO 36

4.3.2. Rheological studies 41
4.3.3. Thermographic analysis of the optimal ink 44
4.3.4. Polarized optical microscopy 46
4.3.5. Conductivity 48
4.4. Chapter conclusion 51
4.5. References 52
CHAPTER 5: SCREEN-PRINTED PAPER ELECTRODE WITH GRAPHENE-OXIDE NANO-INK FOR ELECTROCHEMICAL APPLICATIONS. 55
5.1. Introduction 55
5.2. Materials 56
5.2.1. Chemicals used. 56
5.2.2. Paper-based SPE fabrication process 56
5.2.3. Electrochemical measurements 57
5.2.4. Preparation of g-C_3N_4 nanomaterials 58
5.2.5. Measurement procedure - square wave anodic stripping voltammetry (SWASV) 58
5.3. Results and discussion 59
5.3.1. Morphological and topological Studies of the screen- printed paper-based electrode surface. 59
5.3.2. Cyclic Voltammetry 61
5.3.3. Effects of different scan rate. 62
5.3.4. SWASV detection of Pb (II) and Cd (II) – A comparative study between commercial SPEs and fabricated paper-based SPEs. 65
5.3.5. Simultaneous detection of Pb (II) and Cd (II) with functionalised paper based SPEs. 71
5.3.6. Detection of Cd (II) in spiked wastewater sample. 74
5.4. Chapter conclusion 76
5.5. References 77

CHAPTER 6: CONCLUSION AND RECOMMENDATIONS 79

6.1. Conclusion 79

6.2. Recommendations 80

APPENDICES 81

LIST OF TABLES

Table 2-1: Advantages and disadvantages of electrochemical sensors 4
Table 2-2: Summary of various nanomaterials modified electrochemical sensors for detection of heavy metals. 14
Table 2-3: Summary of various nanomaterials modified electrochemical sensors for detection of heavy metals. 16
Table 4-1:Composition of materials used for the preparation of graphene oxide-based..**Error! Bookmark not defined.**
Table 4-2: Comparison of the various types of graphene inks and their electrical conductivity from literature. 50
Table 5-1: Recommended values from EPA and WHO on the accepted limits of heavy metals in drinking water(Sawan *et al.,* 2020).....64
Table 5-2: Screen-printed paper electrochemical sensors various heavy metals detection ((Yáñez-Sedeño, Campuzano and Pingarrón, 2020).....71
Table 5-3: Physico-chemical Analysis of the wastewater. 74

LIST OF FIGURES

Figure 1-1: Different sensing classes and platforms.....6
Figure 1-2: Representation of various graphene-based screen-printed electrochemical sensors and (bio) sensors (Cinti and Arduini, 2017). 8
Figure 1-3: Research publications on Scopus from the year 2010 to September 2020 with "sensors and nanomaterials" as keywords. 11
Figure 4-1 Raman spectroscopy of GO 37
Figure 4-2: FTIR spectra of GO.....37
Figure 4-3 : UV-Vis spectra of GO.....38
Figure 4-4: XRD pattern of GO. 39
Figure 4-5 : (a) TEM image of GO and (b) FESEM images of GO. 40
Figure 4-6: TGA and DTA curves of GO. 41
Figure 4-7: Rheological parameters of ink 1 to ink 5, the shear viscosity of the different inks as a function of shear rate. 42
Figure 4-8 : Rheological parameters of ink 1 to ink 5 Shear viscosity of the different inks as a function of strain. 43
Figure 4-9: Rheological parameters of ink 1 to ink 5 shear stress of the different inks as a function of strain. 44
Figure 4-10: TGA and DTA curve for ink 3. 45
Figure 4-11: Polarized optical microscope of the different GO Ink: (A)Ink 1, (B) Ink 2 (C) Ink 3 (E)Ink 4 and (E)Ink 5. 47
Figure 4-12: The sheet resistances and thickness of the printed GO ink with different printing passes. 48
Figure 4-13: The conductivity of the printed GO ink with different printing passes. 49
Figure 5-1: Screen -printing process using the DEK 248 semi-automated screen-printer. 57
Figure 5-2: SPE connector to the potentiostat (A) SPE paper sensor and (B) DropSensTM C110 commercial SPE sensor.....58
Figure 5-3: FTIR spectra of g-C_3N_4 and GO and the g-C_3N_4 electrode surface. 60
Figure 5-4: SEM images of (A) g-C_3N^4 and (B) GO and g-C_3N_4 electrode surface. 60
Figure 5-5: Cyclic voltammograms of SPE on the paper substrate in 5mM K3Fe (CN)6 in 0.1 M KCl at a scan rate of 100 mV/s.....61

Figure 5-6: Cyclic voltammogram of commercial electrode sensor (CE), bare paper-based electrode sensor (BE) and functionalised electrode sensor (FE) in 5mM K3Fe (CN)6 in 0.1 M KCl at scan rates 100 mV/s.....62
Figure 5-7: Cyclic voltammograms of functionalised with g-C_3N_4 electrode sensors in 5mM K3Fe (CN)6 in 0.1 M KCl at scan rates of 100 to 500 V/s.....63
Figure 5-8: Linear relationship of the redox peak current (Ip) versus V. 63
Figure 5-9 :SWASV signals for different concentration of Cd (II) Potential vs. Ag/AgCl (0.1 mol/LKCl and pH 4,5) using the bare paper based SPEs. 66
Figure 5-10: SWASV signals for different concentration of (a) Pb (II) Potential vs. Ag/AgCl (0.1 mol/LKCl and pH 4,5) using the bare paper based SPEs).....66
Figure 5-11: SWASV signals for different concentration of Pb (II) Potential vs. Ag/AgCl (0.1 mol/LKCl and pH 4,5) using the commercial SPEs. 67
Figure 5-12: SWASV signals for different concentration of Cd (II) Potential vs. Ag/AgCl (0.1 mol/LKCl and pH 4,5) using the commercial SPEs. 68
Figure 5-13: SWASV signals for different concentration of Pb (II) Potential vs. Ag/AgCl (0.1 mol/LKCl and pH 4,5) using functionalised g-C_3N_4 paper based SPEs.....68
Figure 5-14 :: SWASV signals for different concentration of (a) Cd (II) Potential vs. Ag/AgCl (0.1 mol/LKCl and pH 4,5) using functionalised g-C_3N_4 paper based SPEs. 69
Figure 5-15: Calibration curves for Cd (II) and Pb (II) concentration range 10 to 90 mg/L..69
Figure 5-16: SWASV signals for simultaneous detection of (a) Pb (II) and (b) Cd (II) Potential vs. Ag/AgCl (0.1 mol/L KCl and pH 4,5) using the bare paper-based SPEs with 2 minutes deposition time.....72
Figure 5-17: Calibration curves for Cd (II) and Pb (II) concentration range 10 to 110 mg/L. 72
Figure 5-18: SWASV studies for various concentrations of Cd (II) wastewater. 75
Figure 5-19: Calibration curve for Cd (II) concentration range 30 to 100 mg/L.....76

ABSTRACT

Electrochemical sensors are well-established devices to detect the presence of different analytes in a wide range of fields such as environmental, healthcare diagnostics, and biological applications. Screen-printing technology has offered a low-cost, facile, and highly reproducible approach in the fabrication of disposable electrochemical sensors. The current market of disposable sensors has expensive and non-biodegradable products that are used in the fabrication process such as conductive inks and dielectric materials. Therefore, this study aims to develop a low-cost screen-printed electrochemical electrode sensor for the detection of heavy metal ions in wastewater. Modification of the working electrode with nanomaterials/nanostructures either during or post the fabrication process, has been known to promote the sensors structural and electronic properties and thus improving the electro-catalytic activity. The modified Hummer's method was used to synthesize both the graphene oxide (GO) as well as the conductive ink as it offers strong electrochemical properties and a high conductivity.

Additionally, the synthesized GO ink was used to manufacture a screen-printed electrochemical sensor to detect the traces of $Cd^{2+}$and Pb^{2+} ions in wastewater by stripping anodic square-wave voltammetry. To improve the stability and selectivity of the electrochemical sensors, g-C_3N_4 was used. By using cyclic voltammetry and square wave voltammetry Cd (II) and Pb (II) were detected at a potential close to 0.5 V observing a linear range from 10 mg/l to 110mg/l. Cyclic voltammetry (CV) presented the redox behaviour of the g-C_3N_4 nanoparticles on SPEs with sodium acetate buffer solution as a supporting electrolyte with a pH of 4,5. As the scan rate increases, a shift and an increase in the oxidation and reduction peaks potential were observed.

In conclusion, the GO ink with 30 wt% of the CMC binder exhibited good stability and screen-printing properties. The paper-based screen-printed electrode modified with g-C_3N_4 showed good selectivity in the detection of $Cd^{2+}$and Pb^{2+}ions over a linear range of 10 to 110 mg/l with LOD=0,16 mg/l, and Cd^{2+} ions over a linear range between 10 to 110 mg/l with LOD=0,79 mg/l, for Pb^{2+} ions.

LIST OF ABBREVIATIONS AND SYMBOLS

μPADs Microfluidic Paper-Based Analytical Devices

τij Shear stress (N/m2)

τ Shear stress(N/m)

$\dot{\gamma}$ Shear rate(sec-1)

μ Viscosity (poise

Ag/AgCl Silver/Silver Chloride

Cd (II) Cadmium

CE Counter Electrode

CV Cyclic Voltammetry

FT-IR Fourier-Transform Infrared

GO Graphene Oxide

LOD Limit of Detection

MWCNT Multi-walled carbon nanotubes

Pb (II) Lead

POC point-of-care

RE Reference Electrode

SEM Scanning Electron Microscopy

SPE Screen-Printed Electrode

SWASV Square-Wave Anodic Stripping Voltammetry

Temperature (^{0} C)

Time (s)

TEM Transmission Electron Microscopy

TGA Thermogravimetric analysis

UV UV-Vis absorption spectroscopy

WE Working Electrode

XRD X-ray Diffraction

STRUCTURE OF THE DISSERTATION

Chapter 1 includes a high-level introduction to the dissertation, the motivation, and research questions.

In chapter 2, the background theories and literature reviews on recent developments of screen-printed electrodes and their applications, which demonstrates the merits of using nanomaterial to enhance electrode functions, printed electrode sensors, and the importance of exploring graphene oxide as a material of choice. It also includes electrochemical concepts, designs, and measurements used in this work.

Chapter 3 outlines the methodology section with an overview of the experimental designs, material synthesis, and characterization.

Chapter 4 details the synthesis of the GO nanosheets via the modified Hummers method, ink synthesis, and characterization of the formulated screen-printing ink.

Chapter 5 analyses printed graphene oxide SPEs on a photo paper substrate and characterization of screen-printed graphene oxide. Electrochemical detection of heavy metals in drinking water using commercial SPEs, bare screen-printed SPEs, and functionalized SPEs with graphitic carbon nitride (g-C_3N_4) nanomaterials.

Chapter 6 summarizes the study in this dissertation and recommendations for future studies.

CHAPTER 1: INTRODUCTION

This chapter outlines the background, problem statement, justification, and hypothesis. The research aims and objectives, the overall thesis outline are also included in this chapter.

1.1. Backgroun

Sensors are devices or subsystems, which are made of active sensing material with a signal transducer (Zhang 2010).Their main function is to transmit signals from specific compounds when they detect a change in reaction or events without interference. The sensor devices can produce different types of signals (as shown in Figure 1-1) depending on their application, ranging from electrical, optical, or thermal output signals which can give digital signals output. They are classified on the type of signals that they give out, i.e. Chemical sensors and biosensors (Wang, Wolfbeis 2019). Numerous analytical studies have been done on paper-based microfluidic sensors (μPads) since the successful demonstration with electrochemistry by (Dungchai et al., 2009) on various analytes such as glucose ions, proteins, DNA, or heavy metals. There are various methods for preparing electrodes, but there is no recommended approach because the procedures have drawbacks that affect their electrochemical efficiency. To overcome the shortcomings of bare carbon electrodes for metal detection and maximize the sensitivity of the electrodes, Wang's group used an environmentally friendly metal alteration (Wang, Lu et al. 2001) .

Diagnostic devices made on paper have gained popularity in recent years as a compatible material for the manufacture of wearable devices and sensors as it offers flexibility, high abundance, and low cost to be used in the study of analytical and clinical chemistry. In 1956, the first paper-based device for semi-quantitative glucose detection in urine was introduced; this invention led to the development of immune chromatographic test strips, with the most well-known use being the pregnancy test kit (Comer 1956). Following the advent of engineering microfluidic channels on paper for complex detection analytes, the research emphasis has changed in recent years. This platform offers an opportunity not only for calorimetric techniques to be performed but affords complicated laboratory tests such as electrochemical, chemiluminescence, electrochemiluminescence and electrical techniques to be done on PADs devices.

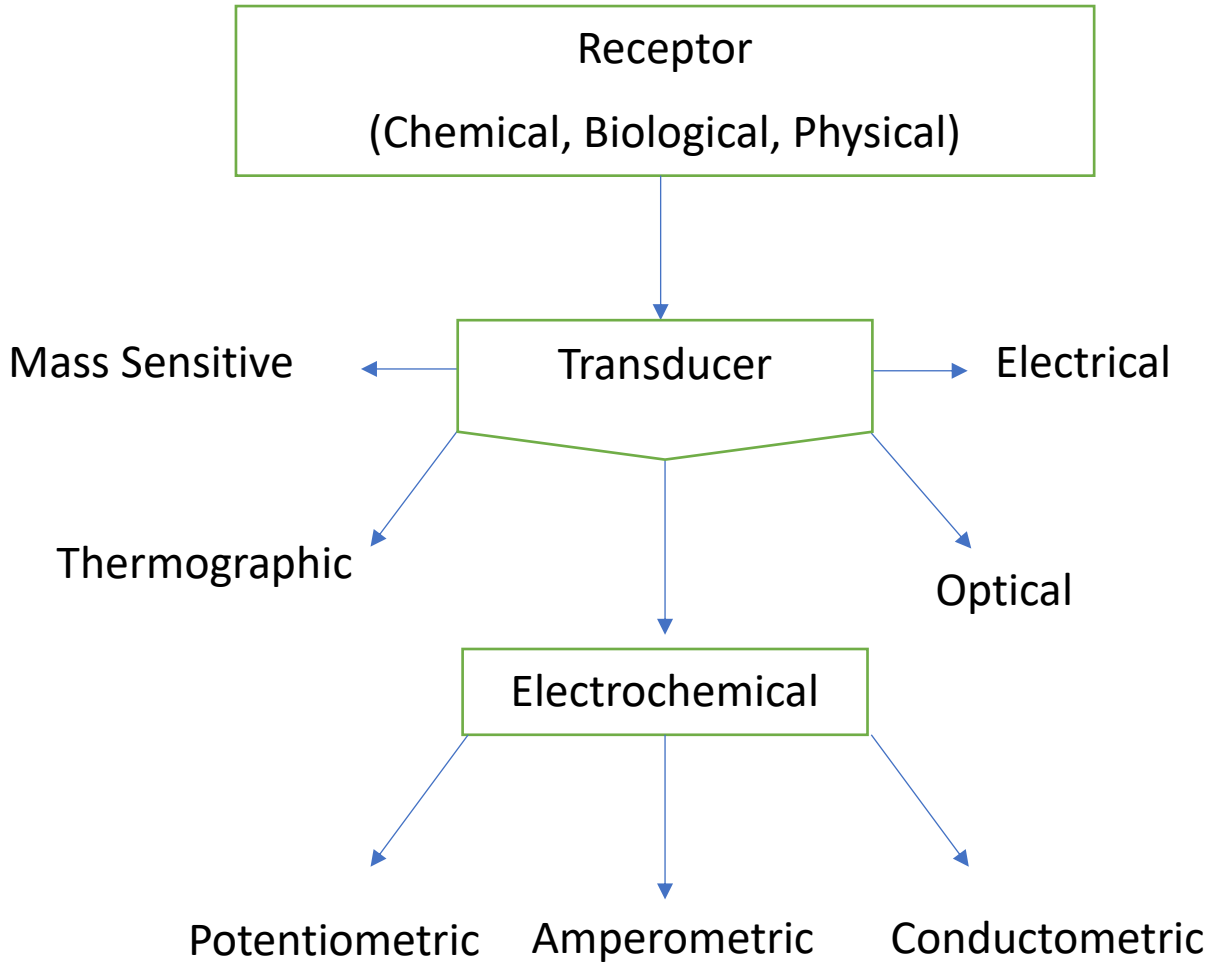


Figure 1-1: Different sensing classes and platforms

Because of the instrument's versatility, low cost, and ease of transport, the electrochemical stripping analysis anodic stripping voltammetry (ASV) technique has long been a preferred tool for heavy metal detention. The replacement of the surface with mercury, gold, silver, bismuth or other materials has been studied to increase the selectivity and sensitivity of the PADs (Li, Li et al. 2012)

Inks containing a conductive factor have become increasingly popular in the printing industry, especially in processes like screen printing and inkjet printing. Reasonable printability, low viscosity, good adhesion to the substrate, pre-and post-printing handling, high electrical ng conductivity, and the ability to densify correctly on the substrate without a "coffee ring effect" are all characteristics of an ideal ink (Tran, Dutta et al. 2018).

Printed electronics devices have been studied using conductive ink formulations made from nanomaterials and polymers over the past ten years. The method of printing to be used for inkjet printing the ink has a big impact on the ink preparation. It must be appropriate for the

substrate being used. Despite these advancements, maintaining the fluidic properties of the ink that meet the parameter specifications, primarily surface tension and viscosity, remains a challenge (Tran, Dutta et al. 2018a)As seen in Figure 1-2, incorporating additive manufacturing processes using inks and pastes that contain a conductive material such as carbon nanotubes, metal nanoparticles, dissolved or scattered conductive polymers, nanowires, graphene sheets, and organometallic compounds and complexes as metal precursors is a favoured option to improve the development of electronic devices. Nanomaterials have arisen as a possible electrode modification because nanoscale materials have a wide surface area, increased conductivity, and quick electrode kinetics. Various nanomaterials, such as metallic nanoparticles, silicon-based materials, and carbon-based materials, as well as graphene oxide materials, have been used (Cinti, Arduini 2017). Thermal resilience, conductivity, durability, foldability, optical clarity, and tolerance to various bending abilities, as well as perfect printing efficiency and electronic device fabrication, necessitate the careful selection of printing process, substrate, ink composition, and conductive materials (Kamyshny, Magdassi 2019).

Environmentally safe, low-cost, and stable conductive materials must be used. Because of its outstanding electrical, mechanical, and thermal properties as a chosen conductive substance, graphene, a two-dimensional carbon lattice, has received high level of recognition (Kamyshny, Magdassi 2019).

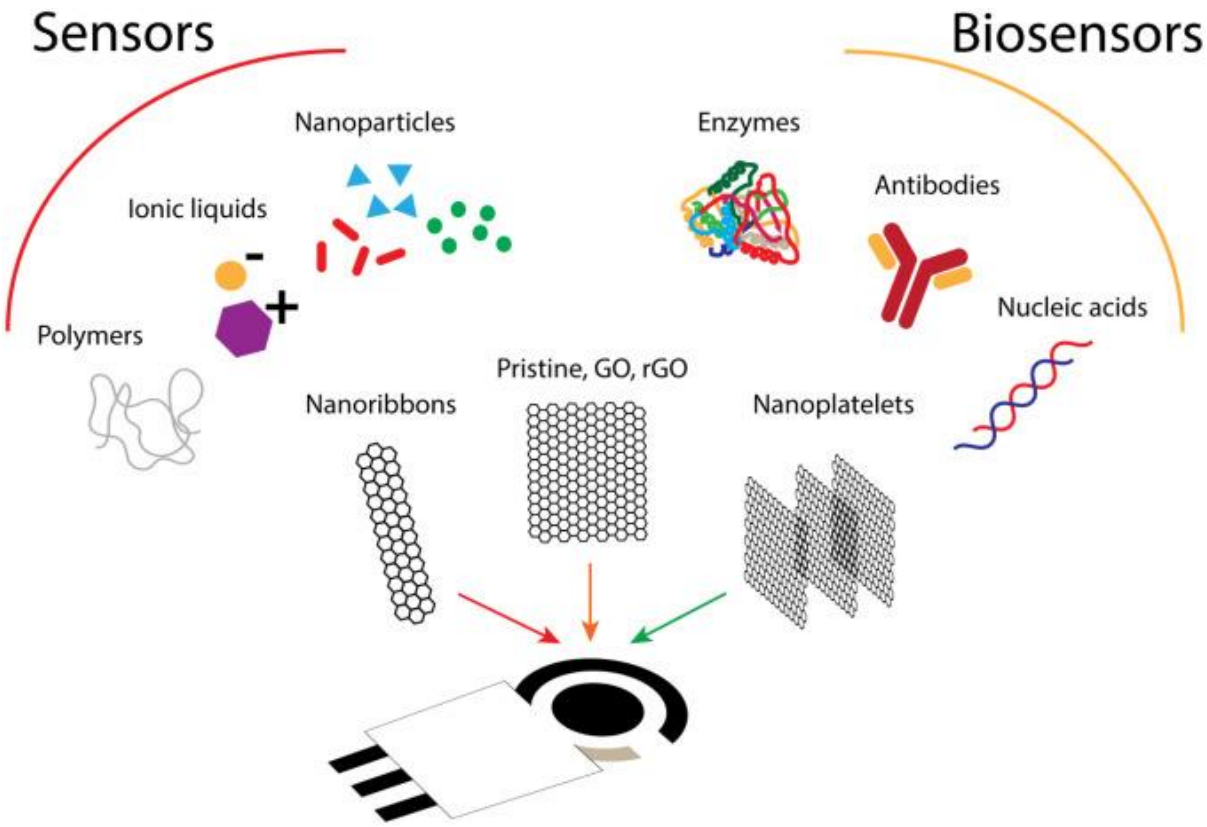


Figure 1-2: Representation of various graphene-based screen-printed electrochemical sensors and (bio) sensors (Cinti and Arduini, 2017).

To date, several methods to produce graphene-based inks have been explored to revolutionise printed electronics by replacing metallic inks and carbon material inks while simultaneously reducing biological hazard and production costs. According to most literature sources, graphene nanoparticles, graphene oxide (GO), and reduced graphene oxide (rGO) are used as fillers in most graphene inks (Tran, Dutta et al. 2018) .Graphene, on the other hand, is hydrophobic and has low solubility in a variety of different solvents. As a result, stabilizers or surfactants must be used to increase the conductive ink's dispersion. The molecular association between surfactants and graphene, which influences the stabilization process of graphene dispersions and surfactant, has not been thoroughly studied (Cinti, Arduini ,2017).

1.1.1. Evolution of paper-based diagnostic devices

The first successful application of litmus paper occurred in the 1700s using woven fibre networks made from cellulose to perform chemical measurements (Carrell, Kava et al. 2019)

This simple litmus paper, made of cellulose paper embossed with pH-sensitive chromophores, allowed pH measurements to be taken in a variety of samples where they had previously been impossible. Maumené developed the first urine analytical instrument in 1850, which looked at the generation of brown-black colour to detect sugars in urine (Credou, Berthelot 2014)Martin and Synge patented paper chromatography a century later, in 1943, to analyse the amino-acid content of proteins. When Müller and Clegg developed a restricted flow channel on paper to produce a preferential elution of a mix of pigments in 1949, they coined the term "paper-based microfluidics" (Credou, Berthelot 2014). In 1956, Kohn developed the first urinary test strips that could be used to measure glucose levels using blood samples. These upgraded strips were a step forward in the advancement of analytical rapid tests that could be used in the field, despite their lack of sensitivity and selectivity. These breakthroughs paved the way for several paper-based device applications, including the lateral flow assay (LFA), a modern medicine hallmark that makes detecting biomarkers and pathogens easier. Law enforcement and environmental monitoring departments began using fluorescent or colorimetric readouts to catch and detect labelled antibodies. One of the most common point-of-care medical diagnostics, blood glucose monitors for diabetes, is launched to the market.

These devices use glucose oxidase, immobilized enzyme, or dehydrogenase on a disposable paper strip with electrodes. The meter connected to the electrode measures current directly or by a redox mediator made while the enzyme catalyses the oxidation of glucose from a drop of blood. Regular blood glucose monitoring across the clinical spectrum is possible due to the enzymes' responsiveness and selectivity. The strips have the advantage of being low-cost reagents that can be packed and kept stable for over a year at temperatures up to 45 degrees Celsius (Akceoglu, Saylan et al. 2021). While modern glucose meters have drastically decreased the number of blood samples used to a few microliters, which is the equivalent of a tiny pinprick on the patient's finger, the major disadvantage of glucose testing with blood is that it requires a blood sample. The interest in the commercialization of non-invasive, non-blood sampling devices has exploded.

The blood glucose sensor is considered the "gold standard" of point-of-care diagnostic medical devices and it is used daily by millions of patients all over the world. Following this advance,

the Whitefield laboratory developed the first µPAD in 2007, which used patterned paper to create multiplexed flow channels rather than spot experiments (Martinez, Phillips et al. 2007). Following this advance, the Whitefield laboratory developed the first µPAD in 2007, which used patterned paper to construct multiplexed flow channels rather than spot experiments (Martinez, Phillips et al. 2007).

The wetting of the cellulose fibres, which is caused by the material's capillary pressure, creates the flow channels on paper. In microfluidics and PADs, the ability to implement multiplexed detection on instruments, as well as the ability to conduct lengthy and complex experimental preparation outside of the laboratory, has opened new possibilities. The field has expanded rapidly since the first research in 2007, with novel techniques for fabricating devices appearing first. Since then, the discipline has expanded and modern methods have emerged, transitioning from a sophisticated and expensive approach including photolithography to screen printing, wax printing, and inkjet printing, and increasing the field's accessibility (Carrell, Kava et al. 2019b)This is combined with new detection methods, with the Henry group being the first to demonstrate the fundamentals of their system's electrochemistry using cyclic voltammetry (Dungchai, Chailapakul et al. 2009) . (Yu, Ge et al. 2011)investigated using chemiminisce to detect uric acid and glucose in artificial urine, and Whiteside et al. (2011) investigated fluorescence. The application has since been expanded to cover initiatives in good and environmental research, in addition to point-of-care diagnostics.

Despite the substantial progress, commercialization of the solutions remains low when compared to µPADs generated by academic research, as seen in Figure 1-1.

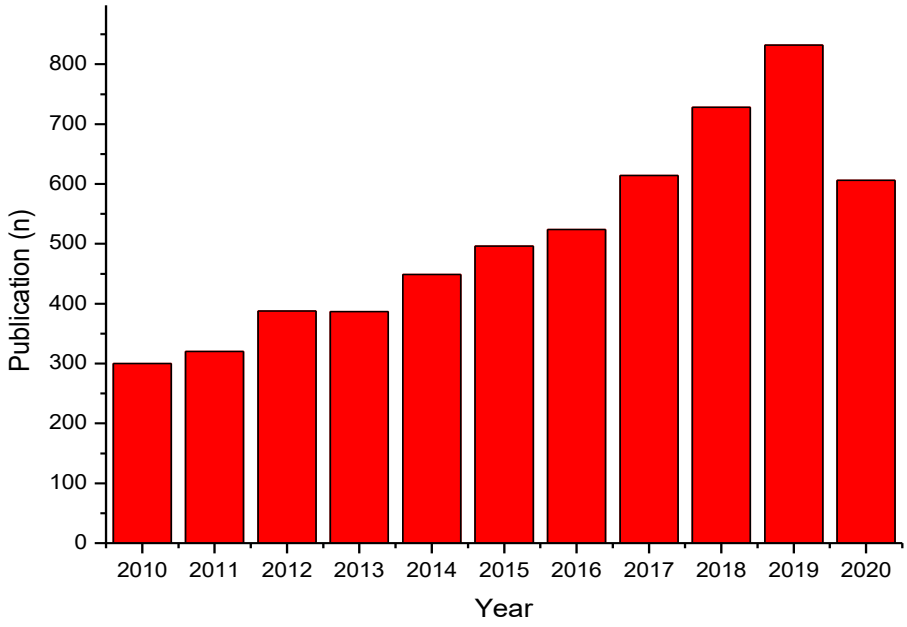


Figure 1-3: Research publications on Scopus from the year 2010 to September 2020 with "sensors and nanomaterials" as keywords.

In 2007, the Whitesides (Martinez, Phillips et al. 2010) introduced a microfluidic pattern on a paper material that controls the fluid flow with photoresist. At this time, microfluidic paper-based analytical instruments, or mPADs, were developed. Two years later, the same group used wax printing technology to create microfluidic patterns on a paper substrate, a simplified and commercially available method (Martinez, Phillips et al. 2007). Since then, there has been an increase in the study and publication of work done on a variety of mPADs using colorimetric detection.

1.2. Problem Statement

Current electrode detection techniques provide a capable platform for lab-on-chip devices, but their sensitivity and selectivity are unreliable. Modification of the surface with mercury, copper, silver, bismuth or other materials is being investigated to increase the SPE's selectivity and sensitivity. Alternative manufacturing processes using inks and pastes containing conductive material such as metal nanoparticles (NPs) and nanowires (NWs), graphene sheets, carbon nanotubes (CNTs), conductive polymers (dissolved or dispersed), and organometallic

compounds and complexes as metal precursors are a favored option to improve the fabrication of electronic products.

1.3. Study Objectives

The main objective of this study is to develop a rapid detecting, sensitive, and selective electrochemical graphene oxide-based electrode sensor for the detection of heavy metal ions in wastewater. The specific objectives of this study are described as follows:

a) The synthesis and characterization of nanomaterials (graphene oxide and graphitic carbon nitride nanoparticles).

b) The formulation and characterization of conductive screen-printing inks for the detection of heavy metal ions in wastewater.

c) To improve electrochemical sensing of heavy metal ions in wastewater for electrodes synthesized by functionalising with graphitic carbon nitride nanoparticles (g-C_3N_4).

1.4. References

1. Akceoglu, G.A., Saylan, Y. and Inci, F., 2021. A Snapshot of Microfluidics in Point-of-Care Diagnostics: Multifaceted Integrity with Materials and Sensors. *Advanced Materials Technologies*, pp. 2100049.
2. Carrell, C., Kava, A., Nguyen, M., Menger, R., Munshi, Z., Call, Z., Nussbaum, M. and HENRY, C., 2019. Beyond the lateral flow assay: A review of paper-based microfluidics. *Microelectronic Engineering*, **206**, pp. 45-54.
3. Cinti, S. and Arduini, F., 2017. Graphene-based screen-printed electrochemical (bio)sensors and their applications: Efforts and criticisms. *Biosensors and Bioelectronics*, **89**(Pt 1), pp. 107-122.
4. Comer, J.P., 1956. Semiquantitative Specific Test Paper for Glucose in Urine. *Analytical Chemistry*, **28**(11), pp. 1748-1750.
5. Credou, J. and Berthelot, T., 2014. Cellulose: from biocompatible to bioactive material. *J. Mater. Chem. B*, **2**(30), pp. 4767-4788.
6. Dungchai, W., Chailapakul, O. and Henry, C.S., 2009. Electrochemical detection for paper-based microfluidics. *Analytical chemistry*, **81**(14), pp. 5821-5826.
7. Kamyshny, A. and MagdassI, S., 2019. Conductive nanomaterials for 2D and 3D printed flexible electronics. *Chemical Society reviews*, **48**(6), pp. 1712-174.
8. Li, Y., Li, M., Li, D. and Long, Y., 2012. Recent developments and applications of screen-printed electrodes in environmental assays—A review. *Analytica Chimica Acta*, **734**, pp. 31-44.
9. Martinez, A.W., Phillips, S.T., Butte, M.J. and Whitesides, G.M., 2007. Patterned paper as a platform for inexpensive, low-volume, portable bioassays. *Angewandte Chemie*, **119**(8), pp. 1340-1342.
10. Martinez, A.W., Phillips, S.T., Whitesides, G.M. and Carrilho, E., 2010. Diagnostics for the Developing World: Microfluidic Paper-Based Analytical Devices. *Analytical chemistry*, **82**(1), pp. 3-10.
11. Tran, T.S., Dutta, N.K. and Choudhury, N.R., 2018. Graphene inks for printed flexible electronics: Graphene dispersions, ink formulations, printing techniques and applications. *Advances in Colloid and Interface Science*, **261**, pp. 41-61.

12. Wang, J., Lu, J., Hocevar, S.B. and Ogorevc, B., 2001. Bismuth-Coated Screen-Printed Electrodes for Stripping Voltammetric Measurements of Trace Lead. *Electroanalysis*, **13**(1), pp. 13-16.
13. Wang, X. and Wolfbeis, O.S., 2019. Fiber-optic chemical sensors and biosensors (2015–2019). *Analytical chemistry*, **92**(1), pp. 397-430.
14. Yu, J., Ge, L., Huang, J., Wang, S. and Ge, S., 2011. Microfluidic paper-based chemiluminescence biosensor for simultaneous determination of glucose and uric acid. *Lab on a Chip*, **11**(7), pp. 1286-1291.
15. Zhang, P., 2010. Chapter 3 - Sensors and actuators. In: P. ZHANG, ed, *Advanced Industrial Control Technology*. Oxford: William Andrew Publishing, pp. 73-116.

CHAPTER 2: LITERATURE REVIEW

This chapter provides a review of the literature on electrochemistry, electrochemical sensors, and the fabrication process for the electrochemical sensors used in the research. The materials used to produce working electrodes, as well as existing field trends. It also looks at several recent studies to help put things in perspective.

2.1. Introduction to electrochemistry

Electrochemistry is the study of interrelations between chemical and electrical effects in the chemistry field (Kaifer, Gómez-Kaifer 2008).Electrochemical sensors consist of chemical and biological elements and electrochemical transduction units, which are applied widely in biological, chemistry, environmental, and medicinal sensing (Banica 2012). The application of the field of electrochemistry is seen in development such as batteries, electroanalytical sensors, fuel cells, large-scale metallic plating, and solar power (Walsh 2001). Therefore, the study of electrochemistry is important to help drive future innovations and discoveries. The main focal point in electrochemistry which differentiates it from other branches of chemistry is that it focuses on the electrochemical interactions of the analyte and the surface of the electrode, as illustrated in Figure 2-1.

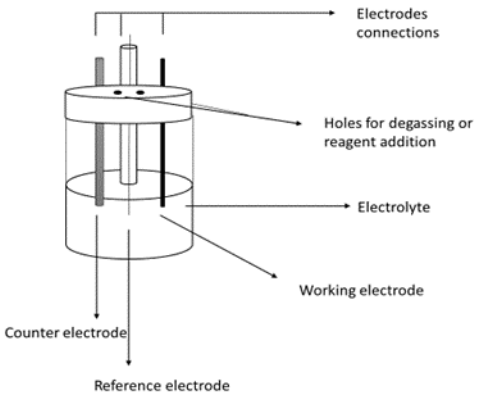


Figure 2-1: Graphic representation of an electrochemical cell.

The study will focus on potentiometry, which uses a static interfacial method to calculate the difference in potential between a working electrode and a reference electrode connected to a voltmeter and submerged in a liquid medium (Barcelo, Petrovic 2007). The counter electrode is used to allow a current to pass through the electrolytic solution while bypassing the reference electrodes (Gianchandani, Tabata et al. 2008).Since the current no longer passes through the electrode, the device becomes stable (Hibbert 1993) (Kaifer, Gómez-Kaifer 2008). Conducting electrodes are submerged in an electrolytic solution, often known as an electrolyte, to use a potentiometric method in an electrochemical cell. These electrodes are referred to as the reference and working electrodes (Reedijk 2014). As presented in Figure 2-1, the reaction takes place on the working electrode inside the electrochemical cell, while the reference electrode retains a static potential that is unaffected by the reaction.

2.2. Types of electrochemical signals

The fundamental of electrochemical reactions are based on the electrode-electrolyte interface, charge separation and mass in Figure 2-1. The process takes places when charges move from the electrode surface and the liquid media (Biesheuvel, Fu et al. 2011). This causes the electrode-electrolyte charge phenomenon which happens when reactions take place in the interfacial electrode surface and the electrolyte solution (Brett, Oliveira Brett 1993).

2.2.1. Cyclic Voltammetry

Cyclic voltammetry (CV) is the most preferred electroanalytical technique, that is used to measure the kinetics of electron transfer and adsorption processes owing to its versatility. The initial step in an electrochemical study of an electrode surface, biological sample, or a compound often begins with cyclic voltammetry (Armstrong, Wilson 2000).The results help rapidly observe redox behaviour over a wide potential range. The results are obtained by measuring the current flowing at the working electrode (WE) during a potential scan. In a single or multiple resulting voltammogram, the direction of the voltage is reversed between two limits, while the potential applied at the WE in both the forward and reverse direction and the resulting current is logged at the same scan rate in the forward and reverse direction (Brett, Oliveira Brett 1993). During a CV experiment, as the potential is scanned negatively the electrode are steadily depleted close to the surface as it is reduced. This suggests that the current increases and later decreases when all the reactant is finished. The concentration of the analyte, the electrode surface, the diffusion coefficient, and the potential sweep rate are factors that determine the current measured during the reaction (Holze 2009). The Nernst equation

(Feiner, McEvoy 1994)shows the relationship between the potential of an electrochemical cell (E) E0′ [V] is the formal potential, E0 [V] is the standard potential, C* [mol. L^{-1}] is the bulk concentration of the studied analyte, and a [mol. L^{-1}] is the activity. A common assumption is to ignore the activity coefficients resulting in E0 =E0'

$$\mathbf{E = E^{0\prime} + \frac{RT}{nF}\ in\ \frac{C_0^*}{C_R^*}} \qquad \text{Equation 1}$$

Peak-to-peak separation refers to the difference between anodic and cathodic peak potentials when the reduction process is chemically and electrochemically reversible. Chemical reversibility shows whether the analyte has reached stability during reduction and can then be re-oxidized. The electron transfers between the electrode and the analyte show electrochemical reversibility (Archer 1989). A change in applied potential causes the Nernstian to reach equilibrium immediately and that results in a low barrier to electron transfer (electrochemical reversibility) and electrochemical reversibility happens when there is a higher barrier to electron transfer. The reactions are more negative and slower potential is needed for reduction reaction or a positive and faster potential for an oxidation reaction (Holze 2009)

2.2.2. Square-Wave Voltammetry

Square-wave voltammetry is the most used tool for electroanalytical analysis to detect analytes especially at extremely low limits of detection to about 1 x 10-8 mol L^{-1}. A square wave plot is generated when the current is sampled over forward and reverses pulses, the response is plotted over a base staircase potential as a non-sinusoidal and with a resultant symmetrical voltammogram (Ramaley, Krause 1969) .When the net current of the forward and reverse current being measured, rather than the single current value, this creates a low limit of detection unlike in cyclic voltammetry (Lovrić 2010).The charging background current can be reduced by this methodological approach. In contrast to other voltammetry techniques, the use of an amplitude decreases the general scan time to seconds besides the advantage of a lower detection limit (Bard, Rubenstein 1996).

Table 1-1: Advantages and disadvantages of electrochemical sensors

Electrochemical sensors	Advantages	Disadvantages
	• Sensitive	• pH dependence and need of supporting electrolyte

Amperometric sensors (screen printed and inkjet-printed sensors, Glucose sensors, modified and unmodified electrodes for sensing in the environment, health, and industry	• Ease of modification for targeted analysis • Real-time and on-site analysis • Redox-active analytes can be detected • Simple Real-time and on-site analysis	• Working electrode surface fouling • Surface modifications are required to achieve higher selectivity • Electro-active species which are not a target cause interference • Low sensitivity
Potentiometric or ion-selective sensors (pH sensors, electrolyte and ion sensors, drug sensors)	• No counter electrode required • Reference electrode stability	• Frequent calibration is required • Fouling on the working electrode surface • Primarily used for ions detection • Non-target ion interferes
Conductometric sensors (Humidity sensors, conductivity meters, gas sensors)	• No reference electrode required • Easy to use	• Low selectivity and sensitivity • Restricted applications • Short shelf life

2.3. Working Electrode carbon material

2.3.1. Graphene

Graphene is a 2D single sheet of carbon atoms organized in a hexagonal network and one of the sought-after carbon nanomaterials since its discovery in 2004. It is the main constituent of all the dimensional graphitic materials which can be wrapped in different forms such as 0D fullerenes,1D nanotubes, and 3D nanotubes or graphite (Zhang, Ren et al. 2011). Since its discovery, there has been a growing interest in scientific and technological research for different applications such as bioscience/biotechnologies, batteries, electronics, energy storage and conversion, supercapacitors, fuel cells, and solar cells (Zhang, Hou et al. 2017) .This is due to its excellent physico-chemical properties such as good thermal conductivity, electric conductivity, the theoretical value of the surface area which records 2630 m^2/g for single-layer graphene which is considered high, and its strong mechanical strength. The first method to obtain pristine structured graphene layers was first reported in 2004 by Geim and his group using the scotch tape method. It uses mechanical exfoliation to produce highly oriented pyrolytic graphite (Novoselov, Geim et al. 2004).Unfortunately, the yield from the method is exceptionally low.

2.3.2. Graphene oxide

Graphene oxide (GO) is obtained from the oxidation of graphene via oxidation, followed by exfoliation in various solvents and dispersion in water. It has excellent dispersibility in various solvents and this is due to the polar oxygen functional group present that gives GO its hydrophilic properties. For this reason, GO makes a good electrode material, it can be deposited on different subtracted in various form to produce conductive films (Chen, Feng et al. 2012)

Silva and Cesarino, (2020) leveraged the synergetic properties of antimony and electronic properties of reduced graphene to formulate a nanocomposite for simultaneous analysis of multiple heavy metals ions in natural freshwater. The group used square-wave anodic-stripping voltammetry (SWASV) to simultaneously detect Cd^{2+}, Hg^{2+}, Pb^{2+} and Cu^{2+}, with a linear range of 0.1 TO 4.5 µmol L^{-1} and the LODs obtained for the metal ions were found to be 45.3, 16.5, 34.1 and 4.8 nmol L^{-1}, respectively.

Baghayeri *et al.*, (2019) synthesised a dendrimer composite with a magnetic graphene oxide nanosheets/poly(amidoamine) and modified a glassy carbon electrode to detect both Cd (II) and Pb (II). They coupled the high adsorption abilities of Fe_3O_4 nanoparticles, together with NH_2 enriched with PAMAM dendrimer to achieve good selectivity and the GO nanosheets'

electronic capabilities, to design the novel sensor that has a low limit of detection (LOD) of 70 ng/l for Cd (II) and 130 ng/l for Pb (II).

Hanif *et al.*, (2019) synthesised a glycine nanocomposite with reduced graphene and polyaniline to modify and improve electrochemical selectivity and sensitivity of glassy carbon electrode. The functionalised electrode exhibited excellent electroanalytical properties with enhanced sensitivity and reproducibility.

Ibáñez-Redín *et al.*, (2018) presented a low-cost functionalised screen-printed carbon electrode on a poly (ethylene terephthalate) (PET) substrate modified with carbon black and reduced graphene oxide nanocomposite This electrochemical sensor was used to detect dopamine, paracetamol, and epinephrine simultaneously which showed remarkable electroanalytical improvements due to the modification.

Akkarachanchainon et al., (2017) compared unmodified electrodes with electrodes modified with hydrophilic graphene oxide to simultaneously detect toxic pesticides carbofuran and carbendazim in agricultural products. The modified electrodes reported having low detection limits of $10\mu g/L^{-1}$ for carbofuran and $5\mu g/L^{-1}$ for carbendazim which are 4 times and 12 times higher compared to the unmodified electrode, respectively.

2.4. Screen-printing

Screen printing has allowed electrochemical experiments to be conducted on a small-scale platform, which is not expensive and can be performed by inexperienced personnel. Despite this, laboratory electrochemical methods need highly technical electrode preparations to build a near-perfect electrode surface free of adsorbents, reactive sites, and grain boundaries. Expensive materials such as gold, platinum, copper, graphite, titanium, and silver are used to make the electrode material (Stetter, Penrose et al. 2003) .As a result, electrochemistry experiments were restricted to the laboratory and could not be used in the field, where disposable platforms are needed. This necessitated the creation of a forum for the development of disposable, mass-production electrodes that do not require pre-treatment, and the use of traditional electrode systems has been steadily phased out after the advent of screen-printed electrodes, which operate in the same way and do not require any pre-treatment or recourse. They are mass-producible and low-cost, making them an excellent solution (Mettakoonpitak, Boehle et al. 2016)

These are the key steps in the screen-printing process, selecting the mesh and designing the panel prototype with the shape and size of the electrodes, (ii) selecting and preparing the conductive inks, as shown in Figure 2-3. (iii)Suitable substrate, (iv) stencil formation, (v) printing of the layer, and (vi) drying through thermal treatment (Couto, Lima and Quinaz, 2015). A thixotropic material such a carbon ink is used in the fabrication of electrodes in screen printing. The carbon ink material is selected according to the application which can be a mixture of carbon black, nanomaterials, graphite, polymeric binders, and solvents. A base substrate is chosen which can make from a thin flexible such as polyester, ceramic, or paper and its properties are carefully considered such as flexibility; longevity; hydrophobicity; and durability (Stradiotto, Yamanaka et al. 2003).The viscosity of the carbon ink plays a major role in the printing process which turns to make the process a difficult one (Hancock, Lin 2004).

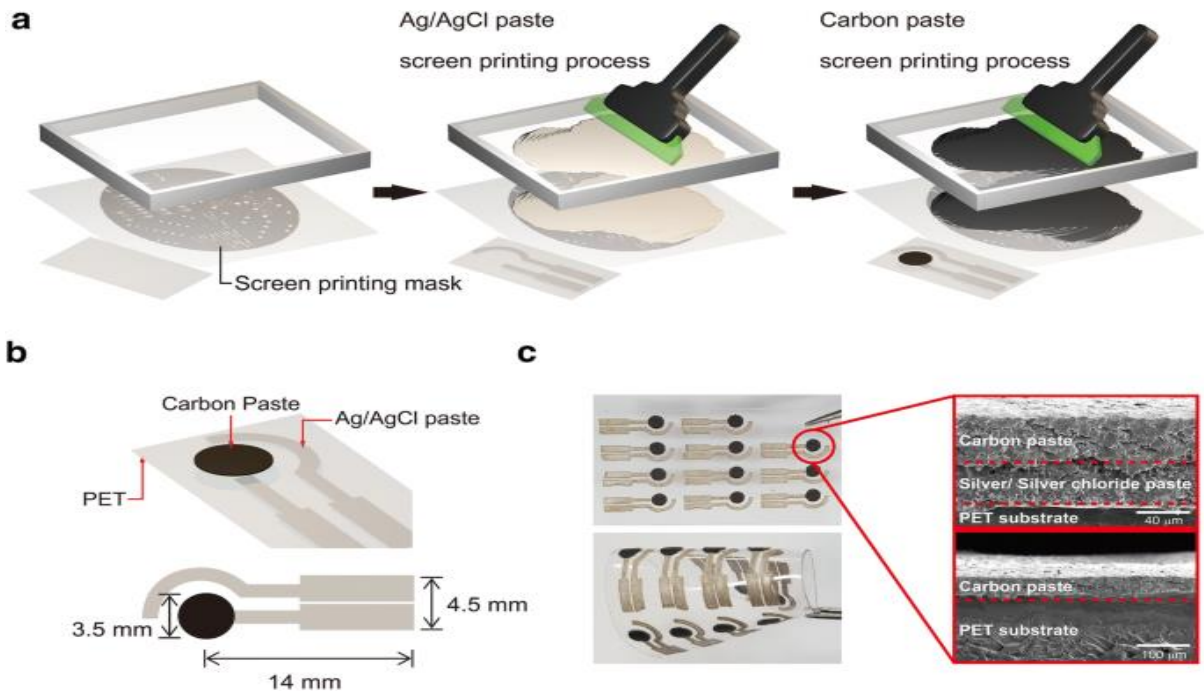


Figure 2-2: Screen-printing process (Park et al., 2019).

A predesigned template has a working, counter, and reference electrodes on a screen mesh which could be on the same or different ink depending on the types of inks to be printed. screen mesh where the ink is pressed using a squeegee blade. The inks are pressed through a screen mesh the counter and working electrodes are mostly printed with the same screen design

template using carbon ink (Park, Yoon et al. 2019). After printing the electrodes are out in the oven to dry and the last reference is printed using a different design template and Ag/AgCl paste is used as common reference material. The reference electrode should have a known potential which is commonly an Ag/AgCl paste, for it to be a redox system. Lastly, to define the microfluidic channels and to restrict flow movement to the working electrode and protect the connections a top layer is printed using a dielectric paste (de Oliveira, Fonseca et al. 2019). The advantages of screen printing include:

- The normal thickness of a screen-printed pattern ranges from tens of micron with one pass of printing, which cannot be achieved by other printing procedures.
- This method allows for various substrates such as paper **(**Figure 2-4), textiles, glass, ceramics, and metal as the ink adheres to various materials.
- A wide range of ink materials is compatible with screen printing as compared to inject printing.
- It is a cheap method, and the cost of printing is masked by the high throughput of the method.

The major disadvantages of screen printing entail the need for mask-the-screen, waste of ink material, and possible contamination of the substrate due to inevitable physical contact between the mask and the substrate. Screen-printed electrodes have had a varied application especially in health diagnostics, the point-of-care glucose monitor is used in hospitals that utilises a screen-printing technology that processes a small sample of blood for blood glucose analysis. This application has seen a sharp rise in the market which is estimated to be 21.5 billion USD by the year 2024 (Maniya, Srivastava 2020)It has resulted in many research projects to find a new direction that investigates different electrochemical techniques, chemical systems, and new application fields such as forensic, environment to use these SPE's.

The application of screen-printed electrodes (SPE) as transducers or electrochemical sensors in various fields has halted the manufacturing of traditional electrochemical sensors because of their advantages and characteristics as compared to other analytical tools. For this reason, carbon ink that is employed in the production of the SPEs is regarded as a good alternative to glassy carbon electrodes and carbon paste electrodes (Kalcher, Svancara et al. 2009) .The properties exhibited by electrochemical sensors such as chemical inertia, low background current (Bolotsky, Butler et al. 2019)due to the crystalline structure of the material, high

signal/noise ratio, and use within a wide potential range has made SPEs extremely attractive as both as electrochemical and transducers detectors. The size of the SPEs is also an added advantage as it makes them portable, allows in situ tests, inline, can be handled and transported with ease, or real-time, without the need for the samples to be transported to the lab (Wang 2002)The ability of the screen-printed electrode to be customised with different electrode material on the same electrochemical device and indirectly increasing the manufacturing of carbon, silver/silver chloride, silver, gold, or platinum on the same support (Jothimuthu, Wilson et al. 2011)

The ability to improve the properties of the electrode through different modification opens them to numerous applications in various industries such as environmental monitoring of wastewater and potable water, forensic sciences in the detection of toxic and antibiotic resistant substances, the management of pesticides/ herbicide in the agricultural sector as well as in the pharmaceutical applications such as glucose, celiac disease or cancer biomarkers (Tothill 2001). Different nanomaterials like carbon-based nanomaterials, silicon, metal, and metal oxide nanoparticles, and polymeric nanomaterials are specially designed to manufacture sensors for the detection of heavy metal ions (Tuantranont 2013) .Surface modification in the development of biosensors using metal oxides and nanostructured metals is still challenging. The modification increases these properties: sensitivity and selectivity due to their large surface-to-volume ratio, a high degree of functionalization, size-dependent properties, and high reactivity (Buledi, Amin et al. 2020). The functionalisation of the nanomaterials is done by different methods namely covalent and non-covalent interactions. In biosensor application, the functionalising of the SPEs introduces different functional groups, and it helps improves the attachment of biomolecules over electrostatic interactions or specific bonds. It also reduces and stabilises the agglomeration of metal and metal oxide nanoparticles. In the environmental application for the detection of heavy metal ions, the numerous ways of functionalisation such as covalent functionalisation, nanocomposite formation, and organic ligand anchoring improve the response sensitivity and selectivity (Buledi, Amin et al. 2020).

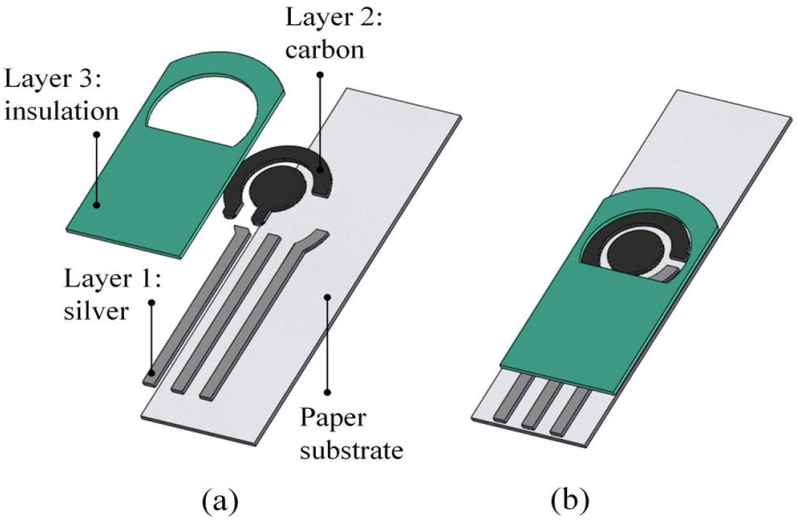


Figure 2-3: Screen-printed electrodes (Smith et al., 2019).

2.5. Heavy metals detection by nanomaterials application

In a study by Ndlovu *et al.*, (2014) an exfoliated graphite electrode that was modified with bismuth (EG-Bi) was used to detect arsenic in water. The EG-Bi modified electrode showed positive implications on sensitivity using SWASV with a detection limit of 5 µg/l. A glassy carbon electrode with bismuth film was modified with gold nanoparticle/graphene/cysteine composite to simultaneously detect Pb^{2+} and Cd^{2+} ions (SWASV) by Zhu *et al.*, (2014). This work provided a good reproducible electrode modified with materials that are biocompatible and non-toxic.

Devasenathipathy *et al.*, (2015) electrodepositing multiwalled carbon nanotubes (MWCNT) reinforced on calcium-crossed linked pectin (CCLP)/AuNP composite. The CCPLP helped to stabilize the AuNPs, which often accumulate and that causes them to lose their electrocatalytic ability. The electrode modified with MWCNT reinforced CCLP/AuNP film, was more sensitive and stable, it was used to determine L-cysteine with a detection limit of 19nM.

For this reason, Ting *et al.*, (2015) used graphene quantum dots to functionalise AUNPs for the simultaneous determination of Cu^{2+} and Hg^{2+} metal ions through the electrochemical detection method. The results demonstrated that Cu^{2+} and Hg^{2+} ions were highly sensitive to AuNPs as synthesized with a low detection limit of .05 nM for Cu^{2+} and 0.02 nM for Hg^{2+} ions.

Xie *et al.*, (2015) presented a hybrid material of graphene/CeO_2 for electrochemical determination of four metal ions such as Cd^{2+}, Cu^{2+}, Hg^{2+}, and Pb^{2+}. This was done using a glassy carbon, with CeO_2 nanoparticles covered by graphene which were synthesized via the hydrothermal method. The incorporation of these prepared CeO_2NPs decorated with graphene materials, improved the sensitivity and selectivity towards Cd^{2+}, Cu^{2+}, Hg^{2+}, and Pb^{2+} metal ions. Bismuth-PSS composite was used to modify screen-printed electrodes for the determination of Cd^{2+} and Pb^{2+} ions in natural water samples by Rorbeto, et al (2016). Electrochemical parameters favoured the detection process of Pb^{2+} ions with an exceptionally low detection limit of 0.27 μg/l and Cd^{2+} ions using the drop method to employ the composite onto the electrode was 0.10 μg/l.

Also, Shi *et al.*,(2017) study showed a simultaneous electrochemical determination of Zn^{2+}, Pb^{2+}, and Cd^{2+} ions using a simple and novel 3D graphene framework/bismuth nanoparticle (Bi NPS). The nanocomposite was formed by dispersing the graphene framework to increase the active and porous surface area, the tuneable nature of the material also played a role. The as-synthesized 3D graphene-framework/BiNPs films were extremely sensitive in detecting Zn^{2+}, Pb^{2+}, and Cd^{2+} metal ions, in water. In the same year Rupesh, et al (2017) demonstrated electrospinning graphene oxide nanofibers onto the screen-printed electrode for the detection of Hg^{2+}, Pb^{2+}, and Cd^{2+} metal ions, with LOD of 0.0075,0.015 and 0.0312 ppb respectively.

Similarly, Sosa Gómez *et al.*, (2015) modified screen-printed electrode by in-situ electrodepositing antimony film and graphene oxide to quantify Cd^{2+}, Cu^{2+}, Hg^{2+} and Pb^{2+} simultaneously. This resulted in a more sensitive and selective electrode. Though, Zhou *et al.*, (2018) presented an electrochemical assay of graphene oxide with $MnFe_2O_4$ nanocomposites and the improved surface assisted in selectively sensing of Pb^{2+} ions. The synthesized mesoporous $MnFe_2O_4$/GO nanocomposites with an average diameter of 400 nm showed good sensitivity towards Pb^{2+} ions with LOD of 0.0883 μM.

Bourquard *et al.*,(2019) fabricated a graphene-ferrocene-doped graphene film onto a disposable low-cost sensor for the determination of metal ions such as Cu^{2+}, Cd^{2+}, and Pb^{2+} with a concentration range of 5 to 10 μg/L. It displayed a detection limit of Pb^{2+} as low as 1 μg/l. Furthermore, Wang *et al.*, (2019) a colorimetry method to detect Ag^{+} ions from water samples, while using fluorescent copper nanoparticles (CuNPs). The diameter of CuNPs was 5.0 ± 0.2 nanometers and the size was uniform with a presented good selectivity for the Ag^{+}

ions with a linear range of 1600 μmol/L to 6000 μmol/L and 2.37μmol/L. for LOD. Moreover, Hwang, et al (2019) studied a novel nano-porous bismuth electrode to electrochemically detect Cd^{2+} and Pb^{2+}. The modified sensor showed good stability and reproducibility and the LODs were 1.3 and 1.5 ppb, respectively.

Table 1-2: Summary of various nanomaterials modified electrochemical sensors for detection of heavy metals.

Nanomaterials	Modification method	Detection method	Analyte	Linear range	LOD	Sample	References
MWCNT and Lead complex	Added in carbon ink	Potentiometry	Pb(II)	4.6 × 10−8–1.0 × 10−1 M	46.0 nM	Contaminated wastewater	(Ali, Hassan and Mohamed, 2016)
MWCNT ionic liquid and Bismuth	Drop-casting	CV and impedance spectroscopy	Cd(II) Pb(II)	1.0–60.0 μg L−1	0.5 μg L−1 0.12 μg L−1	Soil sample	(Wang et al., 2017)
Bismuth modified with CNTs	Added in carbon ink	SWASV	Pb(II) Cd(II) Zn(II)	2.0–100.0 μg L−1	1.3 μg L−1 0.7 μg L−1 12.0 μg L−1	Stream water	(Hwang et al., 2008)
MWCNTs and bismuth film	Drop-casting	SWASV	Pb(II) Cd(II) Zn(II)	4.8–38.4 nM 8.8–70.4 nM 75.0–600.0 nM	0.7 nM 1.5 nM 11.1 nM		(Mandil et al., 2012)
Graphene and graphene oxide	Added in carbon ink	SWASV	Pd(II) Cd(II)	1.0–300.0 μg L−1	0.1 μg L−1	River water	(Shuai and Lei, 2016)

MWCNTs-Multi-Walled-Carbon-Nanotubes, CNTs-Carbon-Nanotubes, MWCNTs-IL-Multi-Walled-Carbon-Nanotubes-Ionic-liqiud, GR-IL-Graphene-ionic-liquid,SWASV-Square-Wave-Anodic-Stripping-Voltammetry,Pb(II)-Lead ions, Cd(II)-Cadmium ions, LOD-Limit-of-Detection, ug/L-Microgram per Liter, nM-nanoMeter, Zn-Zinc ions.

Table 1-3: Summary of various nanomaterials modified electrochemical sensors for detection of heavy metals.

Nanomaterials	Modification method	Detection method	Analyte	Linear range	LOD	Sample	Ref.
GO supported on antimony film	Added in carbon ink	SWASV	Cd(II) Pb(II) Cu(II) Hg(II)	0.1–1.5 μM	54.0 nM 26.0 nM 60.0 nM 66.0 nM	Sewage, fertilizer waste, sea water	(Ruengpirasiri et al., 2017)
GO-PPY nanocomposite	Electrodeposition	SWASV	Pb(II)	5× 10-9mol/L 7.5× 10-7mol/L	4.7 × 10-11mol/L	Tap water	(Seenivasan, Chang and Gunasekaran, 2015)
GO-PVA nanofiber composite	Electrospinning	DPV	Hg(II) Pb(II) Cd(II)	7.5– 1.0 × 103 ng L−1	7.5 ng L−1 15.0 ng L−1 31.2 ng L−1	Field water	(Mishra et al., 2017)
CNPs-BiNPs	Added in carbon ink	SWASV	Cd(II)	1.0–50.0 μg L−1	1.5 μg L−1	Wastewater, Tap water	(Niu et al., 2016)

GO-Graphene Oxide, PPY-rGO- Polypyrrole reduced Graphene Oxide, GO-PVA- Graphene Oxide Polyvinyl alcohol, CNPs-BiNPs- Carbon Nanoparticles Bismuth Nanoparticles - DPV-Differential Pulse Voltammetry – SWASV – Square wave Anodic Stripping Voltammetry, Hg – Mercury, Cu – Copper

2.6. Conductive Inks

Conductive inks are made from carbon, conductive polymers, dispersed metallic and nanoparticles, they are used to print metallic structures of different substrates in the production of low-cost sensing platforms, radio frequency antennas (RFID) amongst others.

2.6.1. Properties of the conductive inks used in printing

(a) Surface tension

A free-falling droplet by aerodynamic, electrostatic, or gravitational forces will always land in a spherical shape, which is caused by the sphere using less energy to form. This usage of less energy or minimized real coverage is due to the surface tension (γ) of the droplet molecules. This is because the molecules at the liquid-air interface or the free surface have higher energy than within the bulk (Levich, Krylov 1969). The resultant force of the surface tension is a consideration when a solid surface has a droplet. This force is perpendicular to a free edge on the surface and acts in the plane of the free surface. The force (F) is proportional to the length (L) of the edge.

$$\mathbf{F = \gamma L} \qquad \text{Equation 2}$$

When the surface tension decreases, the force that resits to the diffusion of wettability to the surface also decreases, and a homogenous, thin layer is stabilized on the substrate.
When the contact surface tension increases, the force that resists the diffusion of dampening solution to the substrate surface also increases.

The shape of the droplet is determined by Young's relation (Wu, Dzenis 2006)which is satisfied at equilibrium.

$$\boldsymbol{\gamma_{sv} = \gamma_{sl} + \gamma_{lv} \times \cos\cos\theta \cos\cos\theta = \frac{\gamma_{sv} - \gamma_{sl}}{\gamma_{lv}}}$$

Equation 3

Were,

γsv = solid/vapour area

γsl = solid/liquid area

γlv = liquid/vapour area

(b) Coffee ring effect

The coffee ring effect is a typical printing phenomenon caused by capillary flow induced by differential evaporation rates transversely the ink drops. When one droplet has immobilised a three-phase contact line, the extra solvent produced at the edge is replaced by solvent located in the middle, forming a radical capillary flow (Soltman, Subramanian 2008). Because of the coffee ring effect, the output of the devices printed submits the pattern deposited on the substrate, which affects the pattern resolution, is directly affected by morphology. When the capillary flow carries the solute in an evaporating droplet near the pinned-three phase contact line while also bringing all the detached material to the side, morphology is formed. This is particularly popular in low viscosity inks (Seo, Jang et al. 2017). A variety of techniques have been used to reduce the coffee ring effect, including drying on a smooth surface or restricting evaporation at the edge with a centrically perforated plate above the drop (Vasileiou 2017). Electro-wetting or drying droplets in an electric field, mixing two or more different liquids with different vapour and surface tensions, and a sufficiently quick increase in viscosity after deposition are two methods used to boost the coffee ring effect (Vancauwenberghe, Di Marco et al. 2013). Traditional conductive inks are made of different functional materials which can be divided into three types, metal-based, carbon-based, and polymer conductive inks. Carbon-based nanomaterials present several possibilities for flexible and printed electronics.

The use of graphene as a preferred material in the fabrication of printed electronics (Song, Mahajan et al. 2017) has risen sharply, this is due to its unique and promising properties. The application includes the production of graphene-based conductive inks as a suitable replacement for other carbon materials inks, metallic inks, and conductive polymer inks, and has the potential to transform the printed conductive field while decreasing production costs and biological hazards (Saidina, Eawwiboonthanakit et al. 2019).

(Majee, Liu et al. 2017) formulated a thermally stable and highly concentrated water-based graphene nanoparticles ink via shear exfoliation and centrifugation of graphene in NMP. The graphene ink was used to make circuit boards, by inkjet printing on a glass substrate and annealed for 150 min at approximately 350°C. This resulted in circuit boards that are near-transparent with a low resistance of 260 ohms per square at~160nm thickness, the conductivity of 1400 S/m and concludes that an ideal ink for screen printing should have a low viscosity at a high shear rate, a high rest viscosity, and fast recovery time. The viscosity of conductive ink for screen printing can be between 0.05 to 5 Pa s. Zhang *et al.*, (2017) used a facile ball milling method to demonstrate a graphene nanoplatelet ink with high conductive properties, with good

electrochemical behaviour. The ink exhibited better film formation and conductivity of 3.5×10^4S/m this makes it suitable for application in printed electrochemical sensors, energy storage devices, functional coatings and smart thin-film heaters. Arapov *et al.*, (2016) used a compression rolling technique to formulate a highly concentrated and colloidally stable polymer binder-based graphene ink paste by gelation which depicted excellent printability down to lines in a width of 40μm and high conductivity of 30 ohms per square. Controlling the thickness of the printed pattern, which is largely controlled by the thickness of the stencils, is the key challenge when using graphene inks for screen printing. Since graphene has a natural propensity to accumulate, it's difficult to create extremely viscous and condensed dispersions (Tran, Dutta et al. 2018)

2.6.2. Rheological Properties of printing inks

(a) Viscosity

Viscosity is defined as the resistance of a fluid (gas or liquid) to flow. When a fluid begins to flow, an external force acting perpendicular to the fluid called force shear stress arises which caused the resistance to flow. An ink has low viscosity when it flows readily, and it has high viscosity when it refused to flow (Patton 1964).The interaction between cone and plate rheometer or disk on a rheometer used to determine properties of an ink characterized the shear-viscosity relationship. Screen-printing inks tend to have a relatively high viscosity. The composition of the ink such as resin, filler, and solvent determine the quality of the ink and the viscosity (Irgens 2014).The solvent properties such as the rate of evaporation during the printing process, solids concentration is always considered during the ink formulation as they affect the viscosity. Viscosity can be described as the ratio of shear stress to shear rate (Patton 1964) as shown in equation 4.

$$\textbf{Viscosity} = \frac{\textbf{Shear stress}}{\textbf{Shear rate}} \qquad \text{Equation 4}$$

Shear stress is the force per unit area and is applied constantly throughout any continuous medium, which is subjected to external forces. Shear rate is the differential change in velocity at which one layer of fluid passes another layer at a right angle, to the direction of the flow (Barnes 2000) .

Measuring the viscosity of a fluid assists in identifying a particular rheological behaviour of screen-printing inks in this instance. These are the following properties and materials that affect viscosity:

1. Shear rate: Most fluids show a decrease in viscosity when the shear rate is increasing, the behaviour denotes a shear-thinning behaviour ((Tanner 2000)
2. Time: The viscosity decreasing with the increase of time, changes in viscosity of fluids can occur over time. The time passed under circumstances of shear affects thixotropic material (Leblanc, Secco et al. 1999)
3. Physical / Chemical Properties: The composition of ink formulation materials affects the viscosity. When this composition is altered, either by changing the proportions of the component filler, solvent, or binder or by the addition of other materials, a change in viscosity happens (Gupta 2000)

The ink shearing behaviour can be used to measure the viscosity and help understand the properties of the ink, Newtonian behaviour happens when the viscosity remains constant no matter what the shear rate. Pseudoplastic or shear-thinning behaviour happens when the viscosity decreases, as the shear rate increases. Dilatant or Shear thickening behaviour happens when the viscosity increases, as the shear rate increases. Bingham plastic happens when the viscosity appears to be infinite unit when a certain shear stress behaviour is achieved (Gupta, 2000).

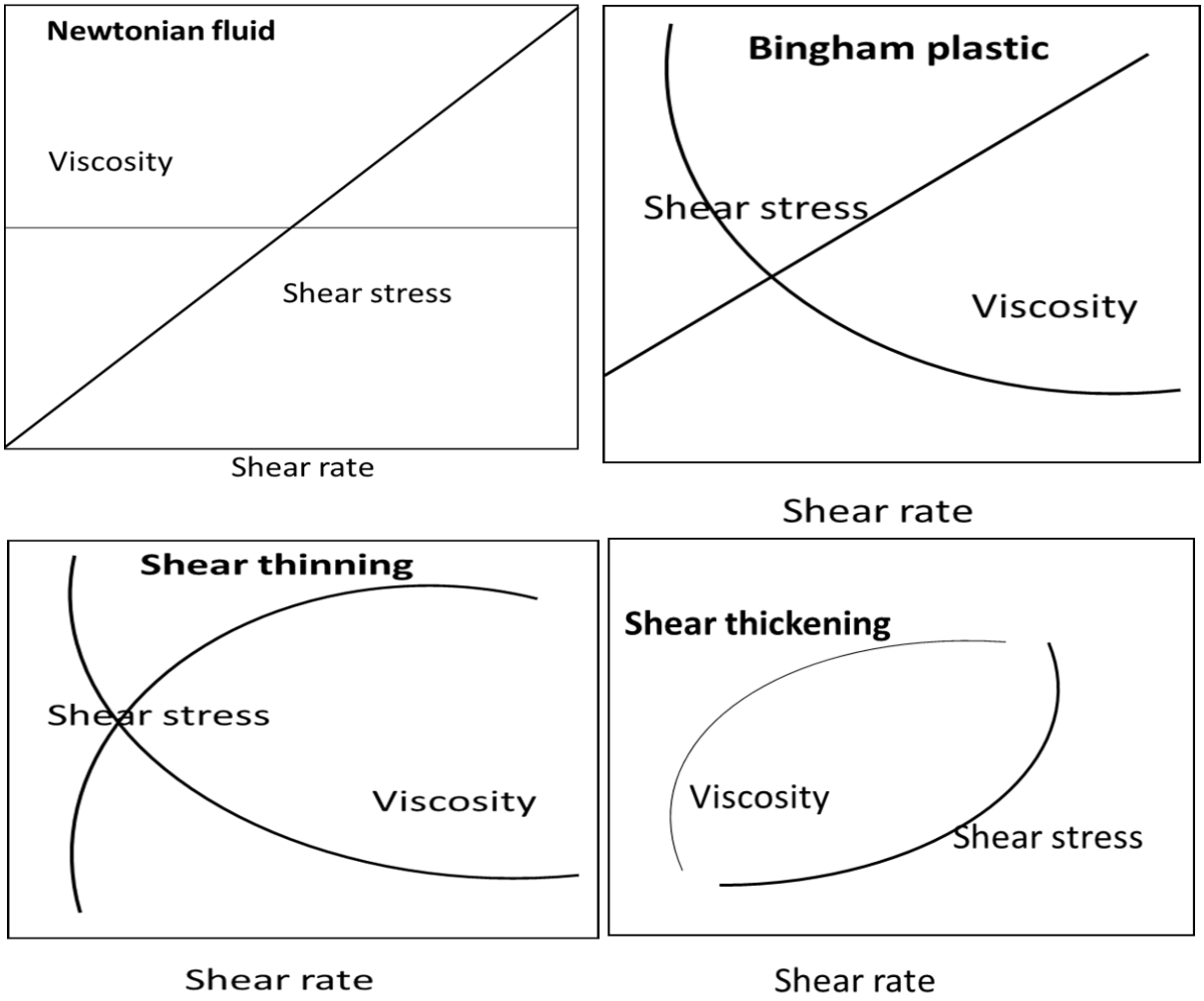


Figure 2-4: Flow and viscosity curves of the four fluid behaviours.

2.7. References

1. Akkarachanchainon, N., Rattanawaleedirojn, P., Chailapakul, O. and Rodthongkum, N., 2017. Hydrophilic graphene surface prepared by electrochemically Reduced micellar graphene oxide as a platform for electrochemical sensor. *Talanta,* 165, pp. 692-701.
2. Ali, T.A., Hassan, A.M.E. and Mohamed, G.G., 2016. Manufacture of lead-specific screen-printed sensor based on lead Schiff base complex as carrier and multi-walled carbon nanotubes for detection of Pb (II) in contaminated water tests. *Int J Electrochem Sci,* 11, pp. 10732-10747.
3. Arapov, K., Bex, G., Hendriks, R., Rubingh, E., Abbel, R., De With, G. and Friedrich, H., 2016. Conductivity Enhancement of Binder-Based Graphene Inks by Photonic Annealing and Subsequent Compression Rolling. *Advanced Engineering Materials,* 18(7), pp. 1234-1239.
4. Archer, M.D., 1989. Genesis of the Nernst equation.
5. Armstrong, F.A. and Wilson, G.S., 2000. Recent developments in faradaic bioelectrochemistry. *Electrochimica Acta,* 45(15-16), pp. 2623-2645.
6. Baghayeri, M., Alinezhad, H., Fayazi, M., Tarahomi, M., Ghanei-motlagh, R. and Maleki, B., 2019. A novel electrochemical sensor based on a glassy carbon electrode modified with dendrimer functionalized magnetic graphene oxide for simultaneous determination of trace Pb(II) and Cd(II). *Electrochimica Acta,* 312, pp. 80-88.
7. Banica, F., 2012. *Chemical sensors and biosensors: fundamentals and applications.* John Wiley & Sons.
8. Barcelo, D. and Petrovic, B., 2007. *Comprehensive analytical chemistry.* Boston.
9. Bard, A.J. and Rubenstein, I., 1996. *Electroanalytical chemistry: a series of advances.* CRC press.
10. Barnes, H.A., 2000. *A handbook of elementary rheology.* University of Wales, Institute of Non-Newtonian Fluid Mechanics Aberystwyth.
11. Biesheuvel, P.M., Fu, Y. and Bazant, M.Z., 2011. Diffuse charge and Faradaic reactions in porous electrodes. *Physical Review E,* 83(6), pp. 61507.
12. Bolotsky, A., Butler, D., DONG, c., Gerace, K., Glavin, N.R., Muratore, C., Robinson, J.A. and Ebrahimi, A., 2019. Two-dimensional materials in biosensing and healthcare: from in vitro diagnostics to optogenetics and beyond. *ACS nano,* 13(9), pp. 9781-9810.
13. Bourquard, F., Bleu, Y., Loir, A., Caja-Munoz, B., Avila, J., Asensio, M., Raimondi, G., Shokouhi, M., RASSAS, I., FARRE, C., Chaix, C., BARNIER, V., Jaffrezic-Renault, N., Garrelie, F. and Donnet, C., 2019. Electroanalytical Performance of Nitrogen-Doped

Graphene Films Processed in One Step by Pulsed Laser Deposition Directly Coupled with Thermal Annealing. *Materials (Basel, Switzerland),* 12(4), pp. 666.

14. Brett, C. and Oliveira BRETT, A.M., 1993. *Electrochemistry: principles, methods, and applications.*
15. Buledi, J.A., Amin, S., Haider, S.I., Bhanger, M.I. and Solangi, A.R., 2020. A review on detection of heavy metals from aqueous media using nanomaterial-based sensors. *Environmental Science and Pollution Research,* , pp. 1-9.
16. Chen, D., Feng, H. and Li, J., 2012. Graphene Oxide: Preparation, Functionalization, and Electrochemical Applications. *Chemical Reviews,* 112(11), pp. 6027-6053.
17. De Oliveira, T.R., Fonseca, W.T., De Oliveira Setti, G. and Faria, R.C., 2019. Fast and flexible strategy to produce electrochemical paper-based analytical devices using a craft cutter printer to create wax barrier and screen-printed electrodes. *Talanta,* 195, pp. 480-489.
18. Devasenathipathy, R., Karuppiah, C., Chen, S., Mani, V., Vasantha, V.S. and Ramaraj, S., 2015. Highly selective determination of cysteine using a composite prepared from multiwalled carbon nanotubes and gold nanoparticles stabilized with calcium crosslinked pectin. *Microchimica Acta,* 182(3), pp. 727-735.
19. Eblanc, G.E., Secco, R.A. and Kostic, M., 1999. Viscosity measurement. *The Measurement, Instrumentation, and Sensors.* CRC Press.
20. Feiner, A. and Mcevoy, A.J., 1994. The nernst equation. *Journal of chemical education,* 71(6), pp. 493.
21. Gianchandani, Y.B., Tabata, O. and Zappe, H.P., 2008. *Comprehensive microsystems.* Elsevier Amsterdam.
22. Gupta, R.K., 2000. *Polymer and composite rheology.* CRC Press.
23. Hancock, A. and Lin, L., 2004. Challenges of UV curable ink-jet printing inks–a formulator's perspective. *Pigment & resin technology.*
24. Hanif, F., Tahir, A., Akhtar, M., Waseem, M., Haider, S., Aly Aboud, M.F., Shakir, I., Imran, M. and Warsi, M.F., 2019. Ultra-selective detection of Cd2+ and Pb2+ using glycine functionalized reduced graphene oxide/polyaniline nanocomposite electrode. *Synthetic Metals,* 257, pp. 116185.
25. Holze, R., 2009. *RG Compton and CE Banks, Understanding cyclic voltammetry.* Springer.
26. Hwang, G.H., Han, W.K., Park, J.S. and Kang, S.G., 2008. Determination of trace metals by anodic stripping voltammetry using a bismuth-modified carbon nanotube electrode. *Talanta,* 76(2), pp. 301-308.

27. Ibáñez-Redín, G., Wilson, D., Gonçalves, D. and Oliveira, O.N., 2018. Low-cost screen-printed electrodes based on electrochemically reduced graphene oxide-carbon black nanocomposites for dopamine, epinephrine and paracetamol detection. *Journal of Colloid and Interface Science,* 515, pp. 101-108.
28. Irgens, F., 2014. *Rheology and non-newtonian fluids.* Springer.
29. Jothimuthu, P., Wilson, r.a., Herren, J., Haynes, E.N., Heineman, W.R. and Papautsky, I., 2011. Lab-on-a-chip sensor for detection of highly electronegative heavy metals by anodic stripping voltammetry. *Biomedical Microdevices,* 13(4), pp. 695-703.
30. Kaifer, A.E. and Gómez-Kaifer, M., 2008. *Supramolecular electrochemistry.* John Wiley & Sons.
31. Kaifer, A.E. and Gómez-Kaifer, M., 2008. *Supramolecular electrochemistry.* John Wiley & Sons.
32. Kalcher, K., Svancara, I., Buzuk, M., Vytras, K. and Walcarius, A., 2009. Electrochemical sensors and biosensors based on heterogeneous carbon materials. *Monatshefte für Chemie-Chemical Monthly,* 140(8), pp. 861-889.
33. Levich, V.G. and Krylov, V.S., 1969. Surface-tension-driven phenomena. *Annual Review of Fluid Mechanics,* 1(1), pp. 293-316.
34. Lovrić, M., 2010. Square-wave voltammetry. *Electroanalytical methods.* Springer, pp. 121-145.
35. Majee, S., Liu, C., Wu, B., Zhang, S.-. and Zhang, Z.-., 2017. Ink-jet printed highly conductive pristine graphene patterns achieved with water-based ink and aqueous doping processing. *Carbon,* 114, pp. 77-83.
36. mandil, A., pauliukaite, R., Amine, A. and Brett, C.M.A., 2012. Electrochemical characterization of and stripping voltammetry at screen printed electrodes modified with different brands of multiwall carbon nanotubes and bismuth films. *Analytical letters,* 45(4), pp. 395-407.
37. Maniya, N.H. and Srivastava, D.N., 2020. Fabrication of porous silicon-based label-free optical biosensor for heat shock protein 70 detection. *Materials Science in Semiconductor Processing,* 115, pp. 105126.
38. Mettakoonpitak, J., Boehle, K., Nantaphol, S., Teengam, P., adkins, J.A., Srisa-Art, M. and HENRY, C.S., 2016. Electrochemistry on paper-based analytical devices: a review. *Electroanalysis,* 28(7), pp. 1420-1436.

39. Mishra, R.K., Nawaz, M.H., Hayat, A., Nawaz, M.A.H., Sharma, V. and Marty, J., 2017. Electrospinning of graphene-oxide onto screen printed electrodes for heavy metal biosensor. *Sensors and Actuators B: Chemical*, 247, pp. 366-373.
40. Ndlovu, T., Mamba, B.B., Sampath, S., Krause, R.W. and Arotiba, O.A., 2014. Voltammetric detection of arsenic on a bismuth modified exfoliated graphite electrode. *Electrochimica Acta*, 128, pp. 48-53.
41. Niu, P., Fernández-Sánchez, C., Gich, M., Navarro-Hernández, C., Fanjul-Bolado, P. and ROIG, A., 2016. Screen-printed electrodes made of a bismuth nanoparticle porous carbon nanocomposite applied to the determination of heavy metal ions. *Microchimica Acta*, 183(2), pp. 617-623.
42. Novoselov, K.S., Geim, A.K., Morozov, S.V., Dubonos, S.V., Zhang, Y. and Jiang, D., 2004. Room-temperature electric field effect and carrier-type inversion in graphene films. *Arxiv preprint cond-mat/0410631*, .
43. Park, H.J., Yoon, J.H., Lee, K.G. and Choi, B.G., 2019. Potentiometric performance of flexible pH sensor based on polyaniline nanofiber arrays. *Nano Convergence*, 6(1), pp. 9.
44. Patton, T.C., 1964. Paint flow and pigment dispersion. *Paint Flow and Pigment Dispersion.* pp. 479.
45. Patton, T.C., 1964. Paint flow and pigment dispersion. *Paint Flow and Pigment Dispersion.* pp. 479.
46. Ramaley, L. and Krause, M.S., 1969. Theory of square wave voltammetry. *Analytical Chemistry*, 41(11), pp. 1362-1365.
47. Reedijk, J., 2014. *Reference Module in Chemistry, Molecular Sciences and Chemical Engineering.* Elsevier.
48. Ruengpirasiri, P., Punrat, E., Chailapakul, O. and chuanuwatanakul, S., 2017. Graphene Oxide-Modified Electrode Coated with in-situ Antimony Film for the Simultaneous Determination of Heavy Metals by Sequential Injection-Anodic Stripping Voltammetry. *Electroanalysis*, 29(4), pp. 1022-1030.
49. Saidina, D.S., Eawwiboonthanakit, N., Mariatti, M., Fontana, S. and Hérold, C., 2019. Recent development of graphene-based ink and other conductive material-based inks for flexible electronics. *Journal of Electronic Materials*, 48(6), pp. 3428-3450.
50. Seenivasan, R., Chang, W. and Gunasekaran, S., 2015. Highly sensitive detection and removal of lead ions in water using cysteine-functionalized graphene oxide/polypyrrole nanocomposite film electrode. *ACS applied materials & interfaces*, 7(29), pp. 15935-15943.

51. Seo, C., Jang, D., Chae, J. and Shin, S., 2017. Altering the coffee-ring effect by adding a surfactant-like viscous polymer solution. *Scientific reports*, 7(1), pp. 1-9.
52. Shi, L., Li, Y., Rong, X., Wang, Y. and Ding, S., 2017. Facile fabrication of a novel 3D graphene framework/Bi nanoparticle film for ultrasensitive electrochemical assays of heavy metal ions. *Analytica Chimica Acta*, 968, pp. 21-29.
53. Shuai, H. and Lei, Y., 2016. Graphene ink fabricated screen-printed electrode for Cd^{2+} and Pd^{2+} determination in Xiangjiang river. *Int. J. Electrochem. Sci*, 11(9), pp. 7430-7439.
54. Soltman, D. AND Subramanian, V., 2008. Inkjet-printed line morphologies and temperature control of the coffee ring effect. *Langmuir*, 24(5), pp. 2224-2231.
55. Song, D., Mahajan, A., Secor, E.B., Hersam, M.C., FranciS, L.F. and Frisbie, C.D., 2017. High-resolution transfer printing of graphene lines for fully printed flexible electronics. *ACS nano*, 11(7), pp. 7431-7439.
56. Sosa Gómez, V., Barceló, C., Serrano, N., Ariño, C., Díaz-Cruz, J. and Esteban, M., 2015. Antimony film screen-printed carbon electrode for stripping analysis of Cd(II), Pb(II), and Cu(II) in natural sample. *Analytica Chimica Acta*, 855.
57. Stetter, J.R., Penrose, W.R. and Yao, S., 2003. Sensors, chemical sensors, electrochemical sensors, and ECS. *Journal of The Electrochemical Society*, 150(2), pp. S11
58. Stradiotto, N.R., Yamanaka, H. and Zanoni, M.V.B., 2003. Electrochemical sensors: a powerful tool in analytical chemistry. *Journal of the Brazilian Chemical Society*, 14(2), pp. 159-173.
59. Tanner, R.I., 2000. *Engineering rheology*. OUP Oxford.
60. Ting, S., EE, S., Ananthanarayanan, A., LEONG, K. and CHEN, P., 2015. Graphene quantum dots functionalized gold nanoparticles for sensitive electrochemical detection of heavy metal ions. *Electrochimica Acta*, 172.
61. Tothill, I.E., 2001. Biosensors developments and potential applications in the agricultural diagnosis sector. *Computers and Electronics in Agriculture*, 30(1-3), pp. 205-218.
62. Tran, T.S., Dutta, N.K. and Choudhury, N.R., 2018. Graphene inks for printed flexible electronics: Graphene dispersions, ink formulations, printing techniques and applications. *Advances in Colloid and Interface Science*, 261, pp. 41-61.
63. Tuantranont, A., 2013. Applications of nanomaterials in sensors and diagnostics. *Springer series on chemical sensors and biosensors (Springer, Berlin Heidelberg, 2014)*, .
64. Vancauwenberghe, V., DI Marco, P. and Brutin, D., 2013. Wetting and evaporation of a sessile drop under an external electrical field: A review. *Colloids and Surfaces A: Physicochemical and Engineering Aspects*, 432, pp. 50-56.

65. Vasileiou, T., 2017. *Studies of Droplet Behavior in Emerging Technologies: Elasticity Effects on Surface Superhydrophobicity and Contactless Acoustophoretic DNA Transfection.* ETH Zurich.
66. Walsh, F.C., 2001. Electrochemical technology for environmental treatment and clean energy conversion. *Pure and applied chemistry,* 73(12), pp. 1819-1837.
67. Wang, H., Zhao, G., Zhang, Z., Yi, Y., Wang, Z. and Liu, G., 2017. A portable electrochemical workstation using disposable screen-printed carbon electrode decorated with multiwall carbon nanotube-ionic liquid and bismuth film for Cd (II) and Pb (II) determination. *International Journal of Electrochemical Science,* 12, pp. 4702-4713.
68. Wang, J., 2002. Real-time electrochemical monitoring: toward green analytical chemistry. *Accounts of chemical research,* 35(9), pp. 811-816.
69. Wang, N., Ga, l., Jia, M. and AI, J., 2019. Synthesis of Fluorescent Copper Nanoparticles and Ultrasensitive Free Label Detection of Ag^{+}. *Journal of Nanomaterials,* 2019, pp. 4089731.
70. Wu, X. and Dzenis, Y.A., 2006. Droplet on a fiber: geometrical shape and contact angle. *Acta mechanica,* 185(3), pp. 215-225.
71. Xie, Y., Zhao, S., Ye, H., Yuan, J., Song, P. and Hu, S., 2015. Graphene/CeO2 hybrid materials for the simultaneous electrochemical detection of cadmium(II), lead(II), copper(II), and mercury(II). *Journal of Electroanalytical Chemistry,* 757, pp. 235-242.
72. Zhang, M., Hou, C., Halder, A., Wang, H. and Chi, Q., 2017. Graphene papers: smart architecture and specific functionalization for biomimetics, electrocatalytic sensing and energy storage. *Materials Chemistry Frontiers,* 1(1), pp. 37-60.
73. Zhang, Y., Ren, L., Wang, S., Marathe, A., Chaudhuri, J. and Li, G., 2011. Functionalization of graphene sheets through fullerene attachment. *Journal of Materials Chemistry,* 21(14), pp. 5386-5391.
74. Zhang, Z., Sun, J., Lai, C., Wang, Q. and Hu, C., 2017. High-yield ball-milling synthesis of extremely concentrated and highly conductive graphene nanoplatelet inks for rapid surface coating of diverse substrates. *Carbon,* 120, pp. 411-418.
75. Zhu, L., Xu, L., Huang, B., Jia, N., Tan, l. and Yao, S., 2014. Simultaneous determination of Cd (II) and Pb (II) using square wave anodic stripping voltammetry at a gold nanoparticle-graphene-cysteine composite modified bismuth film electrode. *Electrochimica Acta,* 115, pp. 471-477.

3. CHAPTER 3: EXPERIMENTAL PROCEDURE

This chapter provides an overview of the chemical reagents and materials used throughout the study, the experimental design and post-treatment methods adopted, the optimization of certain parameters, the Physico-chemical and electrochemical characterization of the prepared materials.

3.2. Materials and Methods

3.2.1. Chemicals

All chemicals used in the study were of analytical reagent grade and were used as received without any further purification. Millipore, deionized water was used to prepare all aqueous solutions. Melamine, Ferri/ferrocyanide ($K_3[Fe(CN_6)]$), Potassium chloride (KCl), Sodium acetate anhydrous($C_2H_3NaO_2$), glacial acetic acid (CH_3CO_2H) ≥ 99 % purity, lead (II) nitrate, ($Pb(NO_3)_2$) and cadmium (II) nitrate ($Cd(NO_3)_2$), Carboxymethyl cellulose sodium salt (CMC) with medium viscosity, glycerol ($C_3H_8O_3$) were purchased from Sigma-Aldrich. Potassium permanganate ($KMnO_4$), sulfuric acid (H_2SO_4,98%), Phosphoric acid (H_3PO_4, 32%), and ethanol (98%) from Merck.

3.1.2. Preparation of reagents for electrochemical analysis

For the electrochemistry measurements, glacial acetic acid was diluted to 0.1M before use. Acetate buffer of pH 4,5 was prepared by mixing appropriate amounts of 0.1M acetic acid and 0.1M sodium acetate. Stock solutions of 1 g/L of Pb (II) and Cd (II) were prepared in 0.1M acetate buffer (pH 4,5) which were further diluted using the buffer to required concentrations for various experiments and the cyclic voltammetry (CV)measurements were done using 0.1 M $K_3[Fe(CN_6)]$ solution containing 1.0 M KCl as a supporting electrolyte.

3.1.3. Synthesis of graphene oxide, graphene oxide ink, and graphitic carbon nitride.

The methodologies that were employed for these syntheses are explained in detail in chapter 4 and 5, respectively.

3.2. Material characterisation techniques

3.2.1. X-ray diffraction (XRD)

To identify the structural phases of the nanomaterials X-Ray diffraction patterns (Aboutalebi *et al.*, 2011) were verified using a Phillips XRD (PANalytical X'Pert PRO, Netherlands). The XRD scans were done for 10 minutes at 0.026° steps from $10 \leq 2\theta \leq 60°$.

3.2.2. Raman Spectroscopy

The Raman employs a technique that uses different vibrational energy levels to excite molecules of a sample and that shows the most prominent characteristic of the samples (McCreery, 2005). GO Raman analysis was done by using an alpha300R (WITec) confocal

laser Raman microscope configured with a frequency-doubled Nd-YAG laser (wavelength 532 nm). Raman spectra were obtained using x50 Nikon objectives.

3.2.3. Fourier transform infrared (FTIR) spectroscopy

The technique (FTIR spectroscopy) was used to determine the functional groups present in the nanomaterials and electrode surface (Ahmad *et al.*, 2020). The analysis was done using a Perkin Elmer Spectrum 100 FTIR spectrophotometer from 400 to 4000 cm^{-1} wavenumber at a 4 cm^{-1} resolution.

3.2.4. Ultraviolet-visible spectroscopy (UV-Vis)

Ultraviolet (UV)-visible spectroscopy used UV-visible light is absorbed by the molecule in the samples. The absorption of the UV-visible radiations causes an excitation of the electrons from lower to higher energy levels and that is how different samples are analysed (Wandelt, 2018). The UV–Vis absorbance was done using a Shimadzu UV-2401 PC spectrophotometer for 200–700 nm wavelength.

3.2.5. Scanning Electron Microscopy (SEM)

SEM produces an image of the samples, which gives information about the surface analysis, morphology, shape, and size of the particles of the sample (Liu et al., 2010). For this work, a field emission scanning electron microscopy (FESEM) on a Zeiss Auriga cobra fib microscope was used, to study the morphology and composition of GO, g-C_3N_4, and the electrode surface.

3.2.6. Transmission Electron Microscopy (TEM)

Transmission Electron Microscopy (TEM) with high resolutions, to study morphology, elemental composition, particle size, defect, and crystalline structure of a sample (Tang and Yang, 2017). High-resolution transmission electron microscopy (HRTEM) on JEOL JEM-2100 was used to confirm the formation of the liquid crystalline phases, the texture patterns of GO were recorded using polarizing optical microscopy.

3.2.7. Rheology

The rheological studies of the GO inks were done by using a rheometer (Rheolab CC Anton Paar Model) with a cone-plate geometry and a temperature-regulating device. The shear rate for conducting these tests was 1 to 100 $s^{-1}$for measuring shear viscosity and the frequency range for measuring loss and storage modulus was 1 to 100 Hz with a 0,5% constant strain amplitude.

3.2.8. Thermographic Analyser (TGA)

Thermogravimetric analysis (TGA) measures sample stability by monitoring weight changes in a material as a function of temperature and/or time under a controlled atmosphere (Trovati *et al.*, 2010). TGA/DTA analyses were performed in an SDT-Q600 thermogravimetric modulus (TA Instruments), using a sample mass of 10 mg in an α-alumina crucible.

3.3. Modification of the paper SPES with g-C_3N_4

2 µL of g-C_3N_4 drop-casted on the SPE surface. The electrodes were incubated overnight or until the electrodes completely dry under a vacuum. After dryness, the SPEs were washed for 2 min with deionized water and incubated for 1 h at 40°C.

3.4. Electrochemical analysis with cyclic voltammetry (cv) and square wave anodic stripping (SWASV)

Electrochemical characterization of the SPEs was carried out by CV in 5mM Ferri/ferrocyanide ($K_3[Fe(CN_6)]$), at a scan rate υ ranging from 100 to 500 mV s^{-1}. For more reproducibility of the experiments and determination of the quantitative values (i.e., peak currents, peak potentials and thus, Ia/Ic and ΔEp), the CV measurements were carried out on triplicates, at a fixed scan rate of 100 mV $s^{-1}$for the different SPEs. Electrochemical analysis of electrodes was carried out by CV and SWASV. The difference being that in SWASV a potential step is applied on the working electrode and not a triangular potential wave-like in CV.

3.5. References

1. Aboutalebi, S.H., Chidembo, A.T., Salari, M., Konstantinov, K., Wexler, D., Liu, H.K. and Dou, S.X., 2011. Comparison of GO, GO/MWCNTs composite and MWCNTs as potential electrode materials for supercapacitors. *Energy & Environmental Science*, **4**(5), pp. 1855-1865.
2. Ahmad, S.Z.N., Salleh, W.N.W., Ismail, A.F., Yusof, N., Yusop, M.Z.M. and Aziz, F., 2020. Adsorptive removal of heavy metal ions using graphene-based nanomaterials: Toxicity, roles of functional groups and mechanisms. *Chemosphere*, **248**, pp. 126008.
3. Liu, F., Lai, Y., Liu, J., Wang, B., Kuang, S., Zhang, Z., LI, J. and Liu, Y., 2010. Characterization of chemical bath deposited CdS thin films at different deposition temperature. *Journal of Alloys and Compounds*, **493**(1), pp. 305-308.
4. Mccreery, R.L., 2005. *Raman spectroscopy for chemical analysis.* John Wiley & Sons.
5. Tang, C.Y. and Yang, Z., 2017. Transmission electron microscopy (TEM). *Membrane Characterization.* Elsevier, pp. 145-159.
6. trovati, G., Sanches, E.A., Neto, S.C., Mascarenhas, Y.P. and Chierice, G.O., 2010. Characterization of polyurethane resins by FTIR, TGA, and XRD. *Journal of Applied Polymer Science*, **115**(1), pp. 263-268.
7. Wandelt, K., 2018. *Encyclopedia of interfacial chemistry: surface science and electrochemistry.* Elsevier.

CHAPTER 4 : GRAPHENE OXIDE NANOPARTICLE CONDUCTIVE INKS: SYNTHESIS, CHARACTERIZATION, AND FABRICATION OF ELECTROCHEMICAL PRINTED PAPER-BASED ELECTRODES.

This chapter presents the materials used in the synthesis of graphene oxide and ink formulation. GO material characterization using XRD, Raman spectrograph, UV-Vis, TGA-DTA, FESEM, SEM and studying rheological behaviour of the ink.

4.1. Introduction

Printed and flexible electronics have the potential to solve key challenges and revolutionize future electronic devices and systems in the near decades. Printing of flexible electronics requires the synthesis of suitable conductive inks that can be printed using various techniques such as screen-printing, inkjet-printing, gravure-based and flexographic while providing the required electrical and mechanical performance (Yazdi, Popma et al. 2016) . Different conductive fillers such as polymers (Perinka, Kim et al. 2013)carbon nanotubes (Han, Kim et al. 2014), and metal nanoparticles or organic metal complexes (Chen *et al.*, 2012) have been studied in the synthesis of different types of conductive inks, focusing more on carbon-based nanofillers such as carbon nanotubes or graphene and graphene-based conductive inks have been successfully applied in printed sensors, supercapacitors, electrodes and conductive patterns ((Yang, Wang 2016); (Tran, Dutta et al. 2018)).

The common problem when it comes to electrochemical sensors is the small surface area of the carbon working electrodes. To overcome this drawback, different nanomaterials have been studied and considered to improve the working electrode due to their large surface area and other properties such as high thermal conductivity and high young modulus. ((Zhang, Huang et al. 2015). Graphene oxide, a kind of promising conductive nanofiller, has recently been studied in the field of printed electronics especially in the production of conductive nano-based inks.

In this chapter, we focus on the synthesis of GO, GO-based conductive ink and its application for the fabrication of screen-printed paper-based electrochemical sensors. With the use of carbon methylcellulose (CMC) as a binder, the obtained conductive ink displayed high stability and permeability as a preferred ink used to fabricate the paper-based electrodes.

4.2. Materials and method

4.2.1. Graphene oxide synthesis

GO was prepared from the modified hummers method (Hummers Jr, Offeman 1958). Graphene flakes (3 g) were placed into a round bottom flask, 360 mL of H_2SO_4, and 90 mL of H_3PO_4 was slowly added. $KMnO_4$(18 g) was subsequently added, and the mixture was placed on a heating stirrer for 12 hours at a constant temperature of 50 °C to complete the oxidation process of the graphene flakes. The reacting mixture was placed in an ice bath to cool to a temperature of 28 °C while adding 8 mL of a 30% H_2O_2 mixture. The resulting mixture brown/dark yellow. To remove the unreacted graphene flakes, the mixture was centrifuged for 20 min at 400 rpm and then washed with deionized water several times. The resulting mixture was filtered and then dried in a vacuum oven at 80 °C for 24 hours.

4.2.2. Ink preparation

4.2.3. Material characterization

To identify the structural phases of GO X-Ray diffraction patterns were verified using a Phillips XRD (PANalytical X'Pert PRO, Netherlands). The XRD scans were done for 10 minutes at 0.026° steps from $10 \leq 2\theta \leq 60°$. The Raman Studies were done by using an alpha300R (WITec) confocal laser Raman microscope configured with a frequency-doubled Nd-YAG laser (wavelength 532 nm). Raman spectra were obtained using x50 Nikon objectives.

Fourier transform infrared (FTIR) analysis of GO were done using a Perkin Elmer Spectrum 100 FTIR spectrophotometer from 400 to 4000 cm^{-1} wavenumber at a 4 cm^{-1} resolution. The UV–Vis absorbance of GO was done using a Shimadzu UV-2401 PC spectrophotometer for 200–700 nm wavelength. To investigate the morphology of the nanomaterial, a field emission scanning electron microscopy (FESEM) on a Zeiss Auriga Cobra FIB microscope and high-resolution transmission electron microscopy (HRTEM) on JEOL JEM-2100 were used. To confirm the texture patterns and ink dispersion images were recorded using polarizing optical microscopy from ZEISS Axio Imager. The rheological studies of the GO inks were done by using a rheometer (Rheolab CC Anton Paar Model) with a cone-plate geometry and a temperature-regulating device. The shear rate for conducting these tests was 1 to 100 $s^{-1}$for measuring shear viscosity and the frequency range for measuring loss and storage modulus was 1 to 100 Hz with a 0,5% constant strain amplitude. The sheet resistance (R_S) of the samples is measured by a two-point probe a Fluke 117 Handheld Digital Multimeter and the measurements were done three times and an average was taken. TGA/DTA analyses were performed in an SDT-Q600 thermogravimetric modulus (TA Instruments), using a sample

mass of 10 mg in an α-alumina crucible. The heating rate varied between 5 °C min^{-1} and 20 °C min^{-1} under inert nitrogen atmosphere flowing at 100 mL min^{-1}, from 30 °C temperature to 500 °C for the conductive inks and from 30 °C temperature to 700 °C for GO analyses.

4.3. Results and discussion

4.3.1. Structural studies on GO

GO was selected because of its dominant carboxyl, hydroxyl, and carbonyl groups which are responsible for the excellent dispersion ability in aqueous media and the strong H-bonding interactions with low dimensional nanofillers with a large aspect ratio (Rattana, Chaiyakun et al. 2012). To achieve higher thermal conductivities in any desired direction, the orientation of the nanofillers can be controlled. Structural characterisation to confirm the presence of GO was done using Raman spectroscopy. The spectra obtained in Figure 4-1show the D which is referred to as the disorder band and G "in phase" vibration band peaks 1350 and 1598 cm^{-1}, which are used to characterise GO. To confirm the formation of GO nanosheets, FTIR spectra analysis in Figure 4-2 was done to show the functional groups available at 3200 to 3500 cm-1 a broad peak is present which is attributed to the stretching of the (OH) hydroxyl group. The stretching of the epoxy-functional group (C-O) at 1230 and 1280 cm^{-1} represents the GO characteristic peaks, the stretching of C-OH unoxidized graphitic domains skeletal vibrations, respectively. The peak at 1730 and 2361 cm^{-1} is confirmation of the stretching of the (C=O) carbonyl function group. The presence of the functional group such as C-O and C=O peaks, confirms the oxidation of graphite into GO as supported by literature (Guerrero-Contreras, Caballero-Briones 2015).

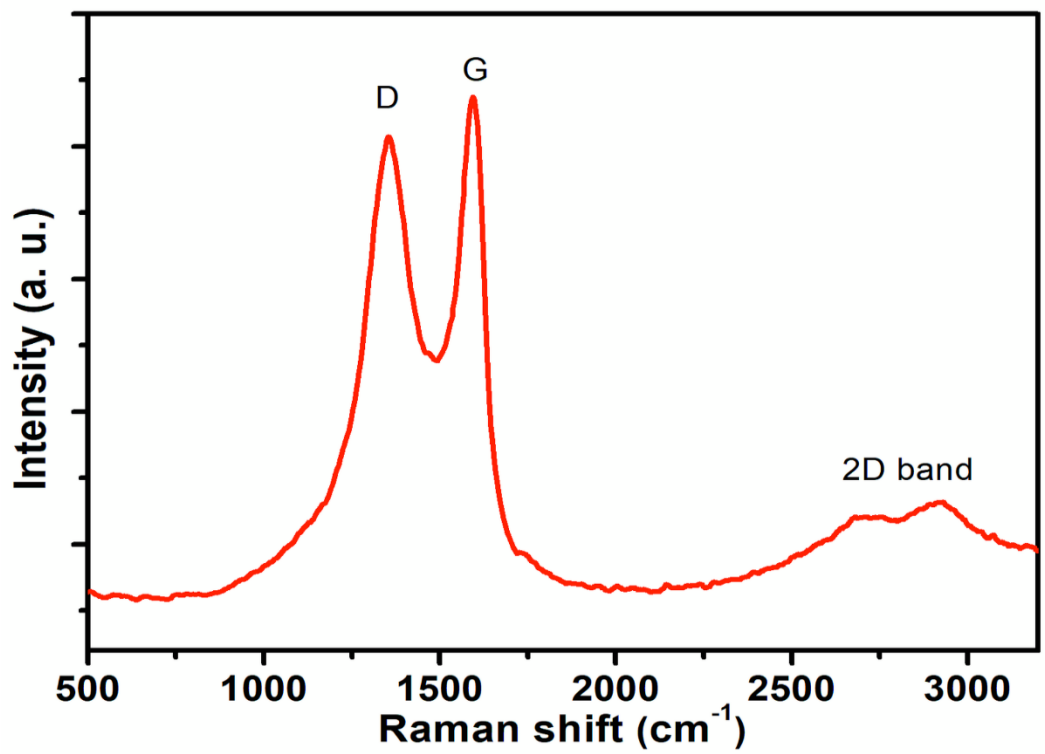


Figure 4-1: Raman spectroscopy of GO

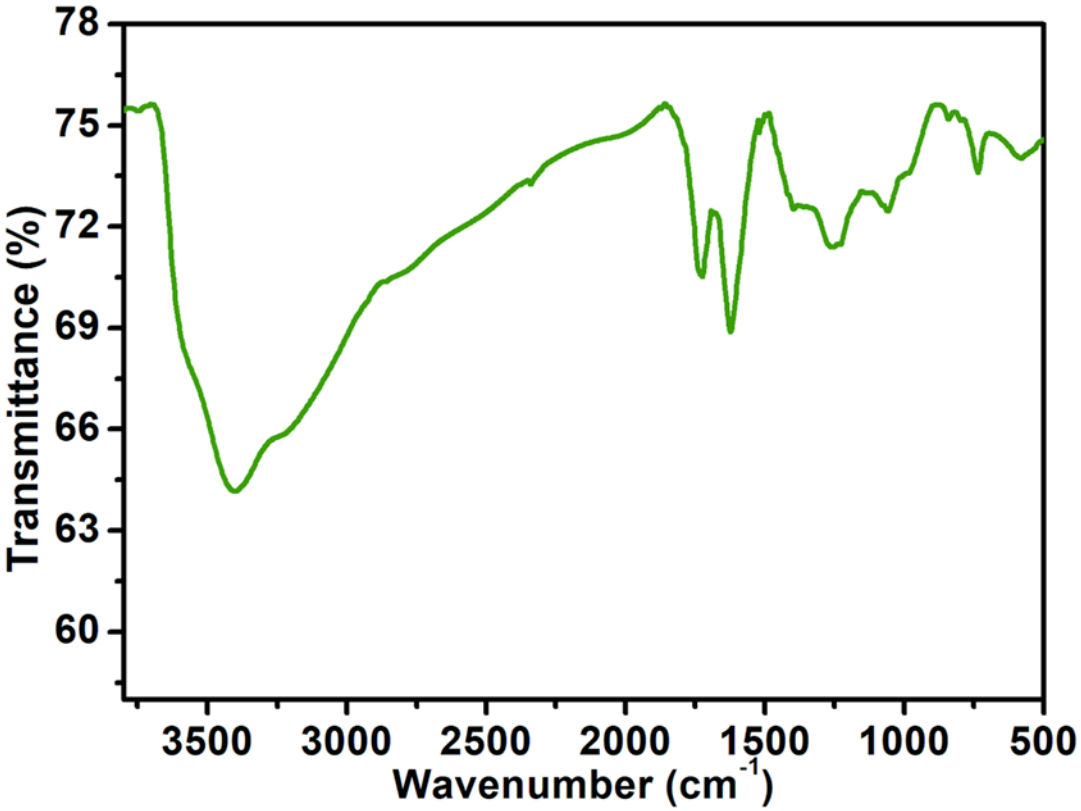


Figure 4-2: FTIR spectra of GO

According to literature (Lai et al., 2012), GO nanomaterials absorb light due to the $n \rightarrow \pi^*$ transition of a carbonyl group and $\pi \rightarrow \pi^*$ at approximately 300nm and 230 nm, respectively which is confirmed in **Error! Reference source not found.** which shows the UV-Visible spectra. As compared to other nanostructures, this promotes a more ordered structure due to the greater preservation of aromatic rings in the basal planes of GO.

The diffraction spectrum of GO inFigure 4-4 shows a peak at 10.44° which was found in the range of 2ɵ of 5 to 50°, this confirms the formation of GO nanosheets and further validates complete exfoliation and chemical reduction of graphite. It also indicated that the characteristic peak reported in the literature which shows the increase of the basal or d-spacing of 0,846 nm. Additionally, the diffraction peak relates to the (0 0 1) plane of GO (Muzyka, Kwoka et al. 2017).

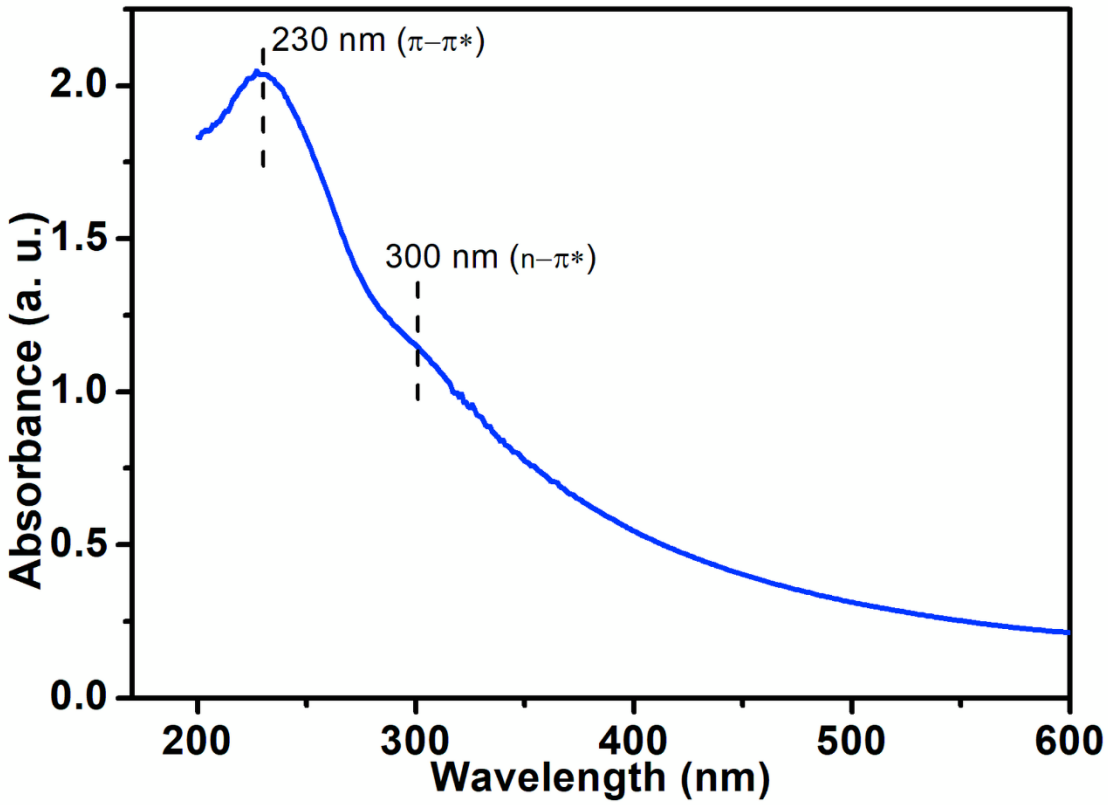


Figure 4-3 : UV-Vis spectra of GO

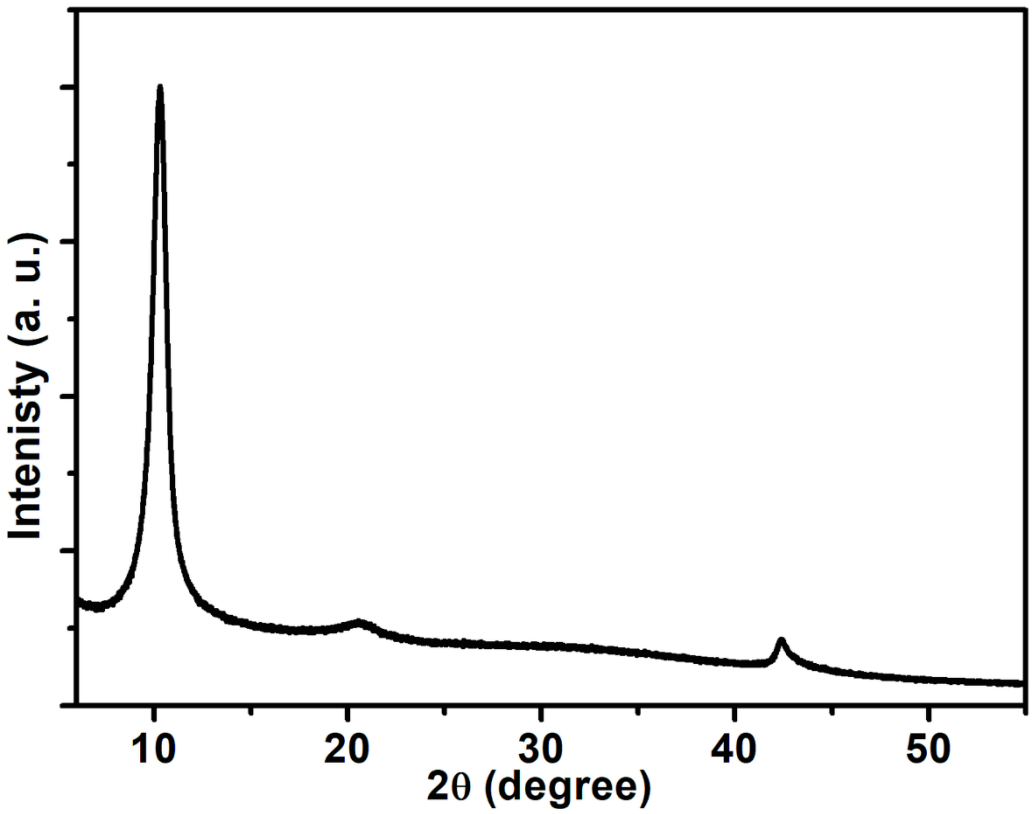


Figure 4-4: XRD pattern of GO.

The FESEM image in Figure 4-5(b), shows many oxygenated graphene flakes with wrinkled and rippled surface morphology with lateral sizes of the sheets which range from several hundred nanometers to microns (Al-Gaashani, Najjar et al. 2019)). **Error! Reference source not found.**(a) shows a TEM image of wrinkled GO which was formed when folding the nanosheets.

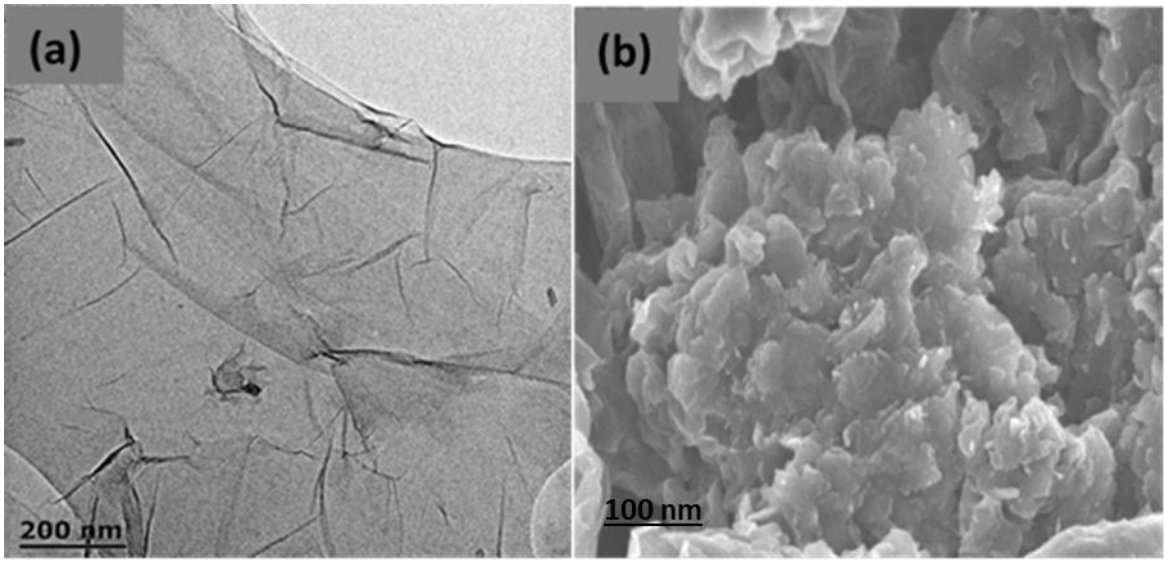


Figure 4-5 : (a) TEM image of GO and (b) FESEM images of GO.

Figure 4-6 represents the TGA and DTA curves of GO, it shows a mass loss in two stages – the dissociation of epoxy and hydroxyl functional groups at approximately 120 °C and 150 °C. The second mass loss is due to bulk pyrolysis of the carbon groups and the DTA curve is consistent with a weight loss curve. The sharp endothermic peak is observed at 150 °C and a broad peak at temperature 250 °c to 600 °c, an endothermic peak (Stankovich, Dikin et al. 2007).

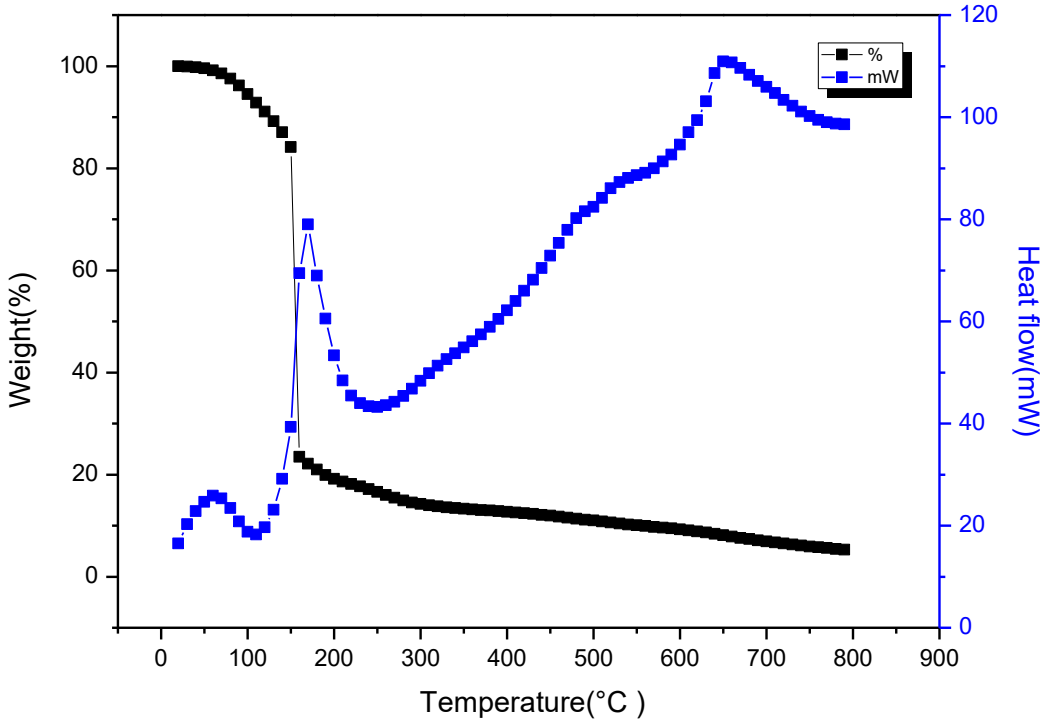


Figure 4-6: TGA and DTA curves of GO.

4.3.2. Rheological studies

Rheological properties of a screen-printable conductive ink influence its printing capabilities such as eliminating bubbles which often causes agglomeration and broad lines with rough edges and thus decrease electrical conductivity (Liang, Tong et al. 2016).The composition of additives used to formulate the ink, need to be considered because of the printable range that is controlled by the rheology of the inks. These additives are dispersant, binder and solvent ((O'Mahony, Haq et al. 2019). Figure 4-7 shows shear viscosity at various shear rate, using a steady-state flow test measurement. This is regarded as a shear shinning behavior which is important for a screen-printing ink (Lin, Chang et al. 2008), this means that when the shear rate increases, the ink becomes thinner, and it flows freely. This property of ink is crucial because during screen printing is the ability of the ink to go through the screen mesh using a squeegee and subsequently drawing pattern over the carrier substrate with good levelling. For the ink to be considered suitable for screen printing it must follow thinning behavior, this

ensures that the ink remains on the screen as it passes through the mesh during screen-printing (Ding, Liu et al. 2016)

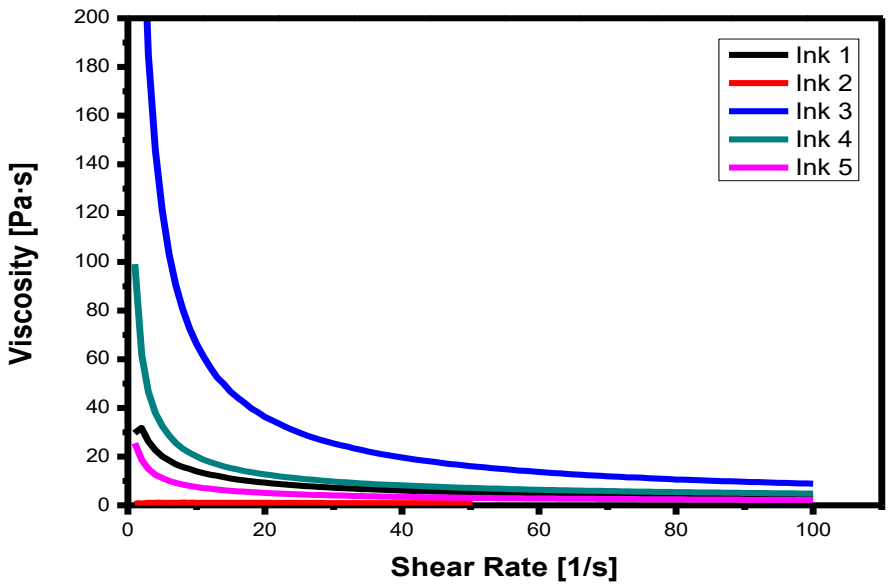


Figure 4-7: Rheological parameters of ink 1 to ink 5, the shear viscosity of the different inks as a function of shear rate.

The result depicts a pseudoplastic fluid when viscosity is decreasing as the shear rate increases, which will prevent the ink from smudging beyond boundaries ink after printing. The pseudoplastic behaviours are influences by organic binders and dispersants which assist in changing the screen-printing ink is dependent on the weight% (wt%) of the binder, not necessarily the concentration of the GO. Ink 1 has the lowest wt% of the binder and ink 3 which is the optimal ink used for printing has the highest viscosity. This means that the rheological behaviour of the ink is dependent on the wt% and the type of binder used, at it, follows the shear-thinning behaviour of the CMC binder. The viscosity of the ink decreases when the combination of the forces happens since it prevents particles from combining instead of breaking the particles with weak physical bonding. To further confirm the characteristic of pseudoplastic fluid. Figure 4-9 shows varying stress against strain to help understand the importance of the binder on the rheology of the screen-printing ink. For the different inks, the curves of shear stress shear strain at show clear elastic-plastic behaviour which can be attributed to the binder rheological behaviour. Viscosity of the ceramic filler to follow a pseudoplastic behaviour. Van der Waals forces and repulsive steric effect causes aggregation

of the suspended particles in the ink which influences pseudo-plasticity, the ink is a non-Newtonian fluid showing a shear-thinning behaviour (Ribeiro, Silva et al. 2013); (Bird, Armstrong et al. 1987)There are three distinct steps during screen printing that can be related to the changes in shear rate during the printing process. The initial step can be associated with the printing ink transfer onto the screen. It is characterised low shear rate and the ink is subjected to low deformation. The second step is during printing when the squeegee strokes onto the mesh surface and induces breakage to the structure of the ink under the shear rate of approximating the 1000 s^{-1}. The third step is where printing happens, levelling the ink onto the substrate and the squeegee returning to its initial state (Neidert, Zhang et al. 2008)simulated these printing steps and Figure 4-7 shows the viscosity evolution with regards to these steps, confirms the shear-thinning (Figure 4-8 as well) behaviour of the ink by decreasing viscosity (Neidert, Zhang et al. 2008).

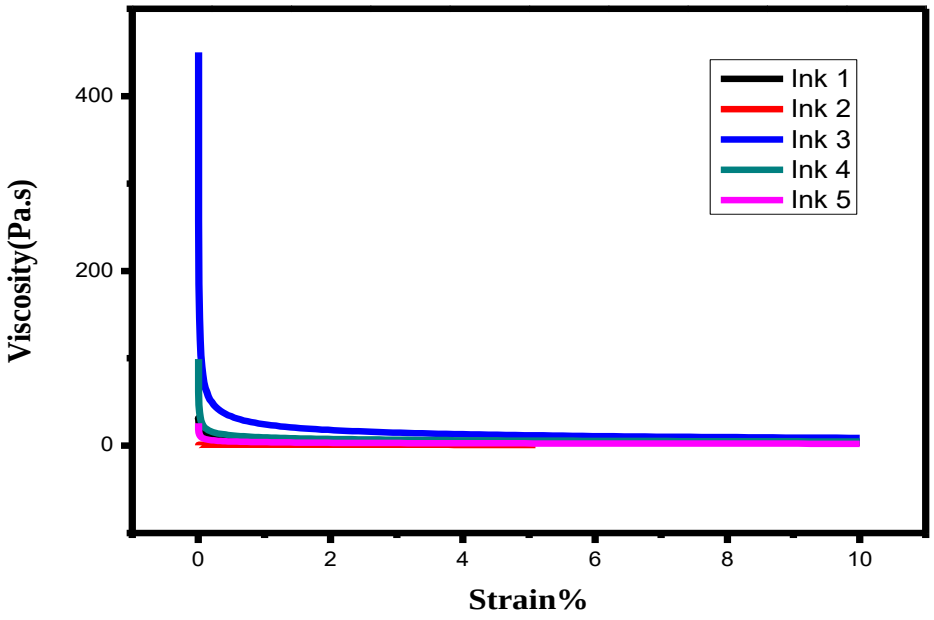


Figure 4-8 : Rheological parameters of ink 1 to ink 5 Shear viscosity of the different inks as a function of strain.

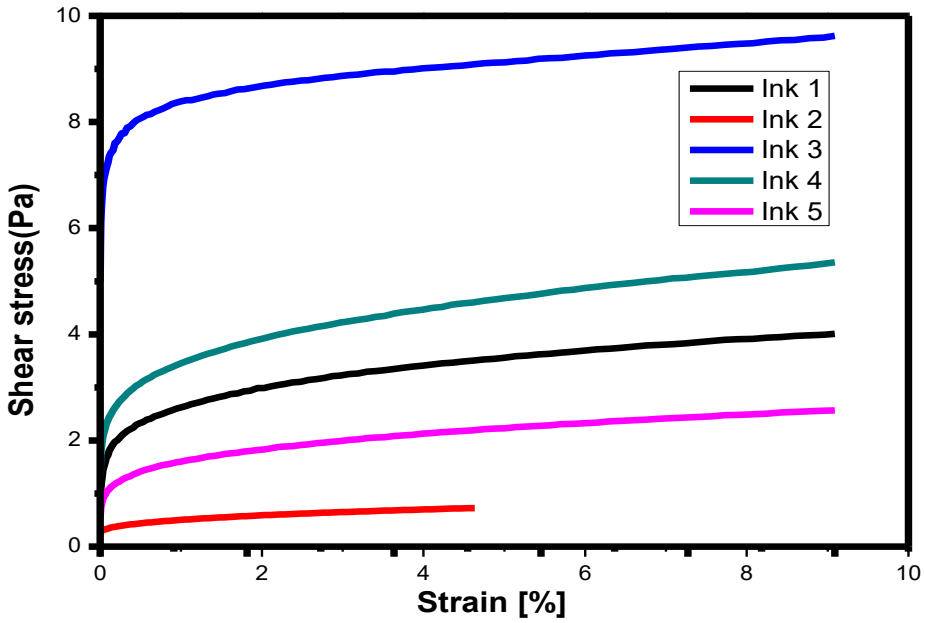


Figure 4-9: Rheological parameters of ink 1 to ink 5 shear stress of the different inks as a function of strain.

4.3.3. Thermographic analysis of the optimal ink

TGA performed on ink 3 is shown in Figure 4-10 ,for Ink 3 which is the optimal ink used in screen-printing, the initial mass loss occurs before 100 °C, which is related to residual water loss. The ink is stable until around 200 °C; after this temperature, further mass losses suggest the start of CMC degradation and after 350°C the mass loss is related to the decomposition of the carbon materials. the DTA curve has two exothermic peaks 50°C and around 200°C which may show the heat released during the decomposition of the binding material and the carbon material under inert environment (nitrogen).

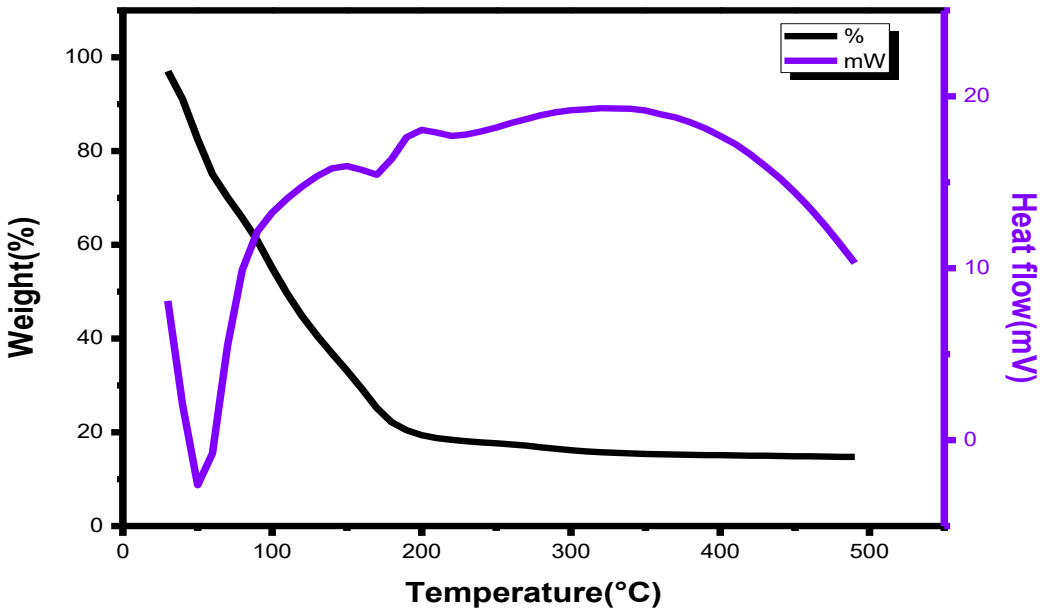


Figure 4-10: TGA and DTA curve for ink 3.

4.3.4. Polarized optical microscopy

The morphological studies were done on the ink samples using an optical microscope to investigate the dispersion behaviour of GO and MWCNTs in the formulation of the inks. Figure 4-11E shows that increasing sonication time and concentration of GO affects the dispersion. Adequate sonication helps exfoliates the GO and forms non-covalent networks which influence shear shinning behaviour thus an important rheological property concerning printing. The ink with less sonication time (Figure 4-11A which represents ink 1) shows the GO and MWCNTs were poorly dispersed, as evidenced by the aggregation and clustering of the fillers. Sonication remained constant for ink 3 and 4 to avoid nanofiller damage, although it has positive outcomes to dispersion as reported in the literature (Guo, Wang et al. 2013). The GO and MWCNTs showed dispersion became more homogenous in and aggregation and clustering were found to decrease (Li *et al.*, 2018). Another possibility is that glycerol promotes hydrogen bonding networks and thus can improve surface wettability. Hydrogen bonding complexes and higher surface wettability of GO /MWCNTs may stabilize the GO sheets in dispersion as well (Cao, Zhao et al. 2016).

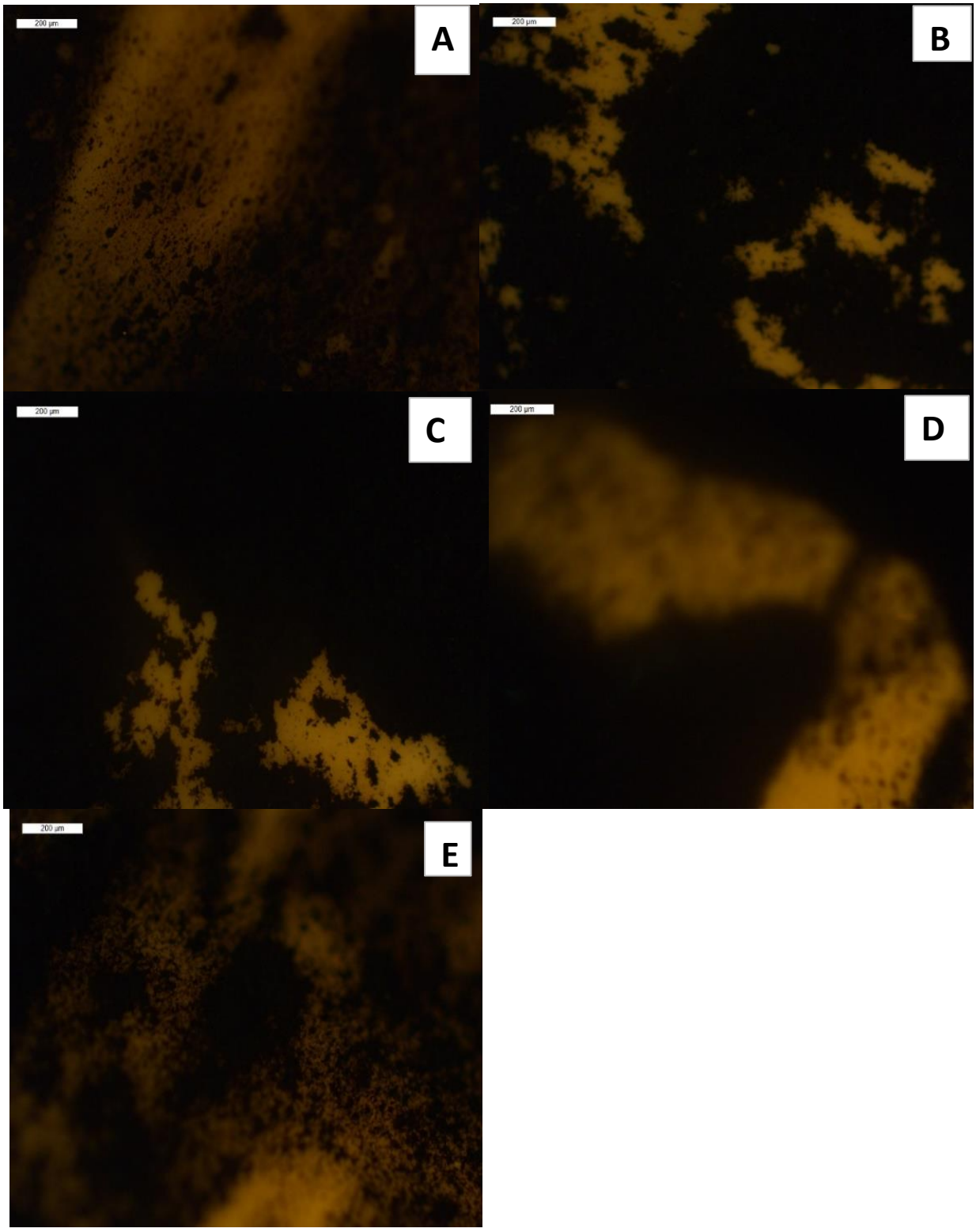


Figure 4-11: Polarized optical microscope of the different GO Ink: (A)Ink 1, (B) Ink 2 (C) Ink 3 (E)Ink 4 and (E)Ink 5.

4.3.5. Conductivity

When the printed layers are increased linearly the graphene oxide ink layer thickens, as shown in Figure 4-12 and the sheet resistance decreases with each added pass. The conductivity of the first layer is 5.0×10^4 Sm^{-1} and is it comparable to the synthesized conductive inks as summarised on Table 4-1. As more layers are printed, there is no significant change it is due to the addition of pattern density as more layers are added as shown in Figure 4-13. It is comparable with other conductivity patterns as depicted in Figure 4-13**Error! Reference source not found.**.

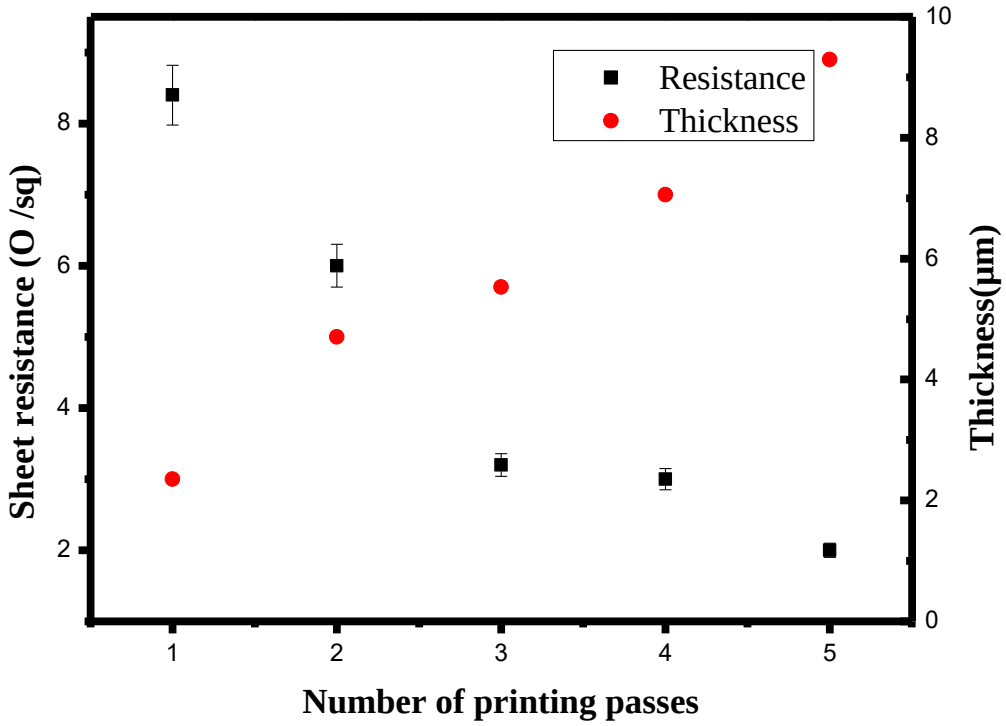


Figure 4-12: The sheet resistances and thickness of the printed GO ink with different printing passes.

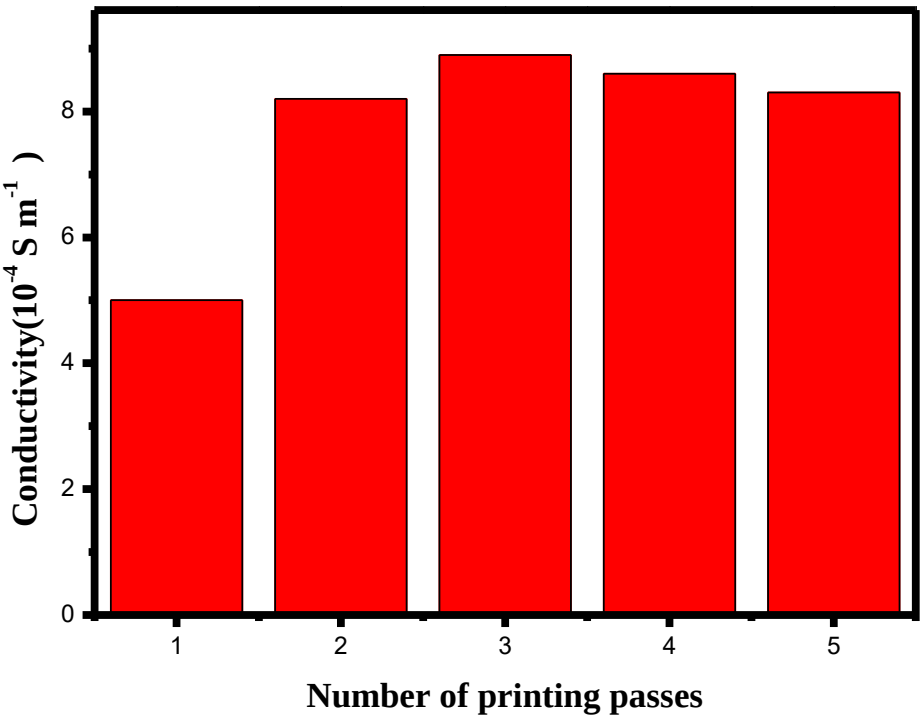


Figure 4-13: The conductivity of the printed GO ink with different printing pas

Table 4-1: Comparison of the various types of graphene inks and their electrical conductivity from literature.

2D materials	Solvents	Binders & additives	Substrates	Conductivity	Ref
Graphite	Glass Varnish/Solvent	-	paper and polyethene terephthalate (PET)	-	((Chen, Yang et al. 2021))
Graphene	Water	Na-CMC	Glass, paper		(Huang *et al.*, 2011)
GO and few-layered GO (FGO)	Water	-	Paper/ poly(ethylene terephthalate) (PET)/polyimide (PI),	$5{,}09\times10^{2}$ S/m and $9{,}09\times10^{2}$ S/m	(Pei and Li, 2017)
pristine GNP	Water	(hydroxypropyl)methyl cellulose	Glass	$3{,}9\times10^{4}$ S/m	(Majee *et al.*, 2017)
rGO	Water	-	Si/SiO_2 and glass substrates	$2{,}48\times10^{4}$ S/m	(He and Derby, 2017)
GO/MWCNTs	Water/Gycerol/Ethanol/Ethylene glycol	Na-CMC	Photo Pa	5.0×10^{4} S m^{-1}	This work

4.4. Chapter conclusion

This chapter presented the synthesis of GO-based ink and CMC as the binding material, for screen-printing application. The electrical conductivity was found to be approximately 5×10^4 S/m and factors such as the weight percentage of the binder and the sonication affected the viscosity and thus the screen-printing ability of the ink. To further characterise the ink, the uniformity of the ink, the resistance of the ink was studied with correlation to the number of printing passes and the width of the printed lines. The inks rheological behaviour shown that the inks covered the suitable printing properties associated with commercially available screen-printing carbon inks. This GO ink showed the potential to be used in the manufacturing of the next generation of low-cost paper diagnostics to advance the medical and environmental diagnostics of limited-resource areas.

4.5. References

1. Yazdi, A.A., Popma, A., Wong, W., Nguyen, T., Pan, Y. and XU, J., 2016. 3D printing: an emerging tool for novel microfluidics and lab-on-a-chip applications. *Microfluidics and Nanofluidics*, **20**(3), pp. 50.
2. Perinka, N., Kim, C.H., Kaplanova, M. and Bonnassieux, Y., 2013. Preparation and Characterization of Thin Conductive Polymer Films on the base of PEDOT:PSS by Ink-Jet Printing. *Physics Procedia,* **44**, pp. 120-129.
3. Han, J., Kim, B., LI, J. and Meyyappan, M., 2014. Carbon nanotube ink for writing on cellulose paper. *Materials Research Bulletin*, **50**, pp. 249-253.
4. Yang, W. and Wang, C., 2016. Graphene and the related conductive inks for flexible electronics. *Journal of Materials Chemistry C,* **4**(30), pp. 7193-7207
5. Tran, T.S., Dutta, N.K. and Choudhury, N.R., 2018. Graphene inks for printed flexible electronics: Graphene dispersions, ink formulations, printing techniques and applications. *Advances in Colloid and Interface Science,* **261**, pp. 41-61.
6. Zhang, L., Huang, Y., Zhang, Y., Fan, W. and LIU, T., 2015. Three-Dimensional Nanoporous Graphene-Carbon Nanotube Hybrid Frameworks for Confinement of SnS2 Nanosheets: Flexible and Binder-Free Papers with Highly Reversible Lithium Storage. *ACS Applied Materials & Interfaces,* **7**(50), pp. 27823-27830.
7. Hummers JR, W.S. and Offeman, R.E., 1958. Preparation of graphitic oxide. *Journal of the american chemical society,* **80**(6), pp. 1339.
8. Rattana, Chaiyakun, S., Witit-Anun, N., Nuntawong, N., Chindaudom, P., Oaew, S., Kedkeaw, C. and Limsuwan, P., 2012. Preparation and characterization of graphene oxide nanosheets. *Procedia Engineering,* **32**, pp. 759-764.
9. Guerrero-Contreras, J. and Caballero-Briones, F., 2015. Graphene oxide powders with different oxidation degree, prepared by synthesis variations of the Hummers method. *Materials Chemistry and Physics,* **153**, pp. 209-220.
10. Muzyka, R., Kwoka, M., Smędowski, Ł, Díez, N. and Gryglewicz, G., 2017. Oxidation of graphite by different modified Hummer's methods. *New Carbon Materials,* **32**(1), pp. 15-20.
11. Al-Gaashani, R., Najjar, A., Zakaria, Y., Mansour, S. and Atieh, M.A., 2019. XPS and structural studies of high-quality graphene oxide and reduced graphene oxide prepared by different chemical oxidation methods. *Ceramics International,* **45**(11), pp. 14439-14448.

12. Stankovich, S., Dikin, D.A., Piner, R.D., Kohlhaas, K.A., Kleinhammes, A., JIA, Y., WU, Y., Nguyen, S.T. and Ruoff, R.S., 2007. Synthesis of graphene-based nanosheets via chemical reduction of exfoliated graphite oxide. *carbon,* **45**(7), pp. 1558-1565.
13. Liang, J., Tong, K. and Pei, Q., 2016. A water-based silver-nanowire screen-print ink for the fabrication of stretchable conductors and wearable thin-film transistors. *Advanced Materials,* **28**(28), pp. 5986-5996.
14. O'mahony, C., Haq, E.U., Silien, C. and Tofail, S.A.M., 2019. Rheological issues in carbon-based inks for additive manufacturing. *Micromachines,* **10**(2), pp. 99.
15. Lin, H., Chang, C., Hwu, W. and Ger, M., 2008. The rheological behaviors of screen-printing pastes. *Journal of materials processing technology,* **197**(1-3), pp. 284-291.
16. Ding, J., Liu, J., Tian, Q., Wu, Z., Yao, W., Dai, Z., Liu, L. and Wu, W., 2016. Preparing of highly conductive patterns on flexible substrates by screen printing of silver nanoparticles with different size distribution. *Nanoscale research letters,* **11**(1), pp. 1-8.
17. Bird, R.B., Armstrong, R.C. and Hassager, O., 1987. Dynamics of polymeric liquids. Vol. 1: Fluid mechanics.
18. Ribeiro, H., Silva, W.M., Rodrigues, M.F., Neves, J.C., Paniago, R., Fantini, C., Calado, H.D.R., Seara, L.M. and Silva, G.G., 2013. Glass transition improvement in epoxy/graphene composites. *Journal of materials science,* **48**(22), pp. 7883-7892.
19. Bird, R.B., Armstrong, R.C. and Hassager, O., 1987. Dynamics of polymeric liquids. Vol. 1: Fluid mechanics.
20. Neidert, M., Zhang, W., Zhang, D. and Kipka, A., 2008. Screen-printing simulation study on solar cell front side AG paste, 2008, IEEE, pp. 1-4.
21. Guo, S., Wang, W., Ozkan, C.S. and Ozkan, M., 2013. Assembled graphene oxide and single-walled carbon nanotube ink for stable supercapacitors. *Journal of Materials Research,* **28**(7), pp. 918.
22. Cao, X., Zhao, N., Li, R., LV, H., Zhang, Z., Gao, A. and YI, T., 2016. Steric-Structure-Dependent Gel Formation, Hierarchical Structures, Rheological Behavior, and Surface Wettability. *Chemistry–An Asian Journal,* **11**(22), pp. 3196-3204.
23. Chen, K., Yang, Y., Yi, Y., Zheng, X. and Tuan, H., 2021. A carbon ink for use in thin, conductive, non-peelable, amphiphilic, antioxidant, and large-area current collector coating with enhanced lithium-ion battery performance. *Journal of Colloid and Interface Science.*
24. Huang, L., huang, Y., Liang, J., Wan, X. and Chen, Y., 2011. Graphene-based conducting inks for direct inkjet printing of flexible conductive patterns and their applications in electric circuits and chemical sensors. *Nano Research,* **4**(7), pp. 675-684.

25. Pei, L. and Li, Y., 2017. Rapid and efficient intense pulsed light reduction of graphene oxide inks for flexible printed electronics. *RSC advances*, **7**(81), pp. 51711-51720.
26. Majee, S., Liu, C., WU, B., Zhang, S.-. and Zhang, Z.-., 2017. Inkjet printed highly conductive pristine graphene patterns achieved with water-based ink and aqueous doping processing. *Carbon*, **114**, pp. 77-83.
27. He, P. and Derby, B., 2017. Controlling coffee ring formation during drying of inkjet printed 2D inks. *Advanced Materials Interfaces*, **4**(22), pp. 1700944.

CHAPTER 5: SCREEN-PRINTED PAPER ELECTRODE WITH GRAPHENE-OXIDE NANO-INK FOR ELECTROCHEMICAL APPLICATIONS.

This chapter presents the characterization of the fabricated screen-printed paper electrodes with ink formulated and synthesis of the g-C_3N_4. The characterization includes SEM studies and electrochemical studies. It also includes the electrochemical detection of heavy metals ions Pb^{2+} and Cd^{2+} using a paper-based electrode, commercial electrodes, and functionalised paper-based electrodes.

5.1. Introduction

The extensive industrialization of various sectors of various sectors has increased in factories and that has escalated environmental pollution (Anwar, Ahmad et al. 2020). The major contributor to water pollution especially heavy metal contamination is from factories and the mining sectors (Addo-Bediako, Rasifudi 2021) South Africa is a water-scarce country and the accumulation of heavy metals, or radioactive or toxic organic compounds being released into our waterways poses a major concern especially with the growth in population density and still most people without access to clean water (Binning, Baird 2001). At present, there is increased bioaccumulation and concentration of heavy metals in the aquatic ecosystems. As a result, the World Health Organization (WHO) has established an international regulatory body that has established standards for heavy metal levels in drinking water as well as an authorized standard for the number of heavy metals in effluent wastewater (Gumpu, Sethuraman et al. 2015). To achieve this aim, lab-on-chip technologies are being developed to employ miniaturized and compact electrochemical sensing capacity to provide low-cost instrumentation that is accessible and requires a limited sample volume, unlike the existing spectroscopic methods on the market (Solhi, Hasanzadeh et al. 2020).

Paper-based electrochemical devices (PEDs) are used in analytical applications because they have excellent properties including low prices, the ability to combine high-density detection, capillary action, disposable/biodegradable, porous, and biocompatible (Oliveira, Dias et al. 2018)

PEDs have allowed unskilled personnel access to this unit, which has been shown to have good sensitivity and only require a limited sample volume for analysis. PEDs are made using a variety of methods on various substrates. To date, screen printing, inkjet printing, photolithography, sputtering, and hand drawing have all been studied. Screen printing has been

used to create sensing devices on a variety of substrates, including paper (as examined in this study), ceramic, alumina, plastic, and glass. This method can print a variety of electrode and cell patterns, including single electrodes, standard three-or-more electrode cells, flexible electrodes, and flow cells, among others. It allows for a diverse range of applications (Barton et al., 2016). Since the electrode configurations on the device can be customized in a variety of ways, such as printing on a different surface, changing the geometry, scale, and shape, mass production is possible (Mishra, Nawaz et al. 2017).Electrode surface modification techniques are used to enhance stripping voltammetric techniques' selectivity, sensitivity, reproducibility, and electron transfer kinetics by increasing the electrode surface area. Mixing ink with nanomaterials, drop-casting of the desired nanomaterial or electrochemical deposition of a metallic precursor may all be used to modify the electrode surface (Li, Tao et al. 2018).The design of a paper-based three-electrode device for square wave anodic stripping analysis (SWASV) for the detection of Pb (II) and Cd (II) metal ions in water samples is presented in this chapter. To produce highly conductive electrode paper sensors, screen printing of graphene-oxide nanoparticle-based inks in combination with graphitic carbon nitride (g-C_3N_4) nanoparticles was used. SWASV analysis was used to electrochemically detect Pb (II) and Cd (II) metal ions in water using industrial, bare, and modified fabricated screen-printed paper-based electrodes.

5.2. Materials

5.2.1. Chemicals used.

All chemicals used in this chapter were used without further purification. Millipore, deionised water was used to prepare all solutions. Glacial Acetic acid, Sodium Acetate, Melamine, Potassium chloride, lead (II) nitrate, and cadmium (II) nitrate were bought from Sigma-Aldrich. The 0.1 M sodium acetate buffer at pH 4,5 was used as the supporting electrolyte. Commercial carbon screen-printed electrodes (DRP-110, DropSens) were purchased Metrohn,South Africa shown in Figure 5-2.

5.2.2. Paper-based SPE fabrication process

A DEK248 semi-automatic screen printer was purchased from Zetech, SA shown in Figure 5-1 was used to print the carbon layers using the formulated ink refer to chapter 4, conductive silver/silver chloride (Ag/AgCl) paste supplied by Gwent Group (Product number C2000215P4, Pontypool, UK), and the insulation layer using a dielectric ink (D210084202, Pontypool, UK) on a photo paper (NB-RC-3GR120) substrate purchased from Mitsubishi

Paper Mills Ltd., Japan. The printing process of the DEK 248 screen printer is controlled by the DEK printing machines 2.4.0 software programme. Screens were supplied by Chemosol (Pty)Ltd (Johannesburg, South Africa) and the mesh size of the screen stretched are 58 x 58cm. The paste was placed in a 6 cm ×6 cm × 2 mm stainless steel frame and cast using a squeegee (Squeegees and flood blades were purchased from DEK, UK) to form a smooth surface.

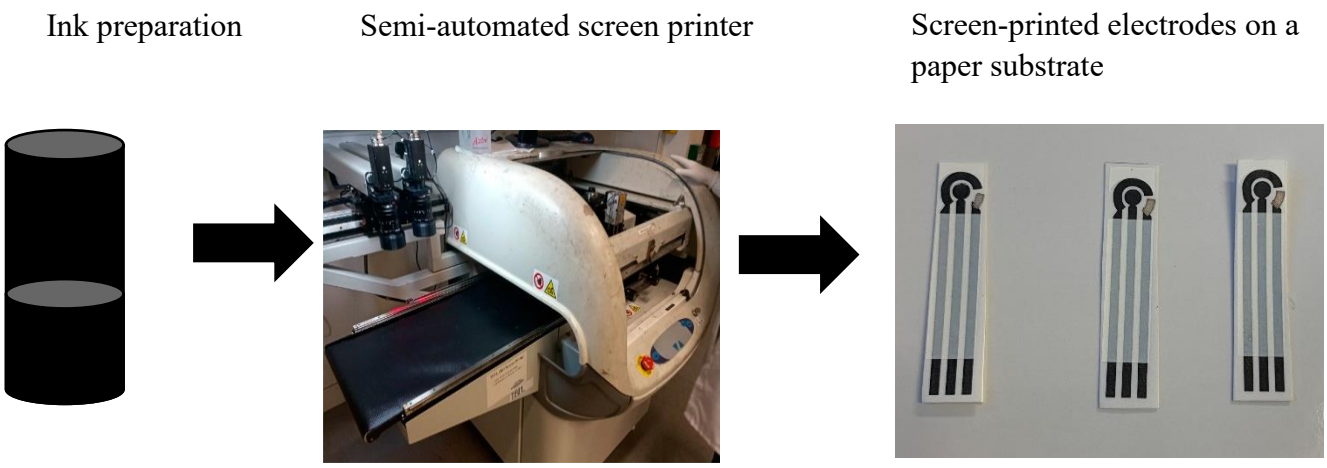


Figure 0-1: Screen -printing process using the DEK 248 semi-automated screen-printer.

5.2.3. Electrochemical measurements

Electrochemical characterization, cyclic voltammetry (CV) and square wave anodic stripping voltammetry (SWASV) analysis was done with a NOVA software (Eco Chemie, The Netherlands) and with the with the commercial sensor was connected to a potentiostat (Metrohm, Autolab PGSTAT101) as shown in Figure 5-2B and a screen-printed electrode sensor on a paper substrate as shown in Figure 5-2A.The design of the commercial SPEs were as follows, a carbon working electrode (4 mm diameter), carbon as counter electrode and Ag/AgCl reference electrode.

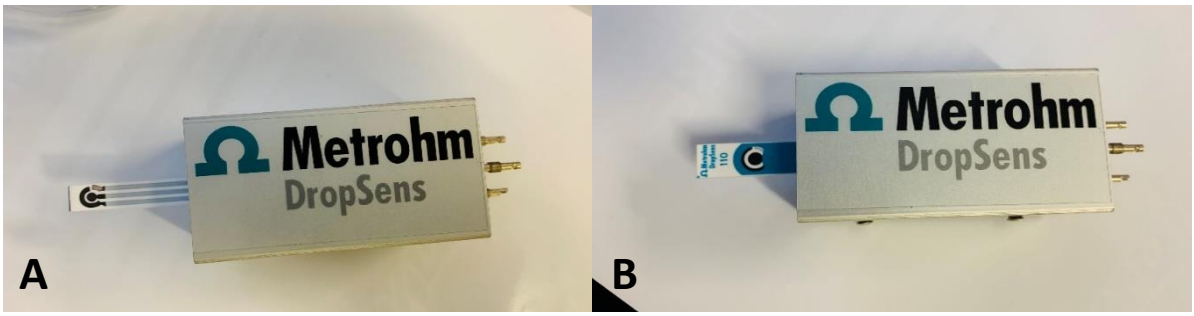


Figure 0-2: SPE connector to the potentiostat (A) SPE paper sensor and (B) DropSensTM C110 commercial SPE sensor.

5.2.4. Preparation of g-C_3N_4 nanomaterials

To prepare pure g-C_3N_4 nanosheets via a direct thermal polycondensation of melamine($C_3H_6N_6$). 5 g of melamine ($C_3H_6N_6$) was mixed with 7 mL of 32% nitric acid (HNO_3) in an alumina crucible. The mixture was placed in a furnace at a heating rate of 10°C/min to 550 ℃ calcination for 2 hours, to obtain a light-yellow polymeric g-C_3N_4 (Gao et al., 2017).

5.2.5. Measurement procedure - square wave anodic stripping voltammetry (SWASV)

Sodium acetate (0,1 M) was used as a supporting electrolyte at pH 4.5. No pre-treatment before the analysis of the working electrode surface. The stripping step using was done using square wave voltammetry (SWV) at a potential range of -1.4 V to 0 V, frequency of 15 Hz, increment potential of 4 mV and amplitude of 25 mV. The disposable sensors were only used for one measurement. A sample volume of 50 µL of different concentration of Pb (II) and Cd (II) with sodium acetate was drop cast on the surface of the electrode to take measurements. The calibration curves were created using the stripping peak current(µA) against the respective heavy metal ions concentration (Zheng, Ntuli et al. 2019) .

The wastewater sample was collected from the Hennops River, in South Africa. A 0.1 mol/L KCl solution of supporting electrolyte was prepared using the wastewater and adjusted the pH with acetic acid. The metal solution was spiked with the heavy metals ions, Pb (II) and Cd (II) to obtain concentrations of 30,50,70,90 and 110 mg/l. The solutions were subjected to the

anodic stripping electrochemical analysis and a calibration line was obtained amongst the concentration of Pb (II) and Cd (II) against anodic peak current.

5.3. Results and discussion

5.3.1. Morphological and topological Studies of the screen- printed paper-based electrode surface.

To study the functional groups, present on the surface of the electrode, FTIR spectroscopy was used. Figure 0-3 shows FTIR spectra for (in black), g-C_3N_4 (in red), GO/g-C_3N_4. The spectra of g-C_3N_4 show distinct peaks at 1230–1634 cm^{-1} which are attributed to the stretching of C-N heterocycles (Hu, Cai et al. 2015) and the stretching vibration of the triazine units is represented by the band at 808 cm−1. The GO/g-C_3N_4 on figure B shows both GO and g-C_3N_4 characteristic peaks at 729,1043,1043,1212,1409,1730 cm^{-1} which represents the epoxide functional group, C-O-C (alkoxy), C-OH, C-0 (epoxy), C=O vibrations (Gao, Wang et al. 2017).The wideband in the range of 3100–3500 cm^{-1} represents the -OH water molecule vibration and the primary and secondary amine. the stretching vibrations of C-N heterocycles and triazine (Niu, Zhang et al. 2012)are located at these peaks' positions 1234, 1316, 1401, 1572, 1634, and 808 cm^{-1}, respectively. Although the band in the range 3100–3500 cm^{-1} for g-C_3N_4 shows weak intensity compared to the GO/g-C_3N_4 surface which confirms the formation of GO/g-C_3N_4.

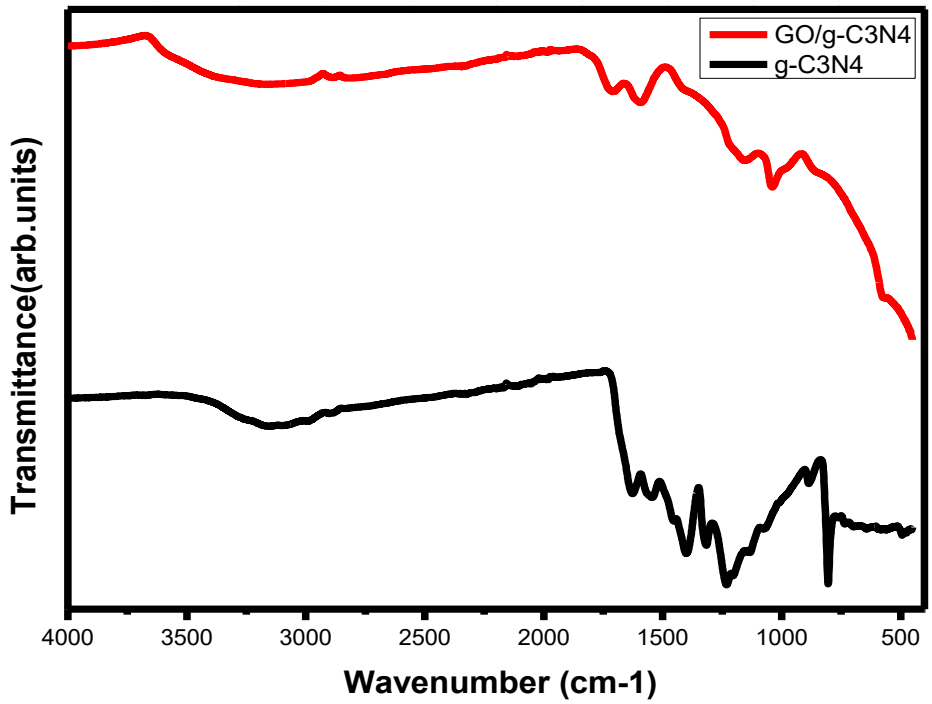


Figure 0-3: FTIR spectra of g-C_3N_4 and GO and the g-C_3N_4 electrode surface.

The surface morphology was further characterized by SEM, Figure 5-4 shows (A), g-C_3N_4 (B), GO/g-C_3N_4. Figure 5-4A shows an image of g-C_3N_4 silk-veil morphology with the layers of stacking graphitic planes. The SEM images of GO/g-C_3N_4 show bulk sheet structure enclosed with wrinkles from the GO structure. The strong functionalities of GO with g-C_3N_4 resulted in a unique electrode surface morphology (Li, Tang et al. 2019).

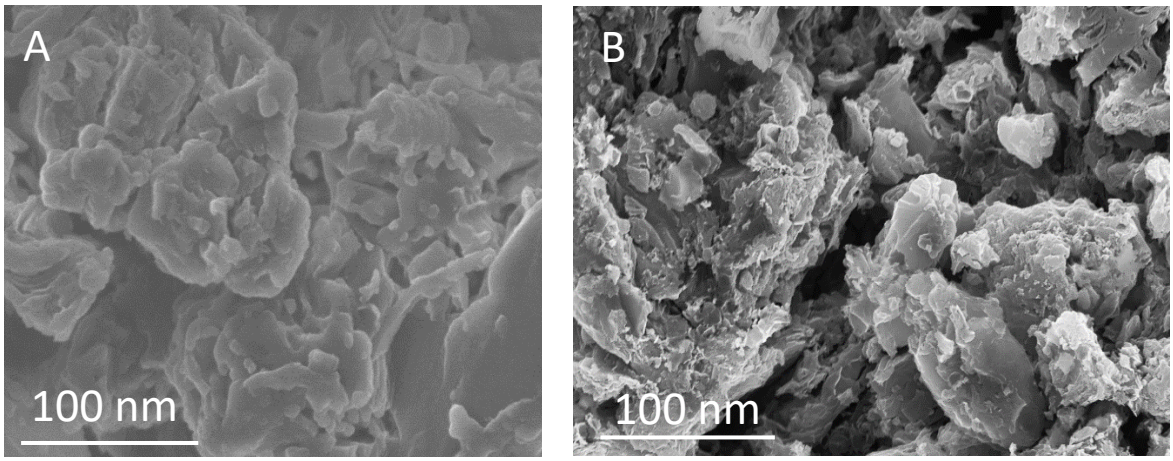


Figure 0-4: SEM images of (A) g-C_3N^4 and (B) GO and g-C_3N_4 electrode surface.

5.3.2. Cyclic Voltammetry

The cyclic voltammetry (CV) measurements were done using 5 mM $K_3[Fe(CN_6)]$ solution containing 1.0 M KCl as a supporting electrolyte. CV scan shown in Figure 0-5 was achieved by a scan rate of 0.1 V/s. and sweeping the potential from 1.0 to −1.0 V. The results in Figure 0-5 show an anodic peak for the forward scan when the potential is varied from −1.0 to 1.0 V and the maximum current was reached when the applied potential was + 0,5 V. The electrode becomes strong oxidation when $Fe(CN)_6^{4-}$ to $Fe(CN)_6^{3-}$ oxidation happens. For the backward scan, the cathodic peak from 1.0 to −1.0 V happens due to the reduction of $Fe(CN)_6^{3-}$ to $Fe(CN)_6^{4-}$ and maximum reduction current was achieved when the potential was −0.3 V.

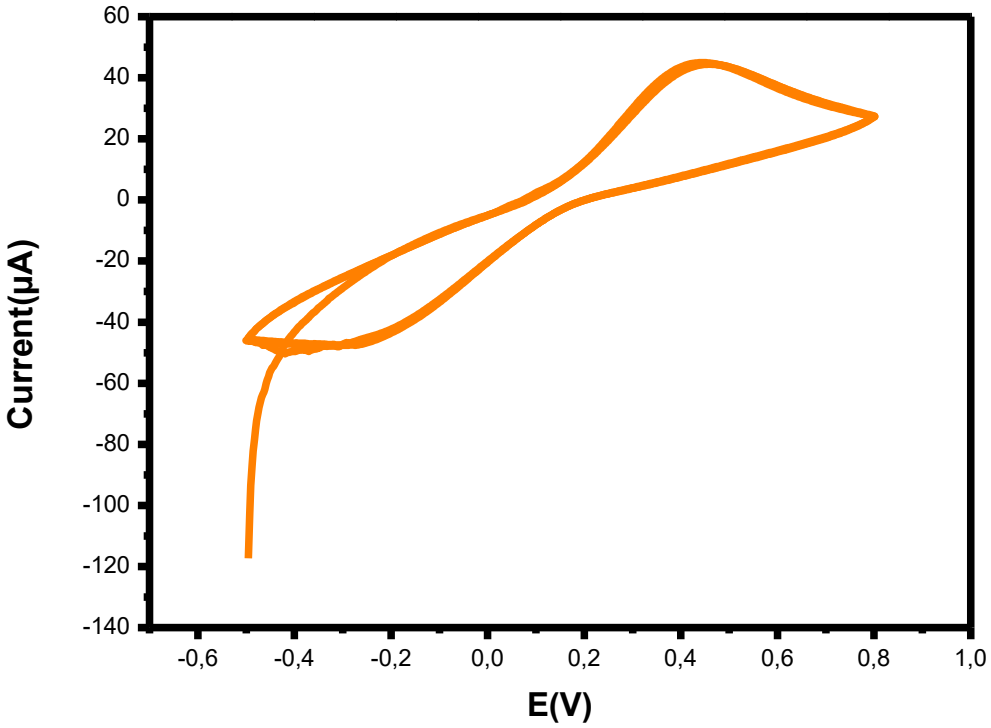


Figure 0-5: Cyclic voltammograms of SPE on the paper substrate in 5mM K3Fe (CN)6 in 0.1 M KCl at a scan rate of 100 mV/s.

Comparing the bare electrodes with the modified electrodes, they showed a lower current density which can be attributed to the reduced conductivities of g-C_3N_4 and GO materials on SPEs as shown in Figure 0-6 . It also showed well defined peaks for all the electrodes.

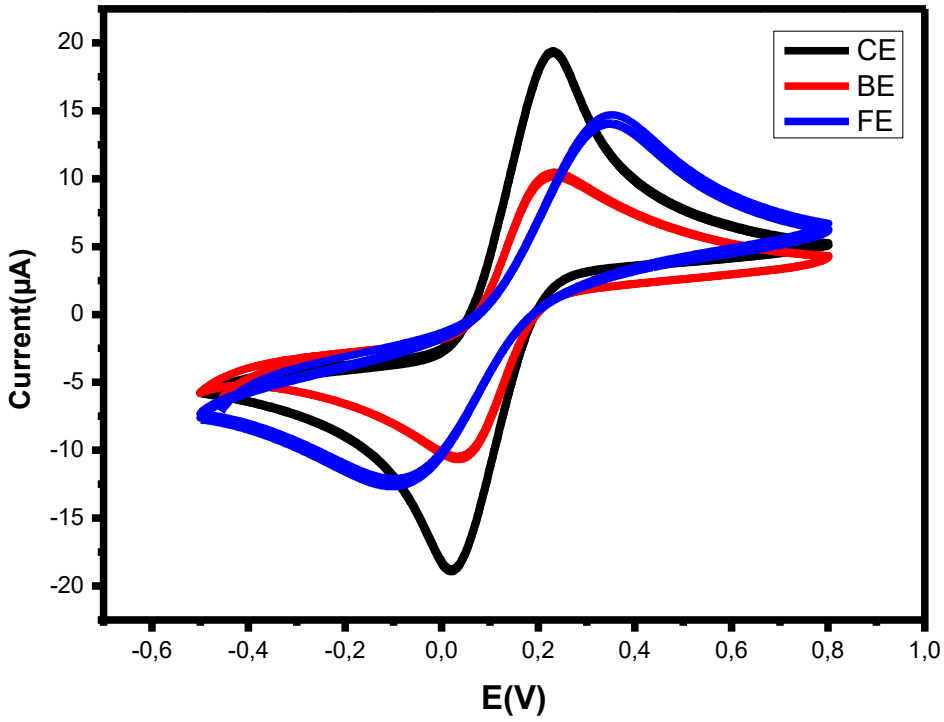


Figure 0-6: Cyclic voltammogram of commercial electrode sensor (CE), bare paper-based electrode sensor (BE) and functionalised electrode sensor (FE) in 5mM K3Fe (CN)6 in 0.1 M KCl at scan rates 100 mV/s.

5.3.3. Effects of different scan rate.

The cyclic voltammograms were done in a solution containing 5 mM ferrocyanide/ferricyanide using the g-C_3N_4 functionalised SPE at a potential scan rate of 100 to 500 mV. s^{-1} as shown in Figure 0-7. Figure 0-7 shows that when increasing the scan rate from 100 to 500.0 mV s^{-1}, the redox peak currents increased similarly with the movement of the redox peak potentials. The peak current (i_p) increases with the scan rate, and the reduction and oxidation peak voltages shift to more negative and positive values, respectively.

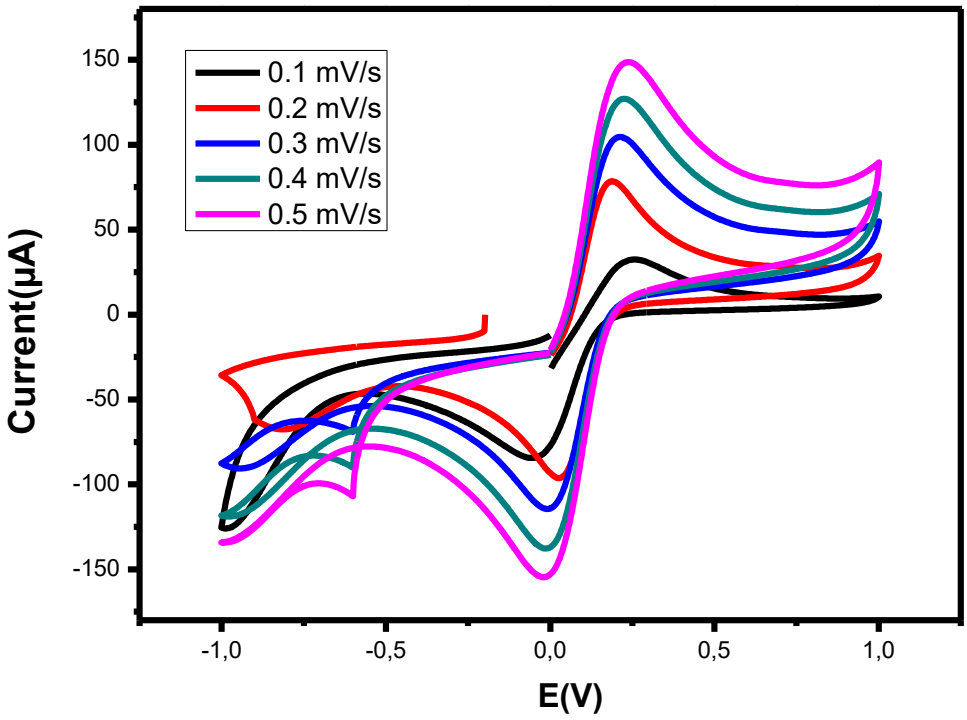


Figure 0-7: Cyclic voltammograms of functionalised with g-C_3N_4 electrode sensors in 5mM K3Fe (CN)6 in 0.1 M KCl at scan rates of 100 to 500 V/s.

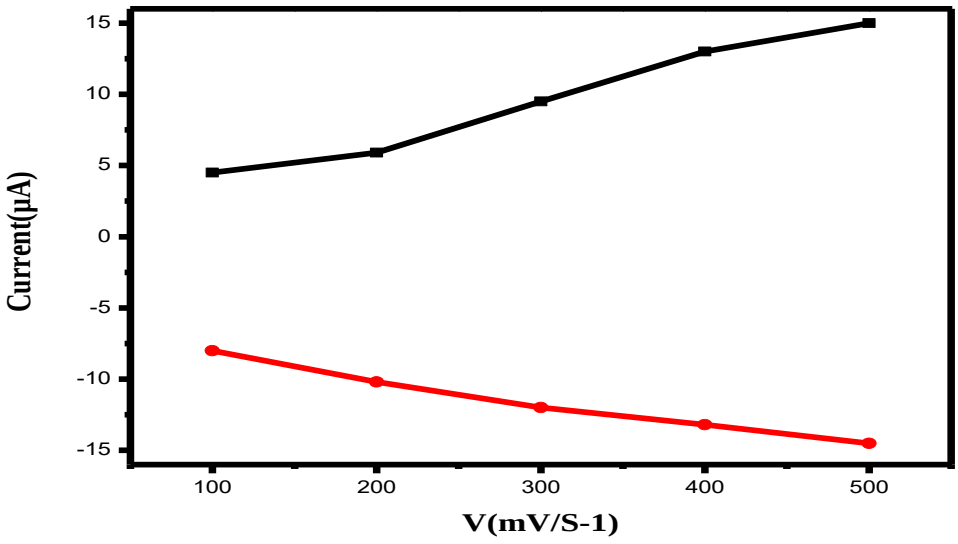


Figure 0-8: Linear relationship of the redox peak current (Ip) versus V.

Good linear relationship between the redox peak currents (Ip) and scan rate (υ) were plotted in Figure 0-8 with two regression equations as Ipc (μA) = 2,4υ + 0.24 (γ = 0.96396) and Ipa (μA) = -7υ – 0,016 (γ = -0.9403), indicating an adsorption-controlled electrode process. The scan rate was varied from 0.1 V s^{-1}up to 0.5 V s^{-1}, as presented in Figure 0-7. The results show that functionalising with g-C_3N_4 improves electron transfer and that electrodes surface have been successfully modified with g-C_3N_4 nanomaterials. The surface of the electrode containing oxygen groups of -OH and -COOH from the GO ink improved the surface wettability and indirectly causing electrochemical accessibility of the ions to the surface of the working carbon electrode (Trick, Song et al. 2017 ;Zhang, Liu et al. 2019).

Table 0-1: Recommended values from EPA and WHO on the accepted limits of heavy metals in drinking water(Sawan *et al.*, 2020).

Heavy metal	Recommended values from EPA in drinkable water (mg/l)	Recommended values from WHO in drinkable water (mg/l)
Arsenic	0,01	0,01
Cadmium	0,03	0,03
Chromium	0,05	0,05
Copper	2	2
Lead	0,01	0,01
Mercury	0,006	0,001
Nickel	0,07	0,02

5.3.4. SWASV detection of Pb (II) and Cd (II) – A comparative study between commercial SPEs and fabricated paper-based SPEs.

The wastewater sample was collected from the Hennops River, in South Africa, A 0.1 mol/l KCl solution of supporting electrolyte was prepared using the wastewater and adjusted the pH. The metal solution was spiked with the heavy metals, Pb (II) and Cd (II) to obtain concentrations of 30,50.70,90 and 110 mg/l.

The solutions were subjected for the anodic stripping electrochemical analysis and a calibration line was obtained between the concentration of Pb (II) and Cd (II) against anodic peak current. For each disposable SPE,one tests was carried for the different concentrations of Cd (II) or Pb (II). The limit of detection (LOD) was calculated using the equation below:

$$\text{LOD} = \frac{3.3\sigma\text{B}}{\text{b}} \quad \text{Equation 6}$$

Limit of detection

Where σ_B is the population standard deviation of the signals and b is the slope of the peak height vs. concentration (Zheng *et al.*, 2019).

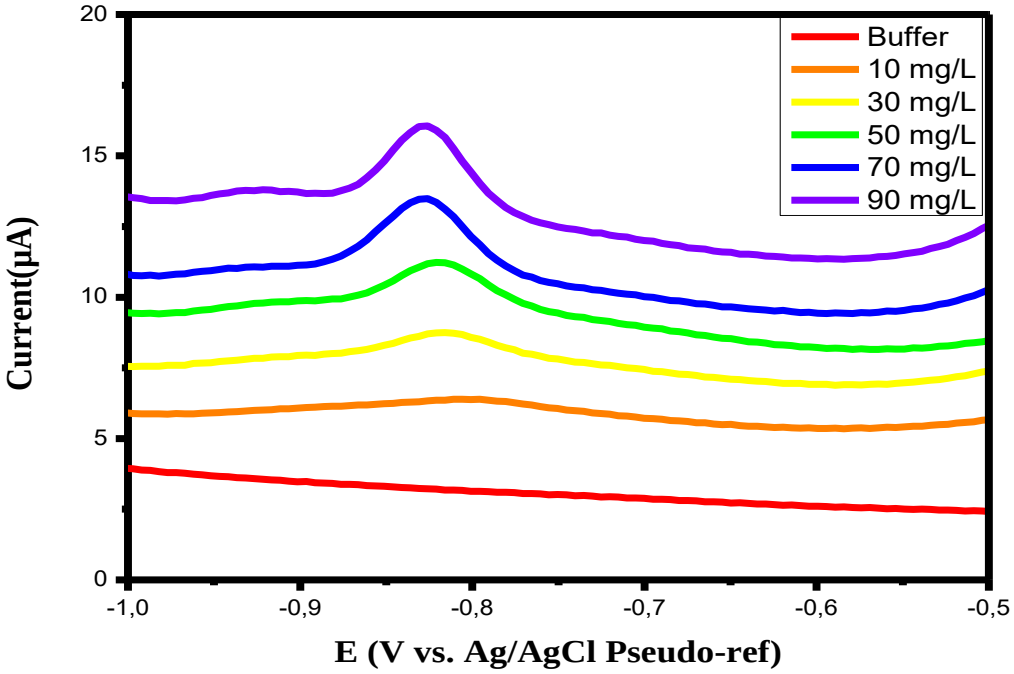


Figure 0-9 :SWASV signals for different concentration of Cd (II) Potential vs. Ag/AgCl (0.1 mol/LKCl and pH 4,5) using the bare paper based SPEs.

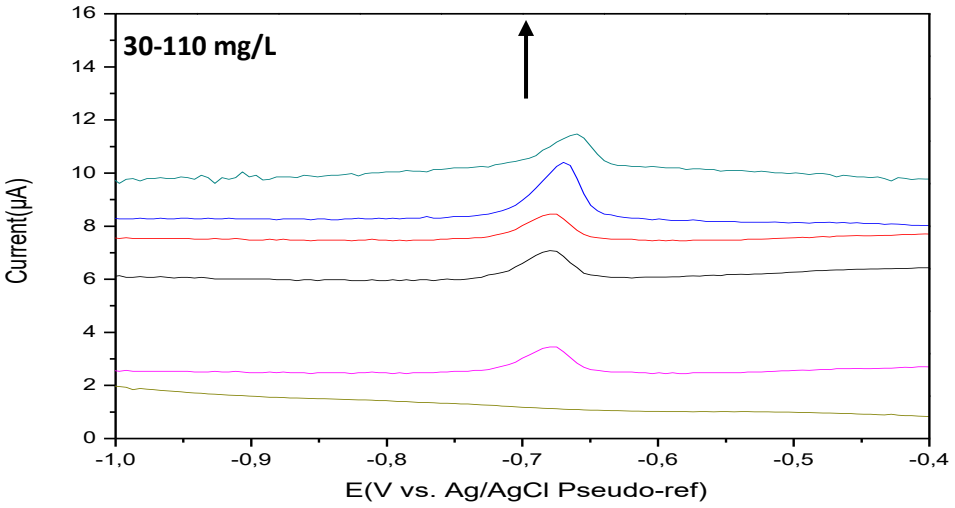


Figure 0-10: SWASV signals for different concentration of (a) Pb (II) Potential vs. Ag/AgCl (0.1 mol/LKCl and pH 4,5) using the bare paper based SPEs).

The SWASV responses for Cd (II) and Pb (II) on bare paper based SPEs were performed with increasing metal ion concentration Figure 0-9 and Figure 0-10 show the SWASV response curves for Cd (II) for concentrations between 30 to 110 mg/l and a slightly skewer curve for Pb (II) responses. The linear equations were (a) Ipa (µA) = 6,84-0,06x(mg/l) (R^2=0,8128 for cadmium ions) and (b) Ipa (µA) =0,0096+1,554x(mg/l) (R^2=0,42846 for lead ions). The detection limits were calculated to be 58,13 mg/l and 90,99 mg/l for Cd^{2+} and Pb^{2+} ions, respectively.

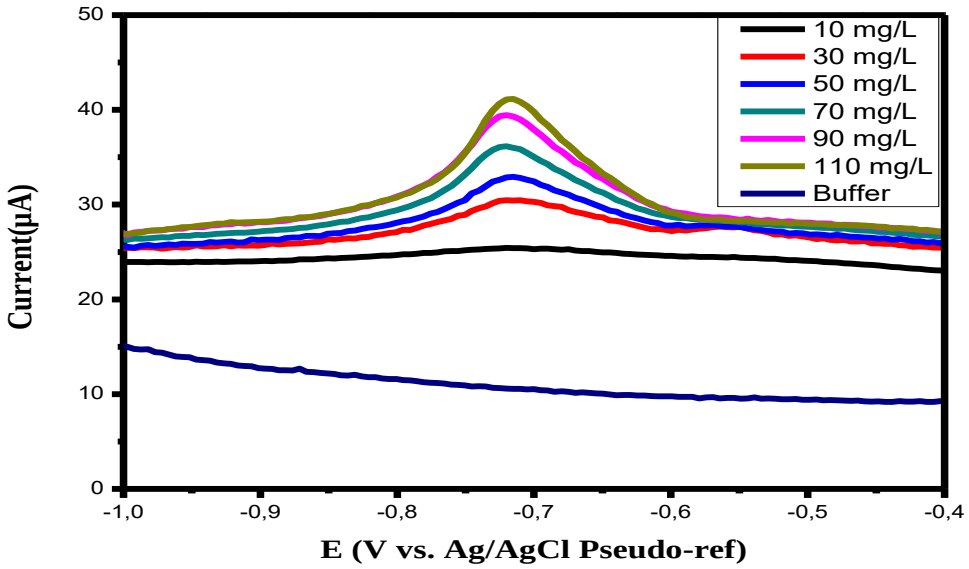


Figure 0-11: SWASV signals for different concentration of Pb (II) Potential vs. Ag/AgCl (0.1 mol/LKCl and pH 4,5) using the commercial SPEs.

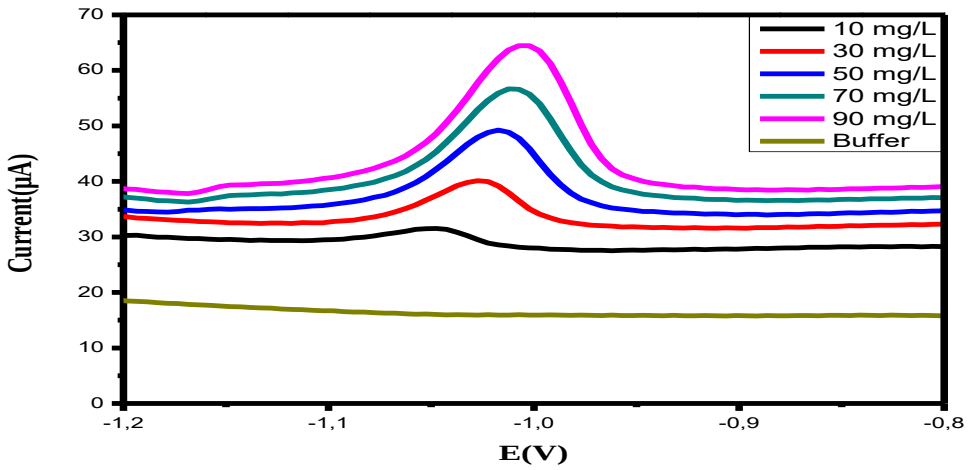


Figure 0-12: SWASV signals for different concentration of Cd (II) Potential vs. Ag/AgCl (0.1 mol/LKCl and pH 4,5) using the commercial SPEs.

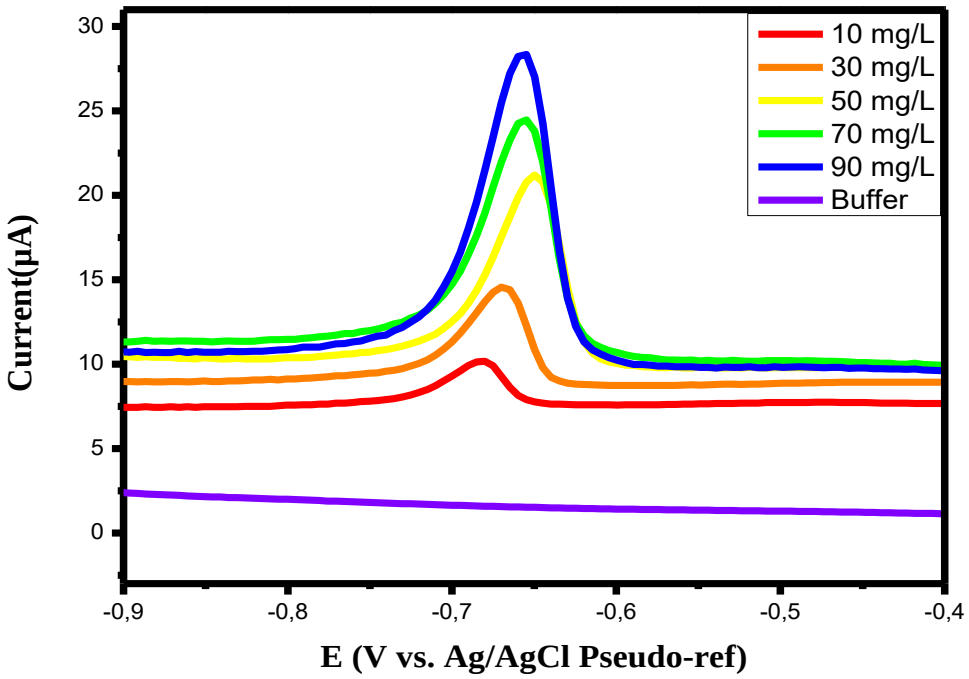


Figure 0-13: SWASV signals for different concentration of Pb (II) Potential vs. Ag/AgCl (0.1 mol/LKCl and pH 4,5) using functionalised g-C_3N_4 paper based SPEs.

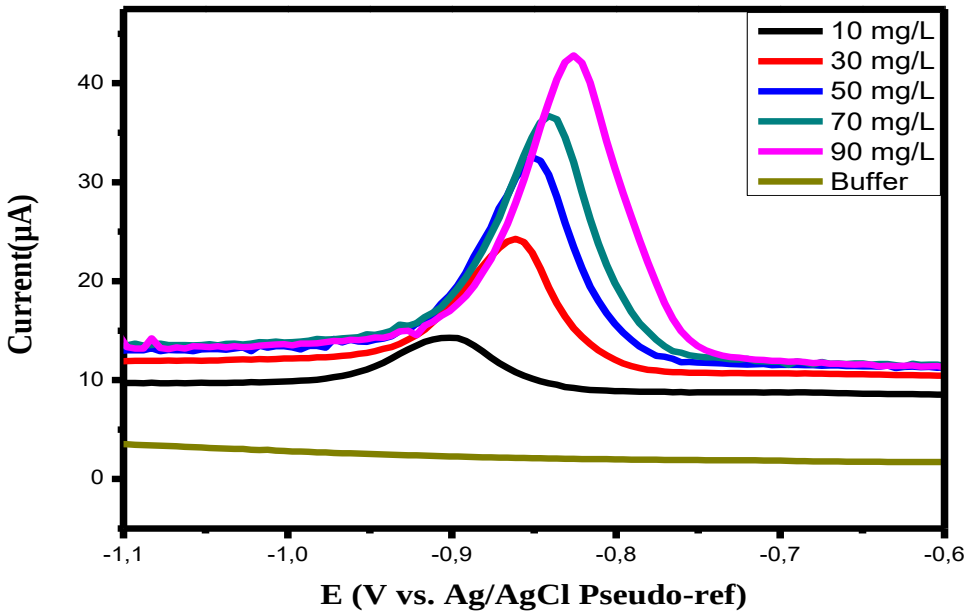


Figure 0-14 :: SWASV signals for different concentration of (a) Cd (II) Potential vs. Ag/AgCl (0.1 mol/LKCl and pH 4,5) using functionalised g-C_3N_4 paper based SPEs.

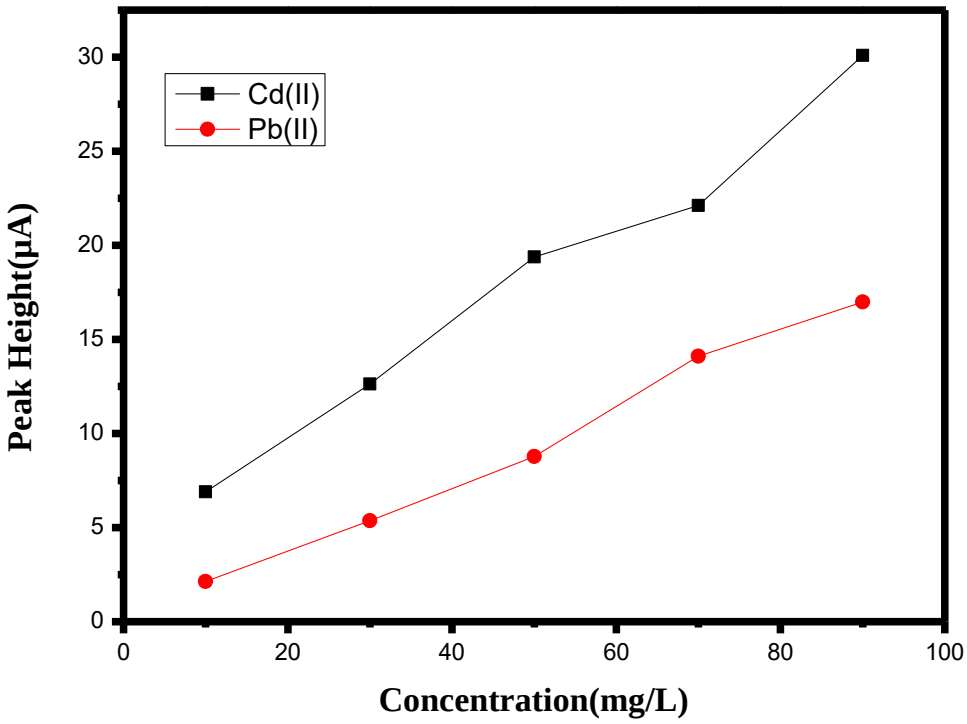


Figure 0-15: Calibration curves for Cd (II) and Pb (II) concentration range 10 to 90 mg/l.

Figure 0-15 presented the stripping currents growth with the increasing of concentration of Cd (II) and P(II). The current showed two linear relationships as Cd (II) and Pb (II)varying in the concentration of 30-90 mg/l: y = y = 0,0559x + 1,4617(Cd^{2+}, R^2 = 0.9761, LOD=0,16 mg/l) and y = y = 0,0385x - 2,0616(Pb^{2+}, R^2 = 0.9803, LOD=0,79 mg/l). The LODs were lower than those found for the unfunctionalized commercial SPEs(shown in figures Figure 0-11 and Figure 0-12) and the bare paper SPEs and was found to be within acceptable limits of the WHO standards.

Table 0-2: Screen-printed paper electrochemical sensors various heavy metals detection ((Yáñez-Sedeño, Campuzano and Pingarrón, 2020).

Nanomaterials	Detection methods	Linear range	Detection limit	Ref.
Carbon black ink/filter paper subtrate	SWV	0.1–0.9; 1–50 μM	0.03 μM	(Jemmeli *et al.*, 2020)
CNTs/Chit/SDS/cellulosic paper with electrodeposited Bi	SWASV	10–200 ppb	6.74 ppb	(Wang *et al.*, 2019)
G/CNTs/ionic liquid/cellulosic paper with electroplated Bi	SWASV	1–50 μg L^{-1}	0.2 μg L^{-1}	(Figueredo, Jesús González-Pabón and Cortón, 2018)
g-C_3N_4/Photo paper	SWASV	10-110 mg/L	-0.16 mg/l Cd(II) 0.79 mg/l Pb (II)	This work

5.3.5. Simultaneous detection of Pb (II) and Cd (II) with functionalised paper based SPEs.

The SWASV characterization (shown in Figure 0-13 and Figure 0-14) was further performed to detect simultaneous determination of Cd (II) and Pb (II). Figure 0-16 show the SWASV responses of the SPEs functionalised with g-C_3N_4 towards the detection of Cd (II) and Pb (II) at different concentrations. Cd (II) and Pb (II) are detected at potentials of −0.85 and −0.65V, respectively.

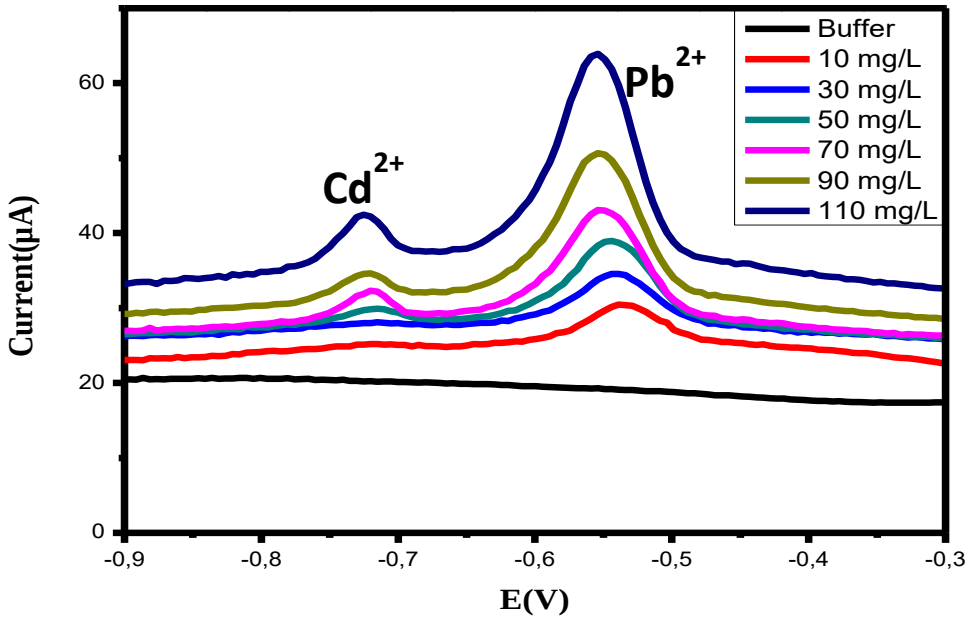


Figure 0-16: SWASV signals for simultaneous detection of (a) Pb (II) and (b) Cd (II) Potential vs. Ag/AgCl (0.1 mol/l KCl and pH 4,5) using the bare paper based SPEs with 2 minutes deposition time.

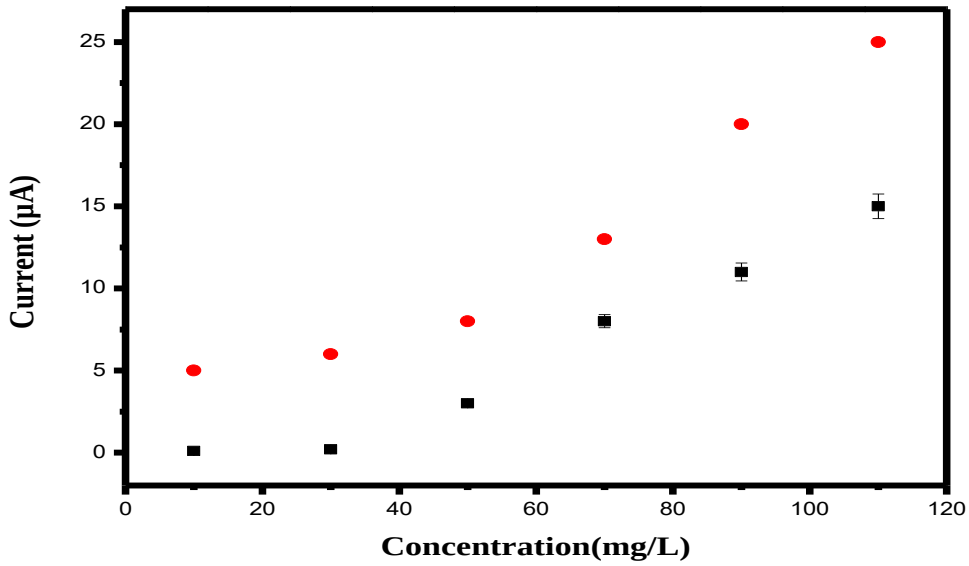


Figure 0-17: Calibration curves for Cd (II) and Pb (II) concentration range 10 to 110 mg/l.

Figure 0-16 show the SWASVs of simultaneous detection of Pb (II) and Cd (II)with different deposition time. The SWASV plots confirmed that the volume concentration of Pb (II) and Cd (II) with concentration ranging from 30 to 110 mg/l (linearly fitting equation Ipa (μA) =0,21*x* +0,2333, Pb^{2+}, R^2 = 0.945, LOD=31,60 mg/l). and Ipa (μA) = 0,15966*x*-3,37476(Cd^{2+}, R^2 = 0.916, LOD=79,41 mg/l) is linearly proportional to the peak current density.

Comparing to other similar studies using modified materials to detect trace Pb (II) and Cd (II) in water, the different parameters of detecting the metals ion while functionalising the surface of the electrodes with different graphene composites are listed in Table 0-2, together with the LODs and the concentration range used in the studies. The current g-C_3N_4 modified electrode has noticeable advantages in Pb (II) and Cd (II) detection. As shown in Figure 0-17, when Pb (II) and Cd (II) were simultaneous, the linear relationships towards them was acceptable and that the presence of the two metal ions did not affect/interfere with the individual detection.

5.3.6. Detection of Cd (II) in spiked wastewater sample.

Table 0-3: Physico-chemical analysis of the wastewater sample used.

Parameters Studied	**Analytical Results**
pH	7.78
Conductivity	109 mS/cm
Resistivity	0.000092 Ω·m
Salinity	0.06 PSU
Oxidation Reduction Potential	221.8 mV
Elemental analysis (AAS)	(mg/L)
Cd	0.0
Pb	0.0
Ni	0.0
Ca	7.021
Fe	0.520
Cu	0.0
Zn	0.322
TOC Analysis	(mg/L)
Inorganic Carbon	9.290
NPOC	0.0010

An extensive analysis of the wastewater in Table 5-3 samples was done to establish the suitability, selectivity and feasibility of the analytical method and physico-chemical properties. The results in Table 0-3 show that water is free of certain heavy metals; however, it has traces of Ca, Zn and Fe and the high value of inorganic carbon and NPOC was found in the water sample. The wastewater was spiked with different concentrations of Cadmium (II) at pH 4,5 in 0.1 mol/l KCl as a supporting electrolyte and the SWASV analysis was done, and results are shown in Figure 0-18.

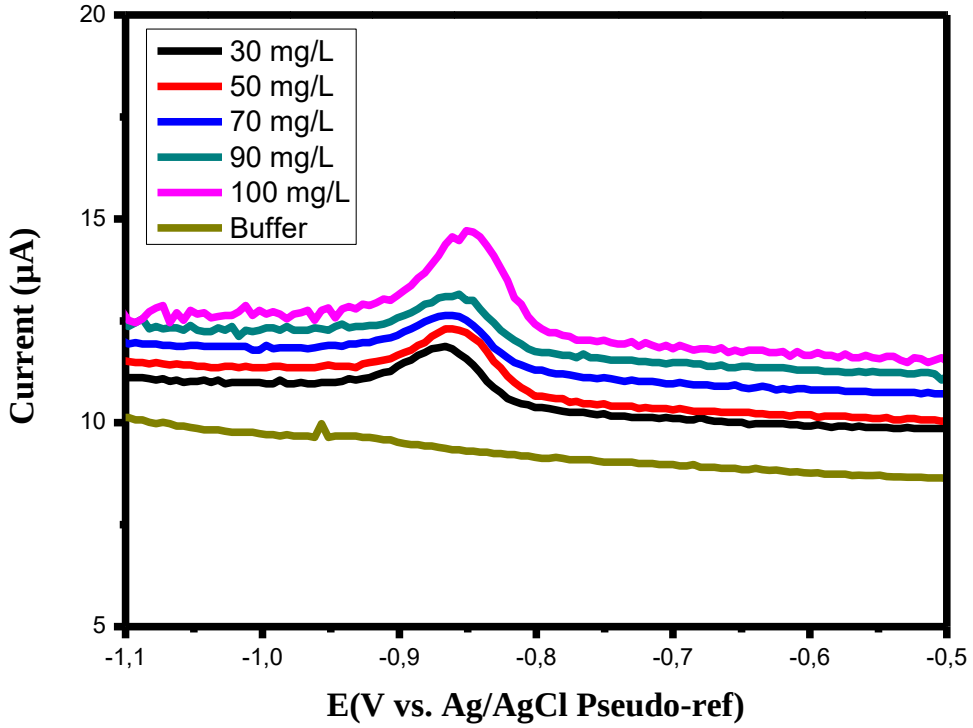


Figure 0-18: SWASV studies for various concentrations of Cd (II) wastewater.

It also shows that the anodic peak current increased gradually with increasing concentration of Cd (II) ions. Figure 5-19 shows the regression line with good linearity between the Cd (II) concentration and anodic peak current as y = 0,0146x + 0,319(R^2 = 0.65825) and LOD = 124,61 mg/l. This shows that the functionalised g-C_3N_4 SPE (with a paper substrate) can be used in qualitative and quantitative detection of Cd (II) from industrial wastewater samples, even though the LOD is ten times higher than the recommended value.

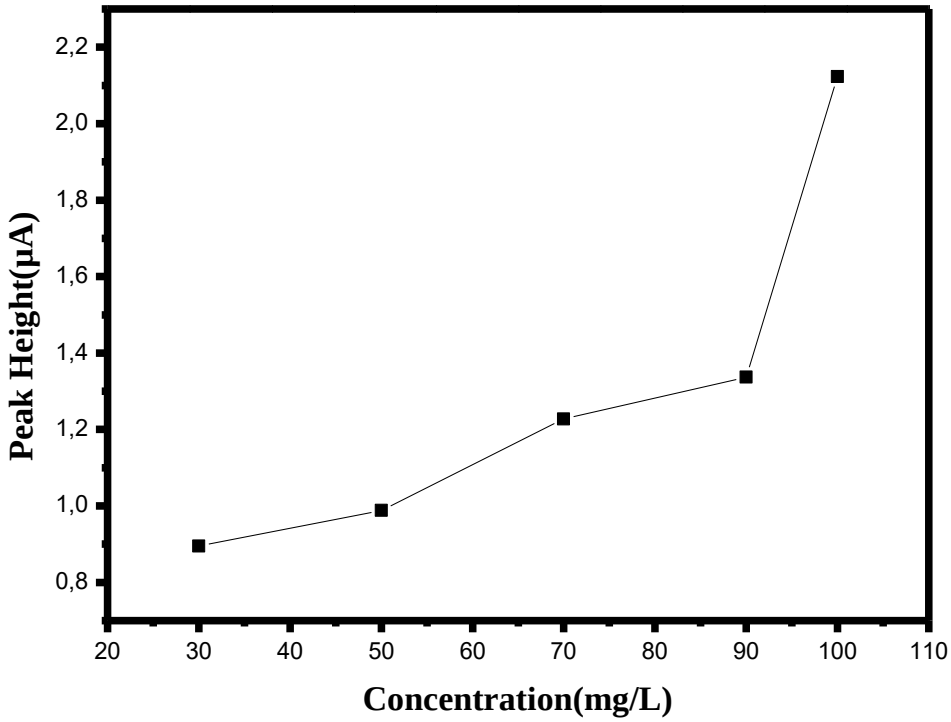


Figure 0-19: Calibration curve for Cd (II) concentration range 30 to 100 mg/L

5.4. **Chapter conclusion**

In this chapter, the fabrication of paper based SPEs was successfully done from the GO ink synthesised These electrochemical sensors offer a competitive analysis towards the detection of Cd (II) and Pb (II) and are comparable with the performance of commercial sensors. g-C_3N_4 nanoparticles were synthesised and used to functionalise the bare paper-based SPEs and successfully improved the sensitivity and selectivity of the electrode sensors. The sensors also demonstrated their ability to detect heavy metals in real polluted water.

Even though the bare screen-printed electrode did not perform as good as the commercial carbon sensors, this was the first attempt at using non-commercial GO ink in the fabrication of the electrode sensors. Further optimization should be directed to improve the GO ink formulation and that will further improve the performance of the resulting electrode sensors and the analytical of other heavy metals such as Ni (II) in water samples.

5.5. References

1. Anwar, A., Ahmad, N. and Madni, G.R., 2020. Industrialization, freight transport and environmental quality: evidence from belt and road initiative economies. *Environmental Science and Pollution Research*, **27**(7), pp. 7053-7070.
2. Addo-Bediako, A. and Rasifudi, L., 2021. Spatial distribution of heavy metals in the Ga-Selati River of the Olifants River System, South Africa. *Chemistry and Ecology*, , pp. 1-14.
3. Binning, K. and Baird, D., 2001. Survey of heavy metals in the sediments of the Swartkops River Estuary, Port Elizabeth South Africa. *Water Sa*, **27**(4), pp. 461-466.
4. gumpu, M.B., Sethuraman, S., Krishnan, U.M. and Rayappan, J.B.B., 2015. A review on detection of heavy metal ions in water–an electrochemical approach. *Sensors and actuators B: chemical*, **213**, pp. 515-533.
5. Solhi, E., Hasanzadeh, M. and Babaie, P., 2020. Electrochemical paper-based analytical devices (ePADs) toward biosensing: recent advances and challenges in bioanalysis. *Analytical Methods*, **12**(11), pp. 1398-1414.
6. Oliveira, V.X.G., Dias, A.A., Carvalho, L.L., Cardoso, T.M.G., Colmati, F. and Coltro, W.K.T., 2018. Determination of ascorbic acid in commercial tablets using pencil drawn electrochemical paper-based analytical devices. *Analytical Sciences*, **34**(1), pp. 91-95.
7. Mishra, R.K., Nawaz, M.H., Hayat, A., Nawaz, M.A.H., Sharma, V. and Marty, J., 2017. Electrospinning of graphene-oxide onto screen printed electrodes for heavy metal biosensor. *Sensors and Actuators B: Chemical*, **247**, pp. 366-373.
8. Li, P., Tao, C., Wang, B., HUANG, J., Li, T. and Wang, J., 2018. Preparation of graphene oxide-based ink for inkjet printing. *Journal of nanoscience and nanotechnology*, **18**(1), pp. 713-718.
9. Zheng, H., Ntuli, L., Mbanjwa, M., Palaniyandy, N., Smith, s., Modibedi, M., Land, K. and Mathe, M., 2019. The Effect of g-C_3N_4 Materials on Pb(II) and Cd(II) Detection Using Disposable Screen-Printed Sensors. *Electrocatalysis*, **10**(2),.
10. Hu, B., Cai, F., Chen, T., Fan, M., Song, C., Yan, X. and Shi, W., 2015. Hydrothermal Synthesis g-C3N4/Nano-InVO4 Nanocomposites and Enhanced Photocatalytic Activity for Hydrogen Production under Visible Light Irradiation. *ACS Applied Materials & Interfaces*, **7**(33), pp. 18247-18256.

11. Gao, J., Wang, Y., Zhou, S., Lin, W. and Kong, Y., 2017. A facile one-step synthesis of Fe-doped g-C3N4 nanosheets and their improved visible-light photocatalytic performance. *ChemCatChem,* **9**(9), pp. 1708-1715.
12. Niu, P., Zhang, L., Liu, G. and Cheng, H., 2012. Graphene-Like Carbon Nitride Nanosheets for Improved Photocatalytic Activities. *Advanced Functional Materials,* **22**(22), pp. 4763-4770.
13. Li, J., Tang, Y., Jin, R., Meng, Q., Chen, Y., Long, X., Wang, L., Guo, H. and Zhang, s., 2019. Ultrasonic-microwave assisted synthesis of go/g-c3n4 composites for efficient photocatalytic h2 evolution. *Solid state sciences,* **97**, PP. 105990.
14. Zhang, X., Liu, H. and Jiang, L., 2019. Wettability and applications of nanochannels. *Advanced Materials,* **31**(5), pp. 1804508.
15. Trick, J.L., Song, C., Wallace, E.J. and Sansom, M.S.P., 2017. Voltage gating of a biomimetic nanopore: electrowetting of a hydrophobic barrier. *ACS nano,* **11**(2), pp. 1840-1847.
16. Jemmeli, D., Marcoccio, E., Moscone, D., Dridi, C. AND Arduini, F., 2020. Highly sensitive paper-based electrochemical sensor for reagent free detection of bisphenol A. *Talanta,* **216**, pp. 120924.
17. Wang, H., Wang, J., Liu, g., Zhang, Z. and Hou, X., 2019. Electrochemical sensing of Pb (II) and Cd (II) in decorative material of wood panel using nano-cellulose paper-based electrode modified using graphene/multi-walled carbon nanotubes/bismuth film. *Int. J. Electrochem. Sci*, **14**, pp. 11253-11266.
18. Figueredo, F., Jesús González-Pabón, M. and Cortón, E., 2018. Low-Cost Layer by Layer Construction of CNT/Chitosan Flexible Paper-based Electrodes: A Versatile Electrochemical Platform for Point of Care and Point of Need Testing. *Electroanalysis*, **30**(3), pp. 497-508.

CHAPTER 6: CONCLUSION AND RECOMMENDATIONS

6.1. Conclusion

- This research aimed to develop paper-based electrochemical sensors using a synthesized nano-based graphene oxide ink. To accomplish this, GO was synthesized using a modified Hummers process and then used to make GO ink with CMC as a binder. The following are some of the work's highlights: GO was successfully synthesize using the modified Hummer's method, structural and morphological studies confirmed the properties present in the sample.
- The GO ink synthesized characterized shear thinning behaviour that is compatible with commercial carbon inks that are used for screen-printing of electrochemical sensors. It was confirmed that the amount of binder used in the formulation process affects the rheological properties of the ink and it is required to maximize the performance of the ink such as printability and conductivity.
- Electrochemical electrode sensors were screen-printed onto a photo-paper substrate to fabricate low-cost analytical devices to detect heavy metals in water. Although, the LOD of the bare electrode was higher than the approved standards
- To further improve the stability, the stability of the SPEs, g-C_3N_4 nanoparticles were used to modify the working electrode surface. The modified electrodes exhibited excellent LODs and were selective in the simultaneous detection of Cd^{2+} and Pb^{2+} and can also be applied in real water samples.

6.2. Recommendations

To further understand the physical properties of the ink versus the substrate used, contact angle measurements need to be performed. Although the SPEs show the ability to detect heavy metals at very low levels, further validation and enhancement of their efficiency is required. Before validation, various criteria such as the effects of the supporting electrolyte and adjusting the pH of the samples should be considered.

APPENDICES

Preparation of Acetate buffer (0.1M, pH 5)

1L volume of **0.1M Sodium Acetate**

$$\textbf{Concentration} = {}^{\textbf{Number of moles}}/_{\textbf{Volume required}}$$

Number of moles required in 1L to make 0.1 mol/L = 0.1 mol

Molar mass of Na-acetate (anhydrous) = 82.03 g/mol

$$\textbf{Number of moles} = {}^{\textbf{Mass required}}/_{\textbf{Molar mass}}$$

Therefore, mass required = 0.1 mol *82.03 g/mol = 8.2 g

Prepare **1L** volume of **0.1M Acetic acid** from glacial (99%) acetic.

$$\mathbf{C_1V_1 = C_2V_2}$$

Molarity (glacial acetic acid) = 17.4 M.

Initial concentration of solution, C_1 = 17.4 M

Concentration of final solution, C_2 = 0.1 M

Volume of final solution, V_2 = 1000 mL

$$\mathbf{V_1} = {}^{\mathbf{C_2V_2}}/_{\mathbf{C_2}}$$

= (0.1 M *1000 mL)/17.4 M

Volume of =5.75mL

Preparation of lead and cadmium ions concentration in 0.1 M Sodium acetate buffer (pH 5) from stock solution (1g/l)

Stock solution dilution

$$\mathbf{C_1V_1 = C_2V_2}$$

$$\left(100\ {}^{\text{mg}}/_{\text{L}}\right) * \text{V}_1 = \left(10\ {}^{\text{mg}}/_{\text{L}}\right) * (100\text{ml})$$

$$\text{V}_1 = 1\text{ml}$$

9 ml buffer + 1 ml stock solution

$$\mathbf{C_1V_1 = C_2V_2}$$

$$(1 * 10^{-7}\,{}^{\mathrm{g}}/_{\mu\mathrm{L}})\mathrm{V_1}=\left(1 * 10^{-11}\,{}^{\mathrm{g}}/_{\mu\mathrm{L}}\right) * (10000\mu\mathrm{L})$$

$$\mathrm{V_1} = 1\mu\mathrm{L}$$



Figure 1: GO ink

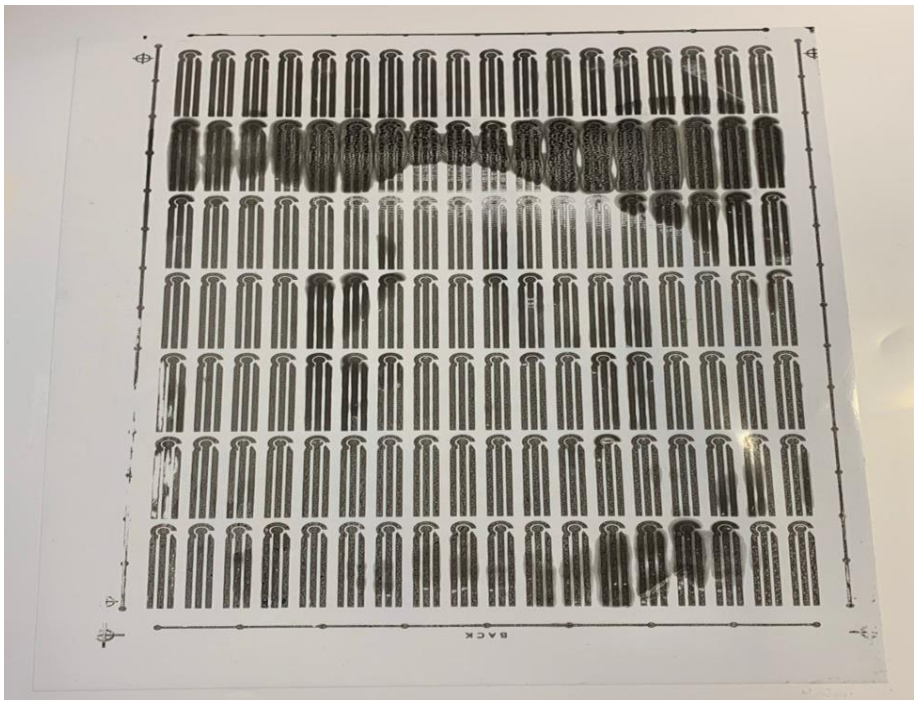


Figure 2: Screen-printed sheet using ink 1

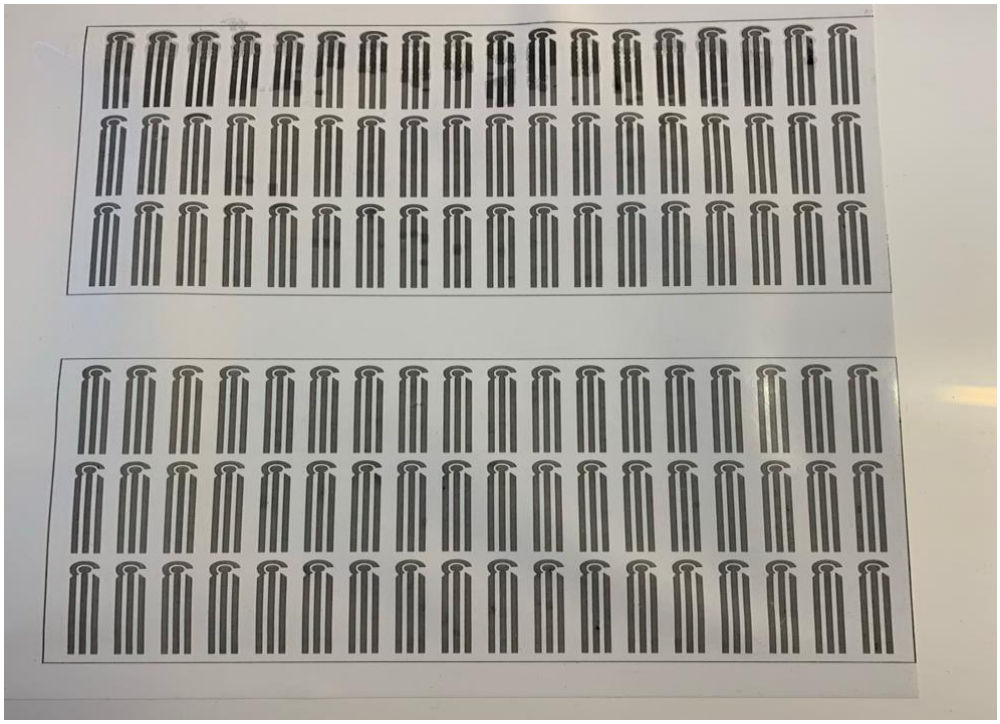


Figure 3: Screen-printed sheet using ink 2

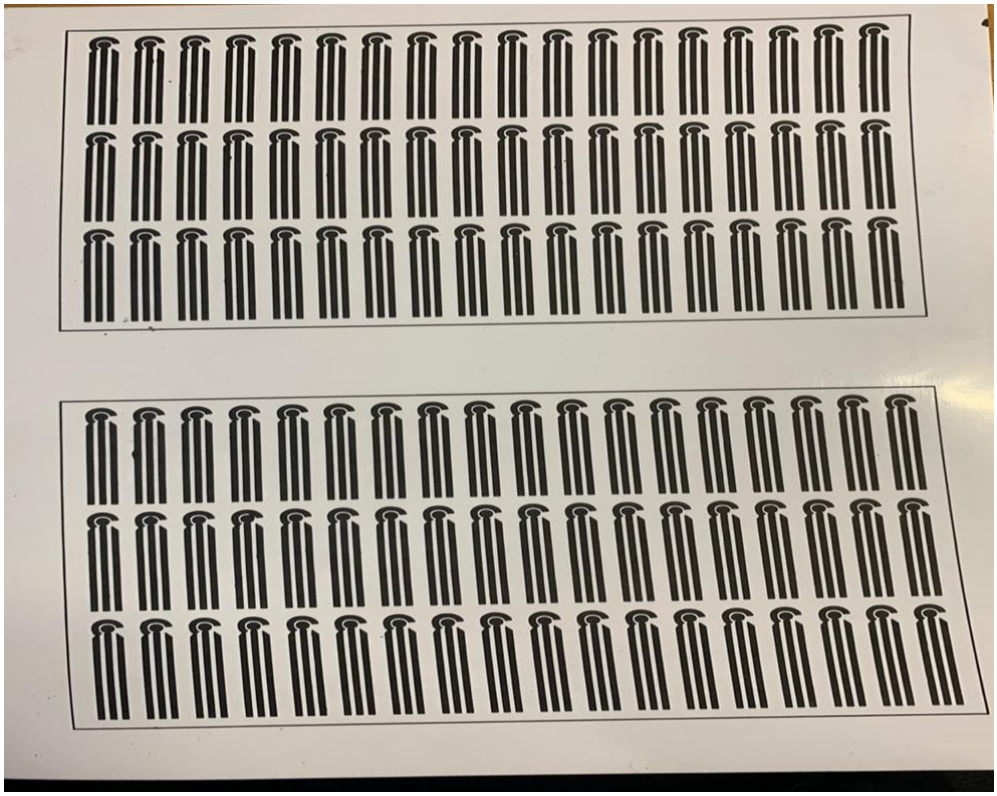


Figure 4: Screen-printed sheet using ink 3

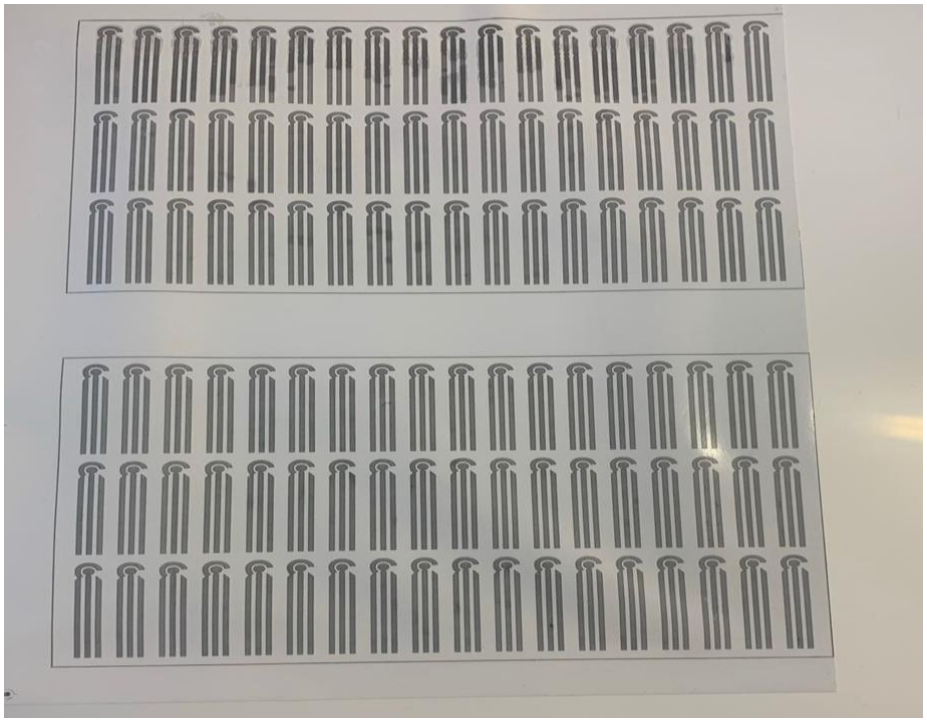


Figure 5: Screen-printed sheet using ink 4

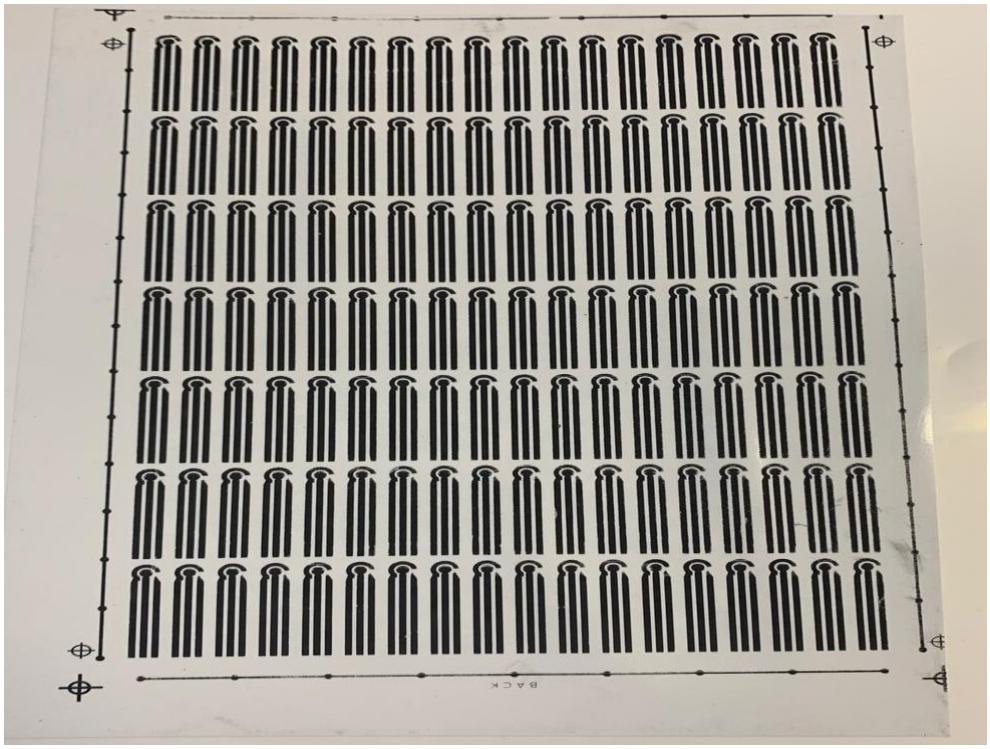


Figure 6: Screen-printed sheet using ink 5

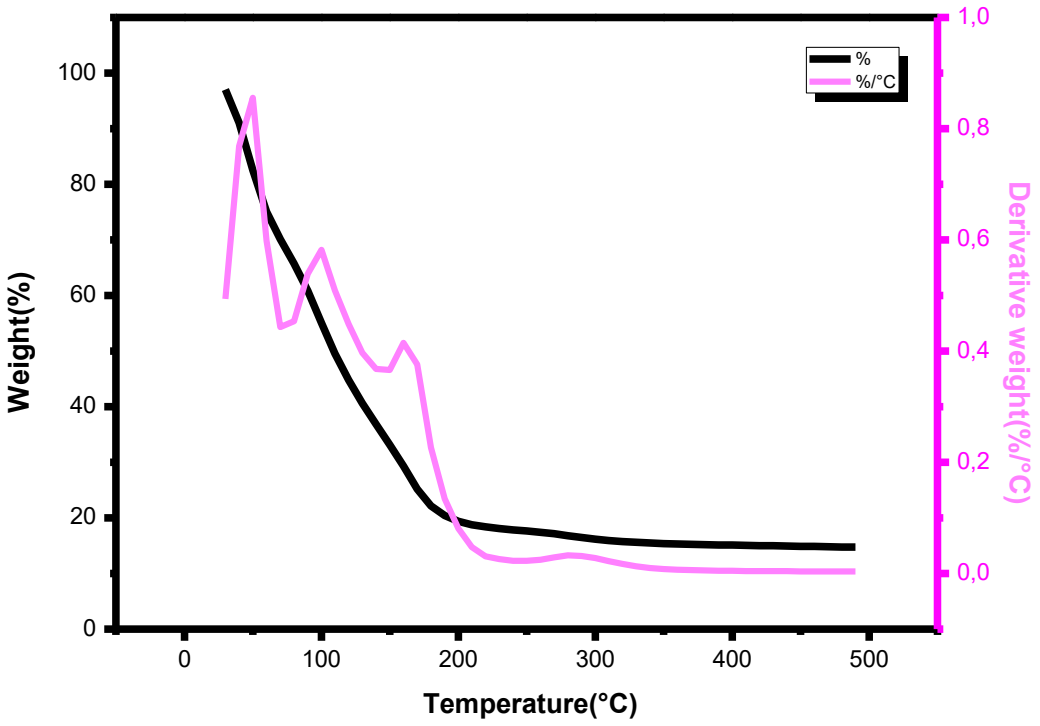


Figure 7: Weight Vs Derivative weight(%/°C) and T(°C)

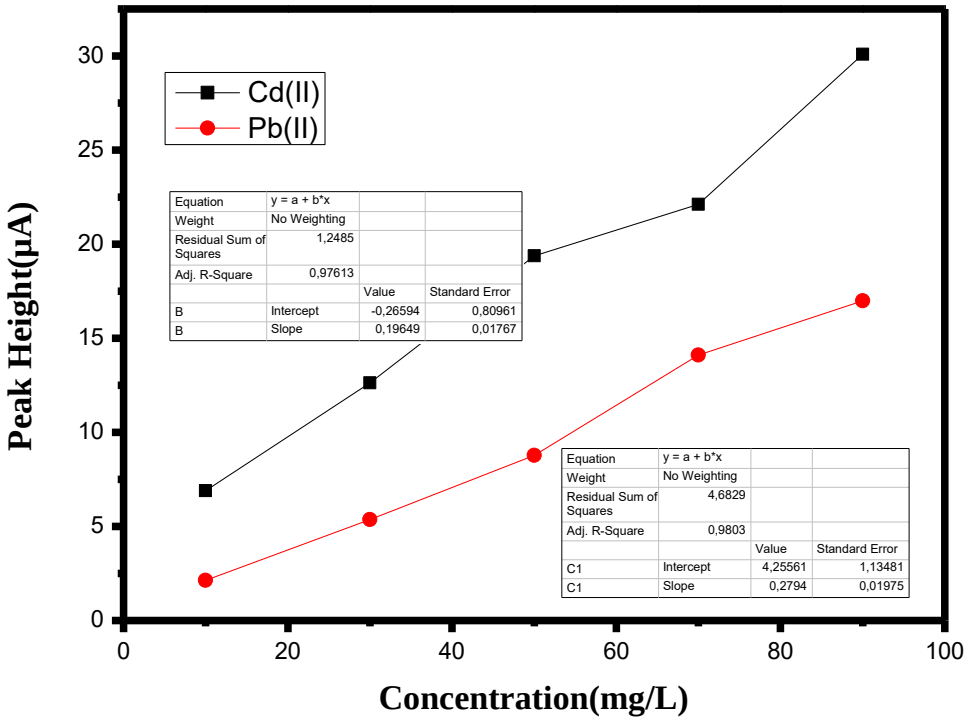


Figure 8: Calibration curves for SPEs with surface g-C_3N_4 modification.

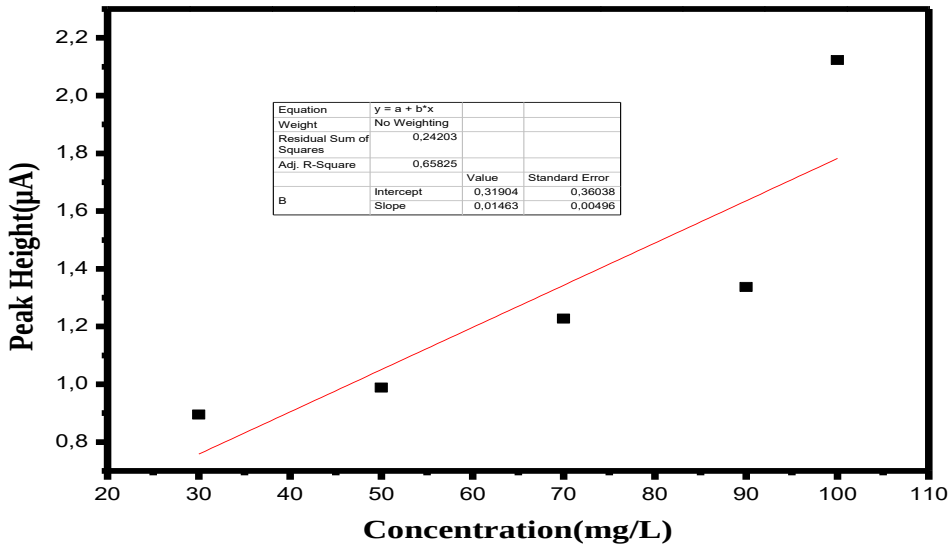


Figure 9: Calibration curves for Cd (II) and Pb (II) concentration range 10 to 90 mg/L.

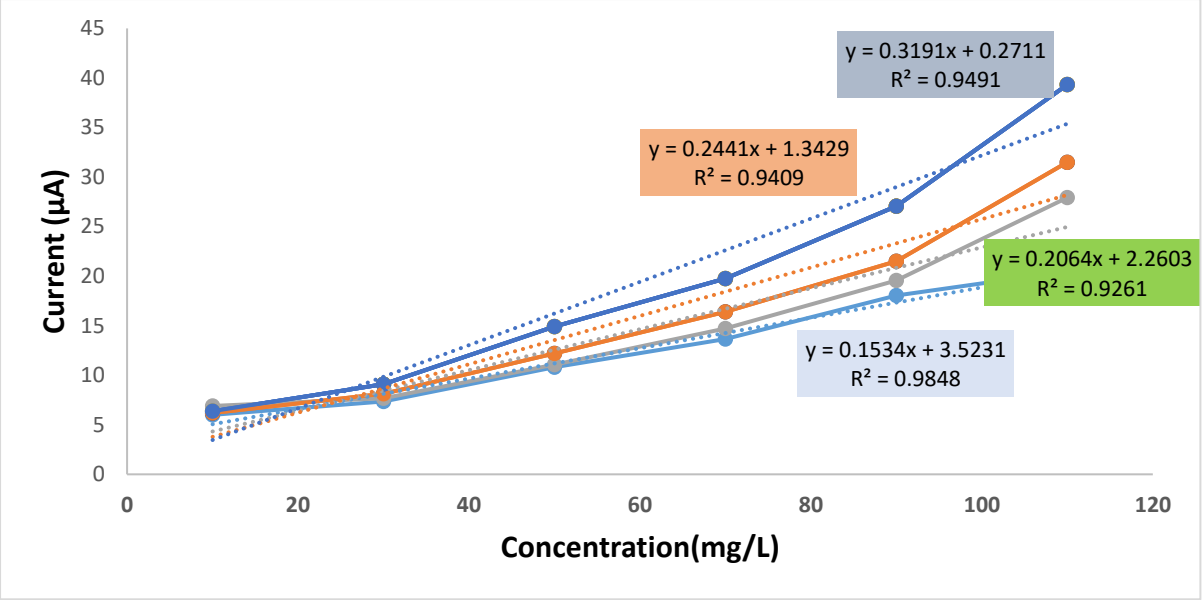


Figure 10: Calibration curves for Pb (II) concentration range 10 to 90 mg/L.

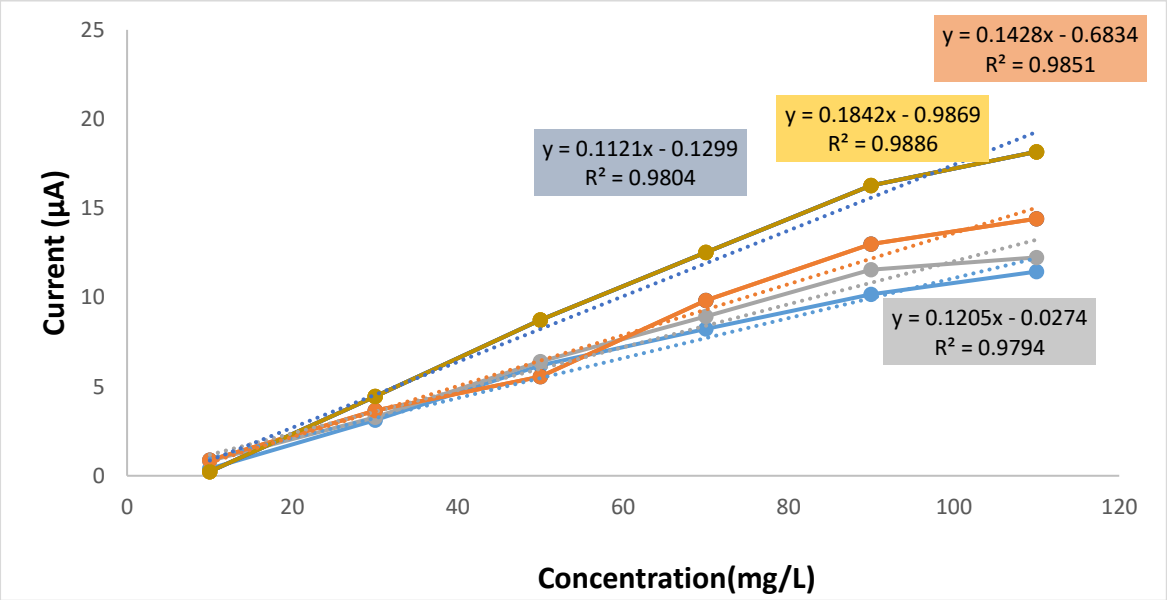


Figure 11: Calibration curves for Cd (II) concentration range 10 to 90 mg/L.

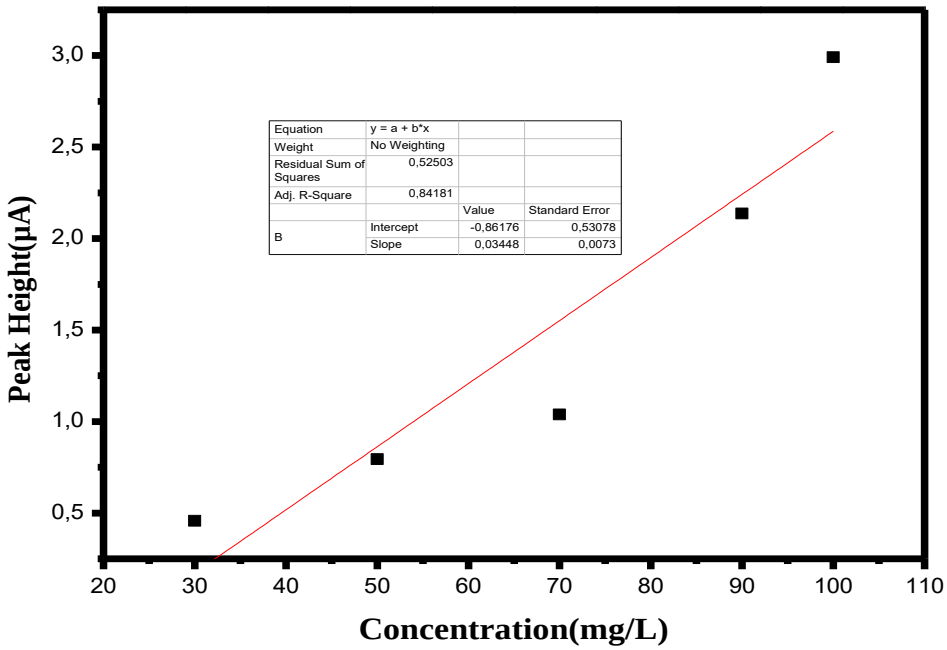


Figure 12: Calibration curves for Cd (II) concentration range 10 to 90 mg/L.

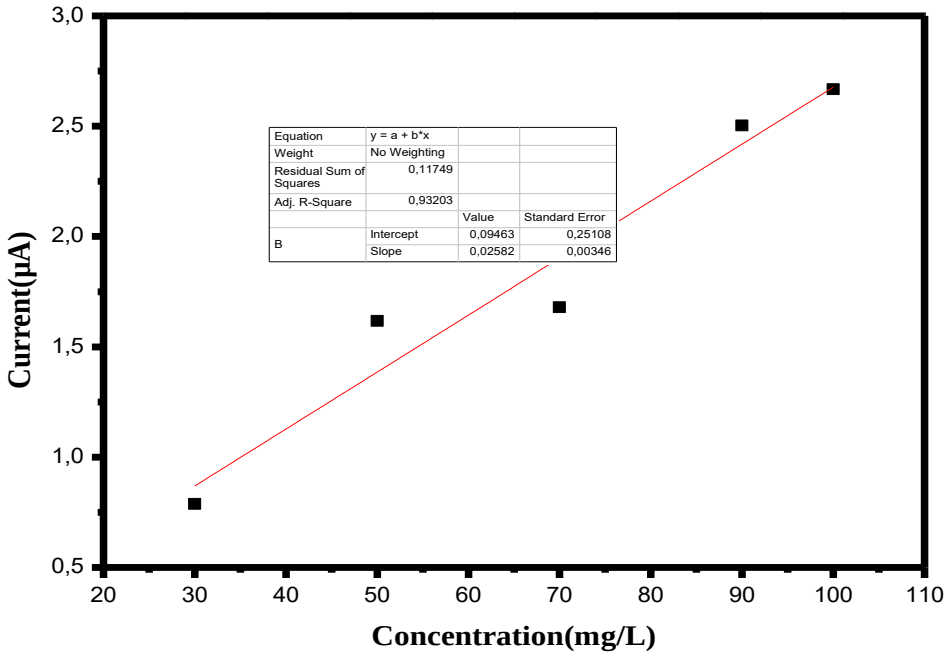


Figure 13: Calibration curves for Pb (II) concentration range 10 to 90 mg/L.